

SLOPE STABILITY OF THE TRIPP PIT NEAR ELY, NEVADA

by

Victor John Miller

---

A Thesis Submitted to the Faculty of the  
DEPARTMENT OF MINING AND GEOLOGICAL ENGINEERING  
In Partial Fulfillment of the Requirements  
For the Degree of  
MASTER OF SCIENCE  
WITH A MAJOR IN MINING ENGINEERING  
In the Graduate College  
THE UNIVERSITY OF ARIZONA

1 9 7 8

STATEMENT BY AUTHOR

This thesis has been submitted in partial fulfillment of requirements for an advanced degree at The University of Arizona and is deposited in the University Library to be made available to borrowers under rules of the Library.

Brief quotations from this thesis are allowable without special permission, provided that accurate acknowledgment of source is made. Requests for permission for extended quotation from or reproduction of this manuscript in whole or in part may be granted by the head of the major department or the Dean of the Graduate College when in his judgment the proposed use of the material is in the interests of scholarship. In all other instances, however, permission must be obtained from the author.

SIGNED:

Victor J. Miller

APPROVAL BY THESIS DIRECTOR

This thesis has been approved on the date shown below:

Richard D. Call  
RICHARD D. CALL  
Lecturer in Mining and  
Geological Engineering

April 25 1978  
Date

## ACKNOWLEDGMENTS

I would like to acknowledge those whose efforts contributed to the successful completion of this thesis. Kennecott Copper Corporation, Nevada Mines Division, provided financial as well as technical support. Within the Nevada Mines Division, John T. Crawford III, mines plant engineer, helped in formulating the thesis and gave valuable guidance throughout the study. William R. Wilson, chief geologist, organized most of the fundamental geologic data and relogged drill-hole samples that were essential to working out the geologic structure in the pit. Discussions with Carl D. Broadbent and Zavis M. Zavodnit of Kennecott's Metal Mines Division Engineering Center added to the ideas presented.

Dr. Richard D. Call, my thesis advisor, deserves special acknowledgment for his guidance and instruction. His efforts and contributions went far beyond what is normally expected from a thesis advisor. Drs. William C. Peters and Jaak J. K. Daemen, who served on the thesis committee, were also helpful. If it had not been for an H.E.W. Domestic Mining Fellowship, which I obtained while a student, completion of the academic work required for a master's degree in Mining Engineering would not have been possible.

## TABLE OF CONTENTS

	Page
LIST OF ILLUSTRATIONS . . . . .	vii
LIST OF TABLES . . . . .	ix
ABSTRACT . . . . .	x
INTRODUCTION . . . . .	1
Purpose of Study . . . . .	1
Brief History of the Tripp Pit . . . . .	2
Slope Stability Studies in the Pit . . . . .	5
GEOLOGY . . . . .	7
General Geology of the District . . . . .	7
Lithology and Stratigraphy of the Tripp Area . . . . .	9
Rib Hill Sandstone . . . . .	9
Limestone Units . . . . .	10
Chainman Shale . . . . .	10
Rhyolites . . . . .	11
Monzonite Porphyry . . . . .	11
Altered Porphyry . . . . .	11
Geologic Structure in the Tripp Area . . . . .	12
Pilot Knob Fault . . . . .	13
Footwall Fault . . . . .	13
Kimberly and Morris Faults . . . . .	13
Smaller Faults and Fault Systems . . . . .	14
Faulting in the South and Southwest Sides of the Pit . . . . .	14
Jointing . . . . .	15
Bedding . . . . .	15
Structural History of the Tripp Pit . . . . .	15
ROCK STRENGTH . . . . .	17
Strength of the Intact Homogeneous Rock . . . . .	17
Strength of the Unfilled Rock Joints . . . . .	21
Strength of the Filled Rock Joints . . . . .	22
The Clay Fault Gouge . . . . .	22
Nature of the Fault Zones . . . . .	22
Tripp Pit Fault Gouge Testing . . . . .	27

TABLE OF CONTENTS—Continued

	Page
GROUND-WATER HYDROLOGY . . . . .	34
Source of Water for the Tripp Area . . . . .	34
Ground Water in the Tripp Pit Area . . . . .	36
SLIDE MORPHOLOGY, MOVEMENT, AND MECHANICS . . . . .	38
Morphology of the Tripp Pit and Slide Locations . . . . .	38
Northwest Tripp Slide . . . . .	39
Morphology . . . . .	39
Structure and Rocks . . . . .	41
Movement . . . . .	41
Slide Mechanics . . . . .	42
Effective Rock Mass Strength . . . . .	43
Transition Zone . . . . .	43
Morphology . . . . .	43
Structure and Rocks . . . . .	45
Slide Movement . . . . .	46
Slide Mechanics . . . . .	46
Effective Rock Mass Strength . . . . .	48
Northeast Tripp Slide . . . . .	49
Morphology . . . . .	52
Structure and Rock Types . . . . .	53
Slide Movement . . . . .	54
Effective Rock Mass Strength . . . . .	56
Back-calculated Strength . . . . .	56
Back-calculated vs. Tested Strength . . . . .	59
Slide Mechanics . . . . .	61
The Complete Wedge . . . . .	61
Mechanics within the NETS . . . . .	62
Estimation of the Net Driving Force . . . . .	66
Morris Failure . . . . .	67
Morphology . . . . .	67
Structure and Rocks . . . . .	67
Slide Movement . . . . .	69
Slide Mechanics and Effective Rock Mass Strength . . . . .	69
Richards Failure . . . . .	71
Morphology . . . . .	71
Structure and Rock . . . . .	71
Slide Movement . . . . .	72
Slide Mechanics and Effective Rock Mass Strength . . . . .	72
Southwest Tripp Slide . . . . .	73
Morphology . . . . .	73
Structure and Rocks . . . . .	73
Slide Movement . . . . .	73
Slide Mechanics and Effective Rock Mass Strength . . . . .	74

TABLE OF CONTENTS—Continued

	Page
SLOPE DESIGN . . . . .	76
Overview . . . . .	76
Safety Factor Approach . . . . .	76
Probability of Failure . . . . .	77
Benefit-Cost Analysis . . . . .	77
Northeast Tripp Slide Slope Design . . . . .	78
Scope of Design Problem . . . . .	78
Design Method . . . . .	79
Slope Height . . . . .	79
Slope Angle . . . . .	79
Dewatering . . . . .	80
Catch Bench . . . . .	81
Tension Cables . . . . .	82
The Adit Solution . . . . .	84
Preliminary Recommendations . . . . .	85
The Other Slides . . . . .	86
Southwest Tripp Slide . . . . .	86
Morris Slide . . . . .	87
Northwest Tripp Slide . . . . .	87
APPENDIX A: DIRECT SHEAR TESTING ON THE TRIPP PIT FAULT GOUGE . . . . .	89
APPENDIX B: BACK CALCULATION OF EFFECTIVE STRENGTH FOR THE NORTHEAST TRIPP SLIDE . . . . .	103
APPENDIX C: NOTATION . . . . .	107
REFERENCES . . . . .	108

## LIST OF ILLUSTRATIONS

Figure		Page
1.	Location of the Tripp Pit and study area . . . . .	3
2.	Aerial photograph of the Tripp Pit area . . . . .	4
3.	Geology and morphology of the Tripp Pit area . . . . . in pocket	
4.	Structural contours of the controlling faults, Northwest and Northeast Tripp slides . . . . . in pocket	
5.	Fault gouge . . . . .	26
6.	Representative results of direct shear tests . . . . .	28
7.	Tested and predicted strengths of Tripp fault gouge . . . . .	29
8.	Tripp Pit slide movement . . . . . in pocket	
9.	Cross sections of north side of the Tripp Pit . . . . . in pocket	
10.	Schematic cross section of the Northwest Tripp slide illustrating slide development . . . . .	44
11.	Block diagrams showing possible failure mechanisms for the transition zone . . . . .	47
12.	Precipitation and wedge velocity of the Northeast Tripp slide over time . . . . .	51
13.	Back-calculated and tested shear strength for the Northeast Tripp slide . . . . .	58
14.	Effective strength of faults controlling the Northeast Tripp slide . . . . .	60
15.	Cross section of the Northeast Tripp slide illustrating its failure mechanism . . . . .	64
16.	Structural and topographic contour map of the Morris slide area . . . . .	68
17.	Pit design with a 200-foot catch bench for the Northeast Tripp slide . . . . . in pocket	

LIST OF ILLUSTRATIONS—Continued

Figure	Page
B-1 Graphic solution to the Northwest Tripp slide . . . . .	in pocket

## LIST OF TABLES

Table		Page
1.	Stratigraphic units found in the Tripp Pit area, Robinson mining district, White Pine County, Nevada . . .	8
2.	Major faults in the Tripp Pit . . . . .	12
3.	Rock substance strength . . . . .	19
4.	Results from Kennecott's triaxial testing . . . . .	20
5.	Unfilled rock joint strength from direct shear tests on similar rock types . . . . .	23
6.	Coulomb's law fit of gouge strength data . . . . .	30
7.	Power law fit of the gouge strength data, $\tau = F\phi_n^f$ . . . . .	30
8.	Atterberg test of fault gouge . . . . .	33
9.	Features of the Tripp failures . . . . .	40

## ABSTRACT

Open-pit mining in the Tripp Pit, which is located 6 miles west of Ely, Nevada, was discontinued by Kennecott Copper Corporation, Nevada Mines Division, in 1971. Economic feasibility of potential copper ore remaining below the present-day pit is marginal. Design of pit slopes will be critical in determining the feasibility of resuming operations.

An estimated 39 million tons of rock are presently involved in six identified slope failures within the pit. Five of these failures are wedge failures, and the sixth appears to be a soil-type circular failure. The 33-million-ton Northeast Tripp slide is the best understood of these six failures. It is a classic wedge failure, which started to fail in 1969 and has moved an estimated 28 feet toward the pit, then later stabilized. The back-calculated strength of the two controlling faults for the Northeast Tripp slide agrees closely with strengths derived from direct shear testing of the high-montmorillonite fault gouge from the area (cohesion = 8.7 psi; friction angle =  $9.6^\circ$ ). The net driving force for this failure may be on the order of  $8 \times 10^6$  lb, which is small compared to the estimated total driving force of  $15.2 \times 10^9$  lb acting on the wedge. Of the stabilization methods discussed, the use of tension cables or a 200-foot catch bench may be the most feasible.

## INTRODUCTION

Most of the Tripp Pit, located near Ely, Nevada, has been involved in slope failures. It is estimated that as much as 39 million tons of rock are incorporated within the six identified Tripp slides. Although Kennecott Copper Corporation, owner of the mine, ceased mining operations in the pit in 1971, 10 to 20 million tons of possible ore reserves still remain below where mining was halted. The economics of mining this ore are marginal, and the critical factor appears to be how the pit slopes can be designed.

### Purpose of Study

The first purpose of this study was to identify and document the failure mechanisms responsible for the Tripp slides. To do this, a detailed geologic structural investigation was completed, followed by a slope stability analysis. For the slope stability analysis it was necessary to run direct shear tests on a montmorillonite fault gouge to estimate the strength of fault zones that were found to control several of the failures.

The second purpose of this study was to make preliminary slope design recommendations. For several slides where there was insufficient data to determine the best slope design, it was only possible to review the alternatives and identify the areas where more data would be required.

### Brief History of the Tripp Pit

The now-idle Tripp Pit was an open-pit copper mine situated in the western portion of the Robinson mining district (also referred to as the Ely or Ruth mining district). The district is in the Egan Mountain range of White Pine County, Nevada, and is located 6 miles west of the town of Ely (Fig. 1). Figure 2 is an aerial photograph taken of the pit and surrounding area.

The district, actively mined since 1908, is currently owned and operated by Kennecott Copper Corporation, Nevada Mines Division. Details of the early history of the district and the Tripp Pit area can be found in reports by Spencer (1917), Parsons (1933), Horton (1960), and more recently by Kreis (1973).

Open-pit mining was first begun in the early 1950s. In 1959 the Tripp Pit was approximately 400 feet deep and had an average overall pit slope of 35 degrees. Even during these early stages a large slide with 1 to 2 million tons of rock in the northwest corner of the pit interfered with mining. The pit design was modified in 1965, based on the design engineer's experience with similar materials in nearby pits, to accommodate an overall slope of 45 degrees (Dimock, 1970). This design was used until 1971 when mining stopped at 625 feet below the surface. Slope instability was a significant factor in the decision to abandon the mine. There has been no mining activity in the Tripp Pit since 1971.

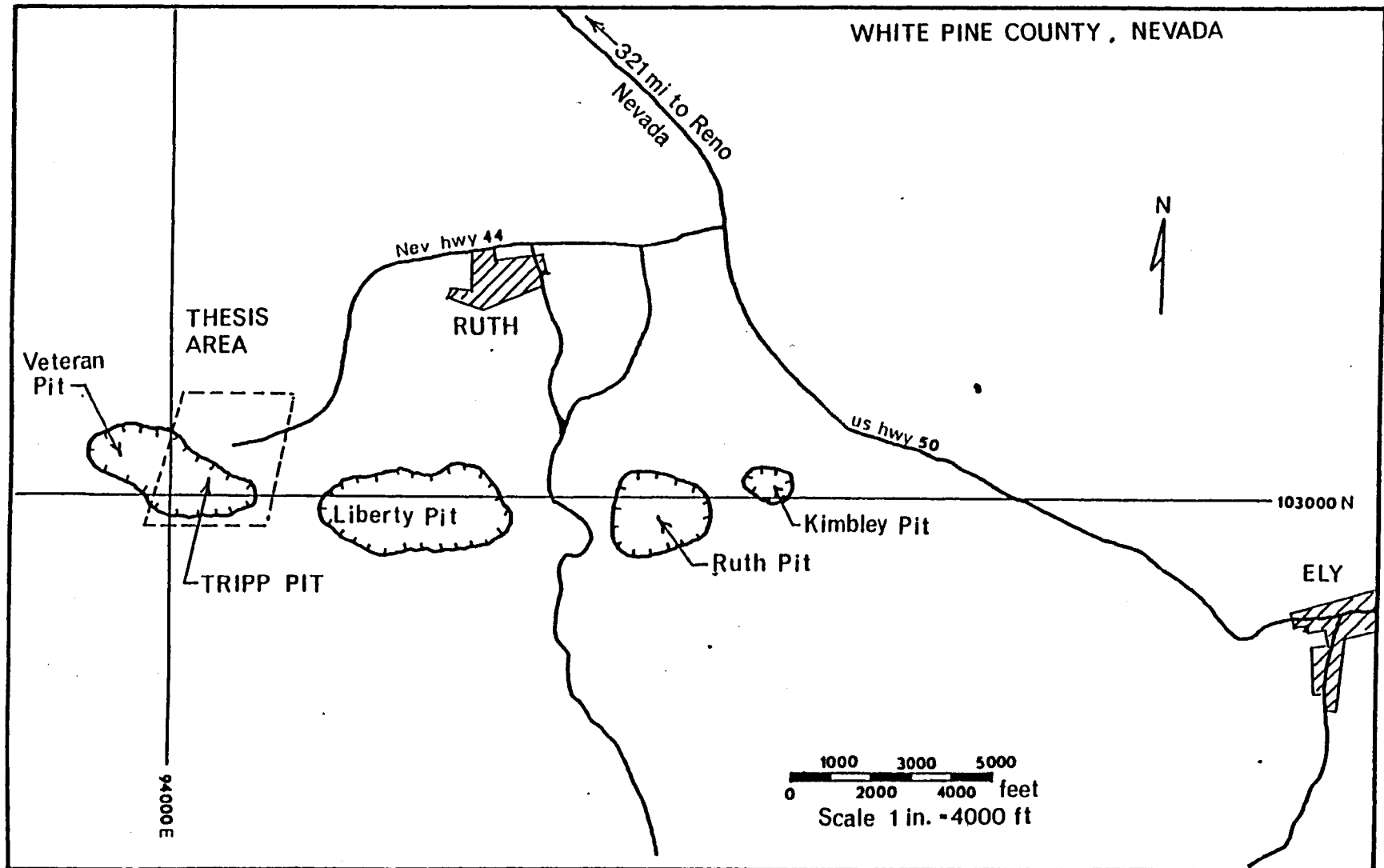


Figure 1. Location of the Tripp Pit and study area

**Figure 2. Aerial photograph of the Tripp Pit area**

**Key to location of features:**

1. Tripp Pit
2. Veteran Pit
3. Shop area
4. Northwest Tripp slide
5. Transition zone
6. Northeast Tripp slide
7. Morris slide
8. Richards slide (below pit rim, not in photograph)
9. Southwest Tripp slide



Figure 2. Aerial photograph of the Tripp Pit area

### Slope Stability Studies in the Pit

From 1968 to 1971 considerable work was done on the Tripp Pit slides. A pit slope monitoring system, using 27 survey stations and extensometers, was established by G. Clayton and R. Dimock of Kennecott. Four diamond drill holes were drilled to further delineate the structure behind the Tripp slide, referred to in this study as the Northeast Tripp slide (NETS).

Personnel from the U.S. Bureau of Mines conducted some of the early microseismic investigations on the north side of the Tripp Pit (Merrill and Stateham, 1970; Stateham and Vanderpool, 1971). Despite some background noise problems caused by nearby mining operations, the results of this study served to relate the microseismic noise to the movement of the pit slope failure.

Much of the slope stability work completed up to 1970 was summarized by Dimock (1970) in an oral presentation at the Open Pit Slope Stability Seminar Workshop, April 30, 1970 at the University of Nevada, Reno. A detailed stability study was completed about this time by personnel of the Kennecott Metal Mining Division Engineering Department, which was reported by Ko (1970). A more recent study by Broadbent (1975) was intended to make design recommendations so that the mine planning department could estimate the economics of possible future mining in the Tripp Pit. Recently, the geologic data from 145 churn drill holes and from the Morris underground workings have been reinterpreted; this has greatly aided in better delineation of the geologic structure that is believed to have controlled the slope failures (Wilson, 1976).

Some preliminary work was done by me on the Tripp Pit failure while employed by Kennecott prior to returning to graduate school. The bulk of the field work for this study was completed between May 16, 1977 and August 12, 1977, while employed as a mining engineer by Kennecott.

## GEOLOGY

Many geological studies have been completed on the Robinson mining district. Early work was done by Spencer (1917), Pennebaker (1932, 1942), Parsons (1933), Bateman (1935), and Beal (1950). More recently, studies were completed by Fournier (1958, 1967a, 1967b), Welsh and Breitrack (1964), Welsh (1965), McDowell and Kulp (1967), Nielsen (1969), James (1972), Kreis (1973), and Westra (1976). A review of the geology of the district was compiled by Bauer et al. (1966).

### General Geology of the District

The orebodies in the Robinson district lie along an east-west-trending zone that obliquely cuts the Egan Mountain Range. This configuration resulted from a complex history of thrusting, igneous activity, and Basin-and-Range faulting. The following list cites in chronological order the events that are believed to have led to the present geological relationships.

1. Deposition of a series of miogeosyncline sediments 7 miles thick.
2. Uplift of the Snake Range to the east, producing westward thrusting, resulting in a large post-Permian pre-Early Cretaceous overturned anticline. The anticline in the Robinson district was cut by several shallow faults during the thrusting. Although thrusting occurred along many of the less competent beds, the most important interface was the Ely-Chainman

contact (Table 1). Based on stratigraphic studies, the thrusting was postulated to have been Jurassic or Early Cretaceous by Welsh (1965).

Table 1. Stratigraphic units found in the Tripp Pit area, Robinson mining district, White Pine County, Nevada—After Welsh (1965)

System	Formation	Original Thickness (feet)	Probable Thickness in Tripp Pit (feet)
Holocene	Pit dumps	0-200	0-250
Quaternary	Alluvium	10-45	0-15
Permian	Rib Hill Sandstone	1100	?
	Riepe Spring Limestone	250	?
Pennsylvanian	Ely Limestone	2200	300-600
Mississippian	Chainman Shale <sup>a</sup>	400-1500	2000
	Joana Limestone	400	160

- a. Ely-Chainman contact was a zone of major thrusting.
3. Intrusion of a large pluton of monzonitic rock (109 m.y.) that was stratigraphically controlled.
  4. Hydrothermal alteration and copper mineralization of the upper portion of the intrusions and nearby sediments. There may have been several stages of igneous and hydrothermal activity, the last of which ended in a monzonitic intrusive event that was

accompanied only by weak hydrothermal activity (Kreis, 1973; Fournier, 1958; Westra, 1976).

5. Basin-and-Range faulting of the area in Oligocene time resulting in normal faulting and reactivation of many old fault zones.
6. Felsic igneous activity resulting in numerous rhyolite plugs, diatremes, dikes, and extrusive ash flows (32 m.y.).
7. Further Basin-and-Range faulting offsetting the rhyolites.
8. Several periods of weathering and erosion.

As will be discussed, the structure in the Tripp Pit as interpreted in this study agrees very nicely with that which would be expected from the series of geologic events for the district.

#### Lithology and Stratigraphy of the Tripp Area

The stratigraphic units listed in Table 1 are those found in the Tripp Pit area. There are few exposures outside the pit because most of the area is covered by shallow pediment deposits. In the northeastern portion, stream alluvium can be found. Recent mining activity has been of much greater significance. Dumps in places are over 250 feet thick (Fig. 3, in pocket) and cover much of the northern and southern parts of the thesis area. Another recent feature is the pit slope failures, which will be discussed in depth.

#### Rib Hill Sandstone

Rib Hill sandstone, consisting of sandstones, calcareous sandstones, and thin-bedded silty limestones with abundant chert, is probably represented by the oxidized sandstone that was mapped along

the south rim of the Tripp Pit. Because of alteration and weathering, the unit appears as a silty quartz-sericite rock with abundant limonite, with the limonite mainly along joints but locally occurring as a rock constituent itself.

### Limestone Units

Distinguishing between the three probable limestone units in the pit was difficult because all the identifiable features were lost due to alteration. Even identification by stratigraphic location has resulted in many disagreements because with all the faulting and thrusting almost any order is possible. Here only the most important lithology, as currently understood, will be discussed. The skarn in the pit is described in detail by James (1972). Extensive calc-silicate skarn is exposed on the north portions of the pit. This skarn is generally high in garnet and pyrite but may also contain considerable biotite, chlorite, nontronite, actinolite, calcite, magnetite, quartz, and sulfides. Where weathered they form a gossan that varies from a mixture of earthy limonites to highly siliceous jasperoid. Marble can also be found on the north wall. Here it is bleached to a grayish white, sometimes containing chert nodules, often skarn lenses, and vary amounts of wollastonite.

### Chainman Shale

The Chainman Shale can be found on the north side of the pit. Unaltered, this unit is a fissile quartz-illite-montmorillonite-kaolinite shale (Westra, 1976). In the Tripp Pit this unit is generally a hornfels that appears to consist of quartz, sericite, biotite, and andalusite to varying degrees. On the surface it is cut by numerous limonitic veinlets

and joints, and at depth diamond drill core shows sulfides below the level of oxidization.

### Rhyolites

Exposed within the pit are numerous rhyolite dikes, diatremes, and breccias. In some fault zones the rhyolites have been weathered to a greenish clay. A breccia in the eastern portion of the pit contains almost all the local rock fragments including a 6-foot-diameter fragment of Chainman Shale-type hornfels. Generally, the fragments range in dimensions from 0.1 to 1.0 foot. In addition, those intrusions can have glassy border zones with varying stages of devitrification (Wilson, 1977).

### Monzonite Porphyry

Hornblende monzonite porphyry, which probably underlies the total thesis area, is exposed on the surface in only one area near the Morris slide (Fig. 1), where it is highly weathered. In drill cores, the appearance of the porphyry varies from fresh to weakly propylitized with or without minor pyrite. Two-inch K-feldspar phenocrysts are common.

### Altered Porphyry

Although for rock mechanics purposes the altered porphyries found in the Tripp Pit area have been lumped into one group, they actually consist of several distinguishable types of alteration. A quartz-sericite porphyry dike is exposed by the Morris slide. In this alteration type the main constituents are a sugary quartz, sericite, and clay (probably kaolinite). Only an occasional remnant ghost phenocryst indicates

that this unit was once a monzonite porphyry. The argillized porphyries form the second major group. Clay alteration varies from that involving just the plagioclases all the way to that including the K-feldspar. Both groups can have varying amounts of sulfides either disseminated or in veinlets. Where exposed, both groups appeared to weather very quickly. The last general alteration type is propylitic. For strength classification propylitically altered porphyry has been included with the fresh unaltered porphyries.

#### Geologic Structure in the Tripp Area

The structural interpretations on the north and northeast sections of the pit are believed by me to be the most accurate. Here, too, most of the geologic data was available. On the south and southwest sides of the pit there were only enough data to indicate this area's very complex nature. Table 2 lists the major faults that were delineated in this study. Figure 4 (in pocket) is a structure contour map of these major faults, which also gives the evidence for the structure.

Table 2. Major faults in the Tripp Pit

Fault	Strike	Dip	Approx. Gouge Thickness (feet)	Origin
Pilot Knob	N. 71° E.	35° SE.	20	Basin-Range faulting
Kimberly	N. 70° E.	33° SE.	10-40	Basin-Range thrusting
Morris	N. 24° E.	31° NW.	5-40	Thrusting
Footwall	N. 64°-37° W.	40°-70° SW.	0-5	Basin-Range thrusting

### Pilot Knob Fault

The Veteran Pit orebody, which lies west of the Tripp area, appears to be offset from the Tripp mineralization by the Pilot Knob fault. This fault has been extensively mapped in the saddle area between the two pits and also intersected by 12 diamond and churn drill holes located in the Tripp Pit. There are not enough data to determine the positive relationship of this fault with the Footwall fault. However, based on the offsetting orebodies and the extension of surface slide cracks which parallel the strike of the Pilot Knob fault, it would appear that the Pilot Knob fault cuts the Footwall fault. For slope stability, only the existence of a system of fault structures that parallel the Pilot Knob fault is important.

### Footwall Fault

The Footwall fault is the major ore-waste contact in the Tripp Pit. It roughly parallels the bedding and can be considered a bedding plane fault. On the hanging wall (southwest) side of this fault are highly altered copper-bearing skarns and intrusive rocks. The footwall (northeast) side contains less altered marble and shale or hornfels. The Footwall fault cuts both the Kimberly and Morris faults.

### Kimberly and Morris Faults

The Kimberly and Morris faults can only be found on the northeast side of the Footwall fault. The Kimberly fault roughly parallels the Pilot Knob fault and may have at one time been a part of that fault system. Above this fault are steeply dipping sedimentary rocks that parallel the Footwall structure, and below is a barren propylitized monzonite

porphyry. The second major fault northeast of the Footwall fault is the Morris fault. It cuts the same rocks as the Kimberly fault. The exact crosscutting relationships at the Kimberly-Morris intersection are not clear, but information from two drill holes (XD-16 and E-166) suggests that the Kimberly fault cuts the Morris fault. The Morris fault is definitely part of a system (Fig. 3). Two parallel faults were mapped, and one of these was used to obtain the gouge samples for strength testing.

#### Smaller Faults and Fault Systems

The Morris underground workings, which were mapped in detail (1" = 20'), offer some insight into the nature of the structure in the Tripp Pit. The first observation is that it is highly complex. Within the 6710 level that covered an area of 500 by 1,000 feet, over 344 faults of varying degrees of importance were mapped. It was found that these smaller faults could be grouped into sets that closely paralleled the major faults. From the Morris headings it was found that both the Morris and Kimberly faults appeared to have been dragged by a left-lateral strike-slip movement on the footwall. Part of the Morris underground mapping that shows this drag is shown in Figure 4.

#### Faulting in the South and Southwest Sides of the Pit

With most of the area now covered by shallow rubble slides and with information from only two diamond drill holes and several churn drill holes, an accurate structural interpretation was not possible. The area contains many more rhyolite breccia intrusions than the north side, which complicates the geologic interpretation of the structure. In addition, a

shallow south-dipping thrust cuts part of the south side (Fig. 3). This thrust (or shallow dipping fault) appears to have the Rib Hill sandstone and Riepe Springs limestone above it. Below the thrust appears to be highly altered Lower Pennsylvanian and Mississippian sedimentary rocks.

### Jointing

As should be expected, where an area is highly faulted there is also a complicated jointing system. Figure 3 shows the results of three detailed lines completed by the staff at Kennecott and the joint set mapping done by me.

### Bedding

The bedding along the north and northeast sides of the pit roughly parallels the Footwall fault (N.  $64^{\circ}$ - $37^{\circ}$ W.,  $40^{\circ}$ - $70^{\circ}$ SW.). Figure 3 and the cross sections in Figure 4 show the bedding. There was evidently a great deal of thrusting within the different sedimentary units. The best example of this is a limestone unit (probably Joana Limestone) 100-200 feet thick that now lies within the thick Chainman Shale unit on the north side of the pit. There is no limestone unit in the middle of the Chainman Shale, so this must be a sliver of one of the other units thrust into the Chainman.

### Structural History of the Tripp Pit

Below is a list in chronological order of the events that may have led to the structural relationships now observed in the Tripp Pit.

1. Regional thrusting from the east forming a large monocline-recumbent anticline. One of the major active faults during this time would have been the Footwall fault, which was tilted to its present position when the monocline formed.
2. Stratigraphically controlled monzonitic intrusion followed by hydrothermal activity. This intrusion tended to assimilate the sedimentary rocks (generally the Chainman Shale) rather than intrude them forcefully. This pluton now lies north and east of the Tripp Pit.
3. Gravity sliding or very low angle normal faulting of the upper alteration halo of this intrusion. The Tripp Pit area was moved generally west. During this period, the Kimberly and Morris faults were active.
4. Normal Basin-and-Range-type faulting. The Footwall and Pilot Knob faults were reactivated downthrowing the south side of the fault to its present position. The last movement on the Footwall fault was strike-slip, which could have occurred when the Pilot Knob fault dropped the whole Tripp area to the southeast and separated it from its sister orebody, the Veteran. In addition, this period was accompanied by considerable rhyolitic intrusive activity with forceful intrusion of the weakened rocks and discontinuities.

This suggested geologic history fits well with what is generally believed to be the geological history of the Robinson mining district.

## ROCK STRENGTH

The strength of the pit slope material has been divided into three categories. First are the strength properties of the intact, homogeneous rock or rock substance (Coates, 1964). Second is the expected strength of the unfilled rock joints. Third, and most important for the Tripp Pit, is the strength of the joints and fault zones filled with gouge.

### Strength of the Intact Homogeneous Rock

Rock substance strengths in the Tripp Pit are much greater than those of joints and faults. The maximum vertical lithostatic pressure expected within the study area should be around 400 psi, which is considerably lower than the measured compressive strength of the intact rocks found in the area. This is not saying that local stress concentrations may not exceed the compressive strength of the weaker intact rocks, only that it should be expected to occur rarely.

Over the last fifteen years, uniaxial and triaxial testing has been conducted on diamond core samples from the Robinson mining district. The testing done by Kennecott at its Engineering Center in Salt Lake City, Utah, was summarized in an interoffice report by Broadbent (1974). Fifty-seven specimens were tested. The second source of data was some uniaxial and Brazilian disk tension tests carried out by U.S. Bureau of Mines personnel in which 12 core samples were tested (Markos, 1971).

Most of the rocks used in these tests did not come from the Tripp Pit. This is believed to be of minor significance because the general petrology of the rocks tested was comparable to that of rocks found within the pit. In addition, the variability in strength properties, even within the same unit, is considerable. For example, 23 subunits have been identified within the Ely Limestone (Welsh and Breitrack, 1964), all with recognizable petrographic and stratigraphic differences. One of these units has large chert nodules, 6-12 in. in diameter, which by themselves would have different strength properties. For this reason, only the general expected range of strength properties will be used. These are given in Table 3.

The cohesion and friction angles obtained from Kennecott's triaxial testing fall somewhere between intact rock strength and the strength expected from an already failed joint. These data can be used to give an estimate of the lower limits of the shear strength of intact rocks. Many objections have been raised regarding the use of triaxial test results to estimate the cohesion and friction angles. Two of the main problems with the test are that only a limited amount of displacement is possible and dilation is not easily measured (Jaeger, 1971). In addition, the use of a "soft" compression testing machine, as was used by Kennecott personnel, increases the difficulty in correctly measuring the residual strength of the already failed rock. With these qualifications, results from the Kennecott testing program are presented in Table 4.

These data were obtained from triaxial tests done by Kennecott Engineering Center (Broadbent, 1974) using diamond core samples mainly

Table 3. Rock substance strength

General Rock Type	Unconfined Compressive Strength, psi		Tensile Strength, Brazilian Disk, psi	Average Young's Modulus	Strength Classifi- cation <sup>a</sup>
	Low	High			
Fresh porphyry	10,000	20,000	untested	$1.3 \times 10^6$	HS
Altered porphyry	700	15,000	<sup>b</sup> 800	1.1	VLS-MS
Shale <sup>c</sup>	2,000	11,500	untested	8.7	VLS-MS
Rhyolite	5,400	15,000	untested	1.8	LS-MS
Limestone <sup>b</sup>	7,000	11,000	1,000	2.4	LS-MS
Skarn- marble	6,700	18,000	600-1200	untested	LS-HS
Fault gouge <sup>b</sup>	450	2,200	untested	9.7	VLS

a. Based on classification system by Deere and Miller (1966): VSH = very high strength; HS = high strength; MS = medium strength; LS = low strength; and VLS = very low strength.

b. Less than three samples tested.

c. Unaltered shale and hornfels are both included in this category, the latter being far more common.

Table 4. Results from Kennecott's triaxial testing

Rock Type	Number of Samples	Cohesion psi		Friction Angle degree	
		$\bar{x}$	s	$\bar{x}$	s
Fresh porphyry	14	675	583	36.4	7.9
Altered porphyry	16	209	179	35.8	4.6
Shale	7	524	513	37.3	4.9
Rhyolite	3	575 to 680		38.0 to 38.5	
Fault gouge	1	165		<sup>a</sup> 38	

a. Does not correlate with the fault gouge direct shear testing done for this study.

from the Ruth Pit area (7,000 feet east of the Tripp Pit). These samples were first tested to failure, usually at zero confining pressure. Then the "failed" specimen was subjected to loading cycles to failure at progressively higher confining pressures, up to 1,000 psi. The data were then reduced by assuming a straight-line Mohr failure envelope to obtain the rock cohesion and friction angle (Broadbent, 1976).

It should be mentioned here that the division between fresh and altered porphyry is gradational. The rock type classification of shale may be too general for strength testing. This class can contain rocks grading from a mainly montmorillonite clay to an andalusite-cordierite-bearing hornfels.

As can be seen from Tables 3 and 4, the strength of the intact rock is considerably greater than the compressive strength expected within the pit slopes. The weakest rock types is the altered porphyry with a cohesion of 209 psi and a friction angle of  $35.8^{\circ}$ . Using the circular failure charts of Hoek and Bray (1977) and assuming a completely water-saturated, 600-foot-high slope, this material could stand at a 90-degree slope (vertical). Even using a cohesion one standard deviation lower (30 psi), a 50-degree slope could be expected to be stable. The steepest slope now existing within the pit is  $43^{\circ}$  and all the existing failures occurred while trying to mine at a 45-degree slope.

#### Strength of the Unfilled Rock Joints

Much of the current literature in slope stability has dealt with describing the properties of the discontinuities within a rock mass. A major portion of these discontinuities fall into the category of unfilled joints. Of all the failures observed within the Tripp Pit, only two of the smaller wedge failures are believed to be controlled on one side by jointing. For this reason, sampling and testing of actual joints were believed unnecessary and in the cases just mentioned, accessibility made sampling impossible.

Because considerable data can be obtained from the slope stability and rock mechanics literature, the strength properties of the joints within the Tripp Pit can be estimated. Although actual testing of the Tripp joints would be ideal, the ranges found by other researchers for similar rock types should more than satisfy the requirements for this study. The joint strengths will be given by the Coulomb failure criteria

of  $\tau = C + \sigma_n \tan \phi$ , where  $\tau$  = the shear strength to be determined and  $\sigma_n$  is the normal stress acting on the joint. The two strength parameters are the cohesion,  $C$ , given in lb/in.<sup>2</sup>, and the friction angle  $\phi$  in degrees. The data presented in Table 5 are the result of direct shear testing on rocks similar to those found in the Tripp Pit.

### Strength of the Filled Rock Joints

#### The Clay Fault Gouge

In the Tripp Pit, the filled joints of importance are the large clay gouge filled fault zones. These zones may range in thickness from several feet up to 40 feet. X-ray analysis of the gouge from the Kimberly and Morris faults done by the KCC Research Center, revealed that the gouge consisted of roughly 50-70% montmorillonite clay, 10-20% kaolinite clay, 10-25% sericite mica, and 5-10% very fine grained quartz. The rocks believed to be the source of the gouge are either the Chainman hornfels or the fresh monzonite porphyry. The hornfels was originally a montmorillonite shale, and it is not surprising that it would yield a high montmorillonite clay gouge. Montmorillonite is also a common alteration product of the monzonite porphyry (Westra, 1976). The 5-10% quartz found in the monzonite may also be the source for the similar quantity of quartz found in the gouge.

#### Nature of the Fault Zones

The nature of the fault zones is important for understanding the expected strength from such a zone. On a large scale, surface irregularities or undulations within the rocks on either side of the fault zones

Table 5. Unfilled rock joint strength from direct shear tests on similar rock types

Rock Types	Cohesion (psi)	Friction Angle (degrees)	Source <sup>a</sup>	Range Expected in Tripp Pit	
				Cohesion (psi)	Friction Angle
Fresh porphyry	0.0	27.5-29.7	2	2-19	29.36
	0.0	29	1		
	0.0-7.1	31.0-36.0			
Altered porphyry	4.9-17.8	26.4-35.8	2	0-7	26-31
	2.6				
Shale	14	16.5	2	0-14	7-23
Hornfels	0.0	31.9	b 3	0-11.6	19-42
	3.7	19	b 4		
	2.4-11.6	19.5-42	5		
Rhyolite	45.0-55.0	29.7-32.6	b 6	14-55	33-55
	14	37.0-55.0	b 7		
Limestone	5	28	8	0-10	28-37
	0	33.0-37.0	9		
	0	36.9	1		
Marble	0	0.45	b 10	0-5	33-35
	5	33	11		
Skarn	0.0-4.7	24.1-31.8	2	0.4.7	24.1-31.8
Fault gouge	0	8.2	b 2	(c)	(c)
	19	6.5	b 2		
	3.5	10	b 12		

a. Key to sources: 1—Coulson (1970); 2—Rock Mechanics Laboratory, University of Arizona (n.d.); 3—Call (1972); 4—Ramos, Guimaraes, and Abrao (1974); 5—Hamel (1972); 6—Jaeger and Cook (1969); 7—Radosavljevic, Colic, and Lokin (1970); 8—Pratt, Black, and Brace (1974); 9—Stagg and Zienkiewicz (1968); 10—Bertacchi and Sampaolo (1974); 11—Abel (1971); 12—Hoek and Bray (1977).

b. Not identical rock type.

c. Discussed on p. 27-33.

could affect the frictional strength. Under low confining pressure, as would be the case in the Tripp Pit, the sliding rock mass would tend to slide up and over these undulations. If the slope of the undulation could be measured, at  $i$  degrees to the direction of the shearing force, the Coulomb equation becomes  $\tau = C + \sigma_n \tan (i + \phi)$  (Jaeger, 1971).

For the large (5-40 feet thick) fault zones, this does not seem to be a likely mechanism. First, the undulation would have to be very large. Second, generally the upper and lower contacts of the fault zones are gradational. An undulation would therefore probably contain many smaller gouge-filled discontinuities that would fail before riding up and over could occur. Finally, the gouge is a plastic material. The gouge tested for this study was observed to flow in the period of a half-hour laboratory shear test at pressures greater than 200 psi. Even if an undulation were strong enough to support riding up, the gouge is not; and over a period of time (measured in days) it would conceivably flow around such an undulation. This flowing would require energy from the sliding block and might tend to dampen the slide, but it would not add to the strength of the fault zone.

Trying to determine the strike and dip or even the inclination to the core axis within the main fault zone can give results that may be very misleading. Lineations of rock clasts or stringers or clay gouge can be oriented in almost any direction to the true orientation of the zone. No study was done on this, but from personal experience with this type of material, if all these smaller orientations were recorded, they would probably exhibit a normal distribution that would have an average equal to the true strike and dip of the main fault. The rock clasts within the

gouge are usually not in contact with each other. This texture is here described as "floating." The matrix is generally a black to grayish-black clay. Where sulfides have been oxidized, this clay has been observed to have a tan-brown appearance probably due to limonites within it. Figure 5 is a photograph of some typical Tripp Pit gouge used for the shear tests.

An interesting phenomenon was observed in the small-scale laboratory direct shear test of this fault gouge. For one test a core sample 1.3 in. in diameter was precut along the shearing surface. The shearing did not occur along this prepared surface. Instead, the sliding occurred along a weaker cup-shaped zone existing approximately 0.1 in. below this cut surface. This occurred several times on different specimens. At confining pressures between 250 and 450 psi, the precut zone usually rehealed, and only the sliding surface, which may or may not have been the precut surface, could be identified. Expanding this concept to a large 20-foot gouge-filled fault, the shearing will occur along the weakest zone within the fault. There is no reason why shearing would not occur along many of these weaker zones within a fault with the differences in movement between these zones being taken up by the multitude of smaller crosscutting subfaults with the main zone and the plastic flow within the gouge. If the zone could be extensively sampled and these samples subjected to shearing tests, the average shear strength of all samples may not be that of the zone itself for this reason. The actual strength could conceivably be close to the strength exhibited by only the weakest samples. This may be one explanation why the

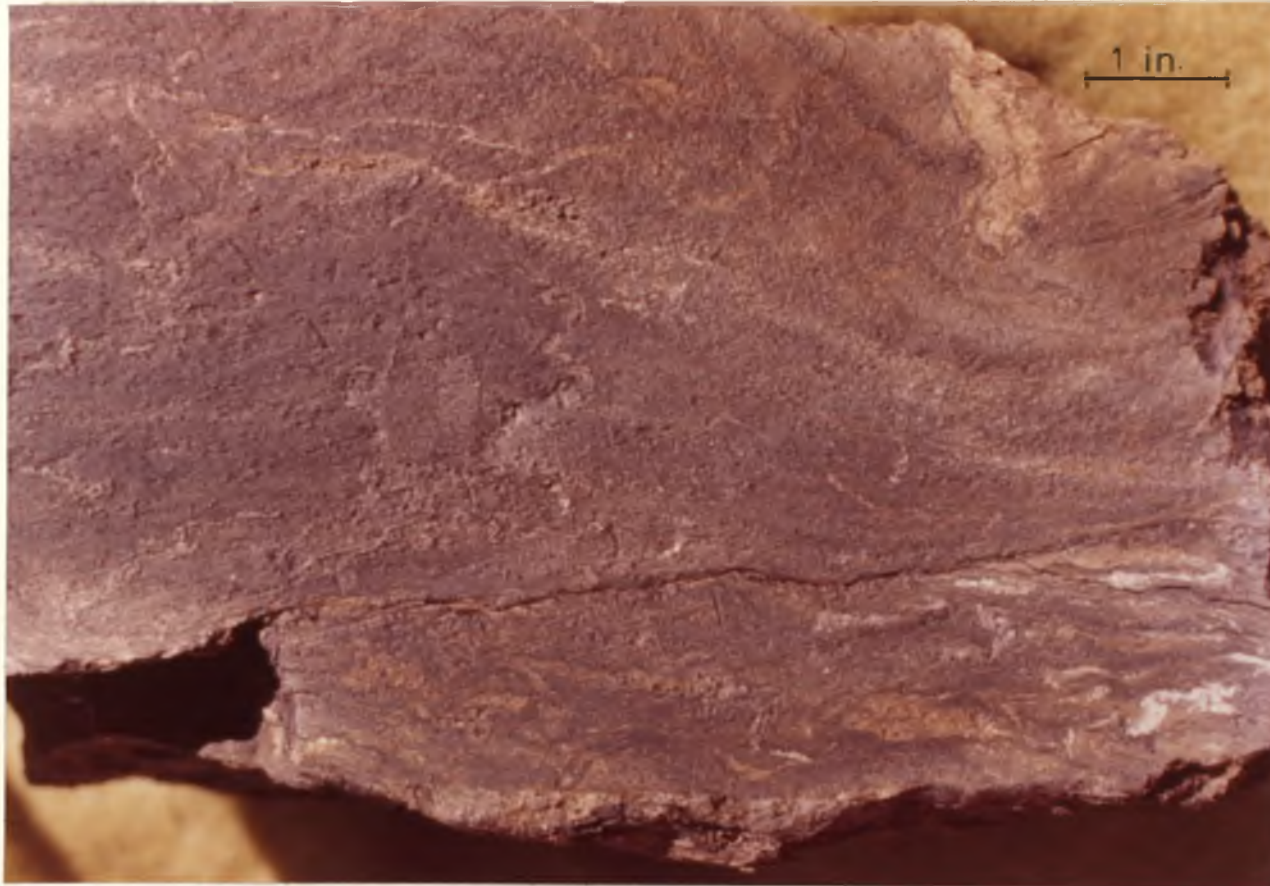


Figure 5. Fault gouge

tested shear strength of the fault gouge in the Tripp Pit was slightly higher than the back-calculated strength from the actual failures.

### Tripp Pit Fault Gouge Testing

Obtaining large samples from the controlling faults in the Tripp Pit was impossible. Only a very limited amount of core was available, which had badly deteriorated after sitting for seven years in core boxes. Instead, a 5-foot-thick fault zone on the northeast side of the pit rim about 200 feet from the old Tripp skip was sampled. This fault parallels the Morris fault and can be considered a part of the Morris system. The surrounding rocks and the physical appearance of the fault gouge were identical to those in the core from the major slide-controlling faults. Details of the sample preparation and direct shear testing can be found in Appendix A. The tests were run in a Soiltest small direct shear machine. Each test yielded the peak and residual shear strength for one normal stress. For several of the samples, it was found that additional data on the residual strength could be obtained by increasing the normal pressure after the first residual strength was reached. Figure 6 shows the results of some direct shear tests. The complete test data are included in Appendix A.

The results of all the tests can be analyzed by plotting the normal stress versus the shearing stress as was done in Figure 7. As can be seen, the peak strength of the gouge was roughly twice the residual strength. Using Coulomb failure criteria to evaluate the data, a linear regression on the peak and residual shear strengths yielded the results shown in Table 6.

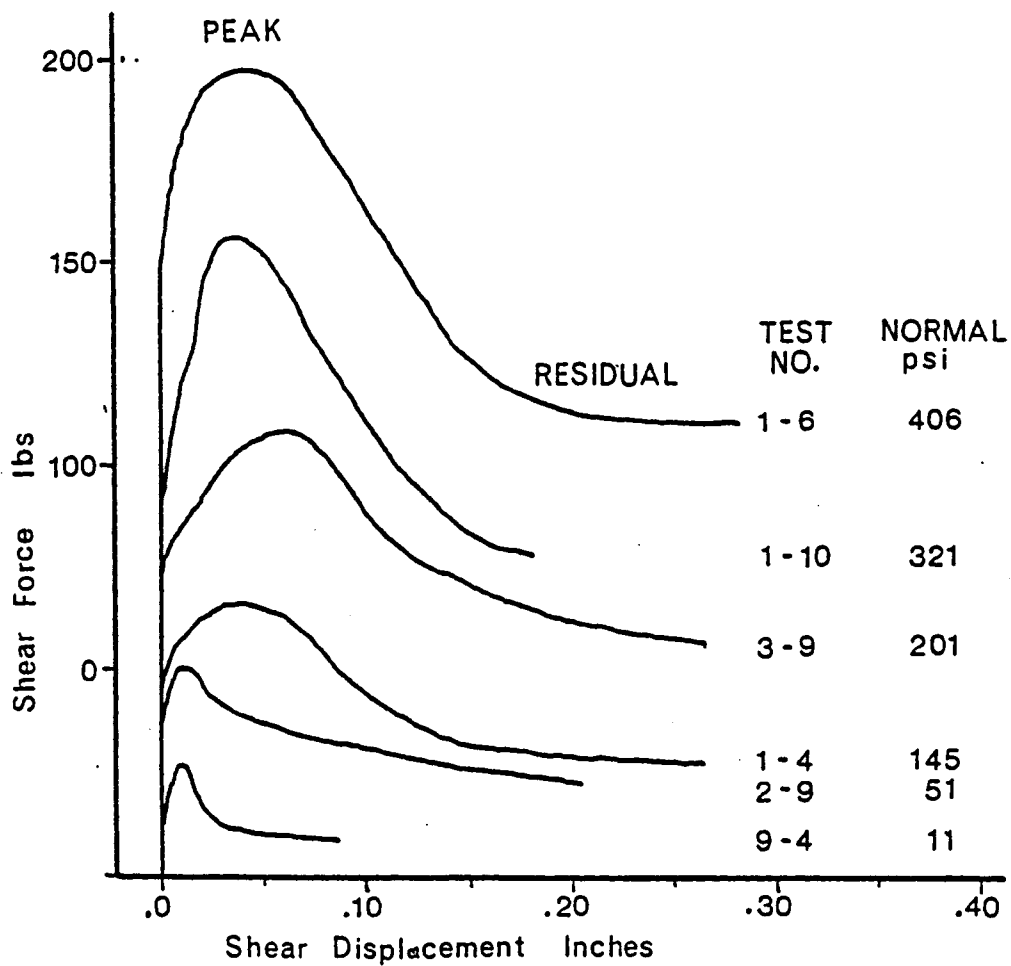


Figure 6. Representative results of direct shear tests

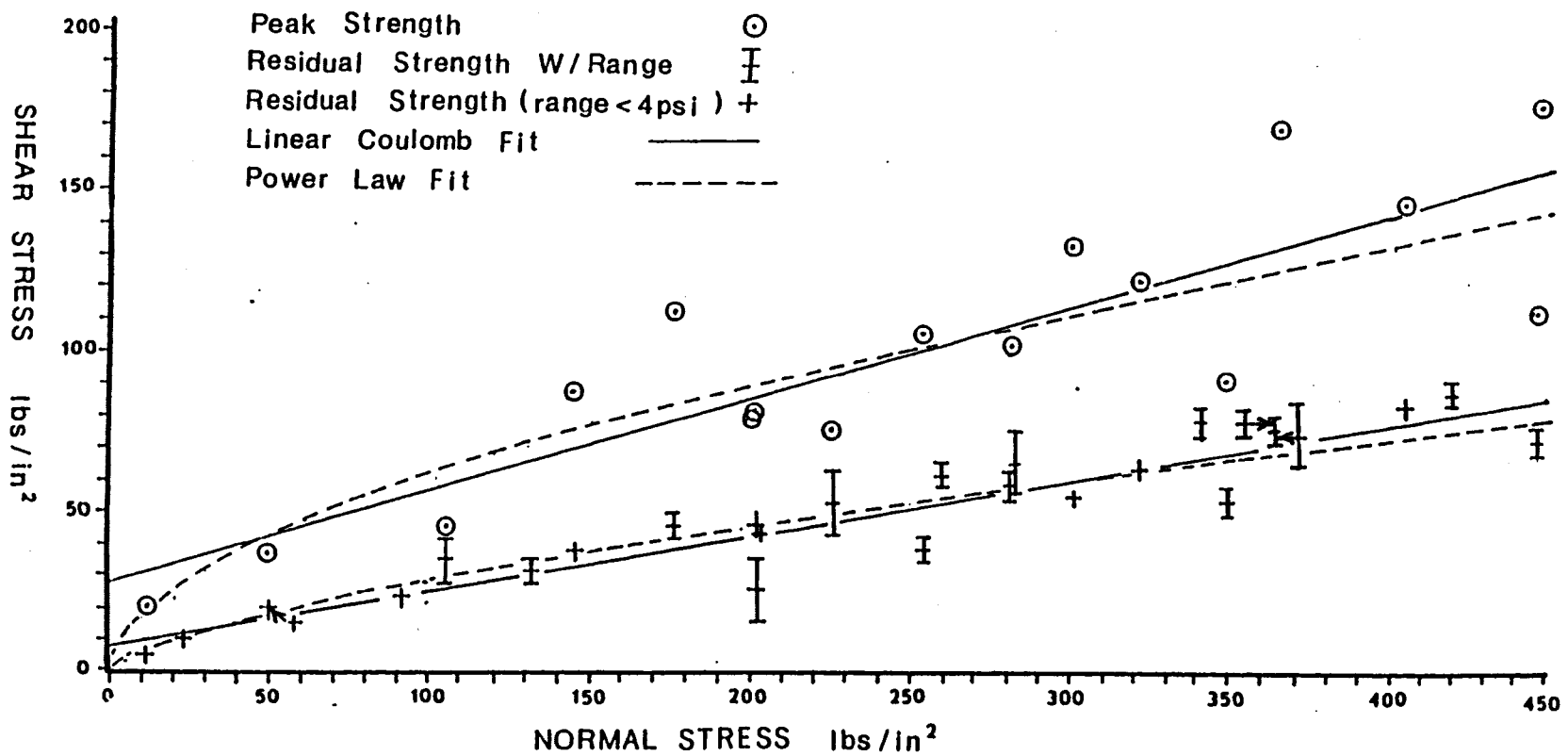


Figure 7. Tested and predicted strengths of Tripp fault gouge

Table 6. Coulomb's law fit of gouge strength data

	Cohesion, psi		Friction Angle (degrees)		Correlation Coefficient r	Number of Data Points
	$\bar{x}$	s	$\bar{x}$	s		
Peak	27.9	12.2	15.8	2.3	0.86	17
Residual	8.7	3.2	9.6	0.7	0.95	27

Coulomb failure criteria may not be the best way to represent the shear strength of the gouge. Jaeger (1971) noted that the power law tends to fit data that turn down at the lower normal stresses. As can be seen in Table 7, the power equation does fit the data slightly better than a linear equation.

Table 7. Power law fit of the gouge strength data,  $\tau = F \sigma_n^f$ 

	F	f	$\tau$	Number of Data
Peak	4.70	0.556	0.93	17
Residual	1.13	0.694	0.97	27

The strength predicted from both the linear Coulomb analysis and the power law analysis is plotted on Figure 7. Except for the peak strength, the power law does not fit the data significantly better than the Coulomb analysis.

The question arises as to which strength, the peak or the residual, represents the actual strength of the controlling faults in the Tripp Pit. The back-calculated strength will be discussed later in detail, but it will be sufficient here to mention that these strengths compare closely with the residual strength.

The major problem in performing direct shear tests on high clay material, like the Tripp fault gouge, is in the nature of the material itself. The two properties that could not be adequately dealt with were the moisture content of the sample and its plastic behavior.

Even though the tests were run with the shear box filled with water, very little of this water entered the sample. The estimated permeability of the gouge is roughly 0.0015 in./hr (Sultan, 1977). Because of this, below 150-200 psi normal pressure, the tests were essentially run at less than full saturation. Above 200 psi, the samples were observed to sweat water, indicating that they were behaving as a saturated clay. The tests were run at very low strain rates (0.8 in./hr) to allow the water contained in the sample to escape. A single test took from 0.5-1 hr to run from the time of initial loading to the time when a distinguishable residual strength was reached. The degree of saturation could be one explanation for the slightly higher friction angles at the lower normal stresses.

When the samples were prepared, their cross-sectional area perpendicular to the normal load was 1.3 in.<sup>2</sup>. At the end of these tests, and especially for the higher normal stress tests (greater than 200 psi), the samples were observed to have swelled laterally. Evaluating the effect of this plastic flow is difficult. Ideally, 20 percent swelling would

decrease the area in contact and increase the normal stress. On several of the stress-strain curves, the residual strength was difficult to determine (Fig. 6, tests 3-9 at 201 psi) because it tended to require a continuous decrease in shearing force as the test progressed. One possible explanation of this is that the swelling was increasing the bearing area faster than the shearing was decreasing it, thus causing the normal stress to decrease along with the stress required to shear the sample.

There was also a great deal of variability between the gouge samples themselves. In one sample, an unusually long core was first sheared, then slid up 0.3 in., then sheared again. The first test had a normal stress of 350 psi, a peak strength of 120 psi, and a residual strength of 70 psi. The second test had a lower normal stress of 283 psi, a higher peak strength of 135 psi and a higher residual strength of 80 psi (tests 6-9 and 7-9A, respectively). An attempt was made to correlate the downward slope of the residual shear strength with the normal stress. If it was due to the plastic swelling of the gouge at higher normal stresses, the residual shear strength should decrease at a more rapid rate. No correlation could be found probably because of a high degree of variability in the plasticity of the test samples.

Some other properties of the gouge that could be useful if this material was eventually to be compared to other gouges is its water content and its Atterberg plasticity index (Lambe and Whitman, 1969; Krynine and Judd, 1957). Three samples heated at 140°F for 24 hr yield 21.6 to 31.5 percent by weight water with an average of 25.8 percent. The results from the Atterberg test are presented in Table 8. The

extremely low value from Sample 3 (Table 8) is another indication of the variability within the gouge itself.

A high montmorillonite clay gouge would be expected to swell. Between the depth of 100 feet and the center of the pit at 600 feet, the swelling pressure should be less than the pressure exerted by the weight of the material above the gouge. Krynine and Judd (1957) mention swelling pressures as high as 147 psi. Brekke and Selmer-Olsen (1965) investigated the properties of montmorillonite-carrying joints and faults. Using their charts for swelling pressure versus allowed swelling, a maximum expansion pressure for the Tripp Pit gouge was estimated at 71 psi. The results obtained from the gouge direct shear testing should contain this effect; that is, when calculating whether a slope will be stable using a limiting equilibrium analysis, this swell pressure should not have to be subtracted from the normal pressure exerted on the controlling fault(s). The reason for this is that above 200 psi normal stress, the test samples are believed to have been saturated (sweating off water). Thus the swell pressure within the test specimen would have been acting against the normal stress being applied to the sample.

Table 8. Atterberg test of fault gouge

Sample	Liquid Limits % H <sub>2</sub> O	Plastic Limits % H <sub>2</sub> O	Plasticity Index
1	70.1	64.8	14.3
2	77.7	66.9	10.8
3	61.8	58.2	3.6
Average	72.9	63.3	9.6

## GROUND-WATER HYDROLOGY

The importance of the water conditions that exist behind the pit slope cannot be overstated. For frictional sliding, the water pressure in a joint or fault zone will act directly against the normal forces on that joint (Hoek and Bray, 1977), thus directly decreasing the frictional force. For the Coulomb failure equation with a water pressure of  $u$ , the frictional resisting stress becomes

$$\tau = C + (\sigma_n - u) \tan \phi$$

Similar changes can be made in the power equation.

### Source of Water for the Tripp Area

Before discussing the actual or suspected ground-water conditions in the Tripp area, the source of the water should be reviewed. There are no lakes or ponds in the immediate area, and a wash north of the Tripp Pit was not observed to have held water during my three years at the mine. The main source of the ground water for the area must be rainfall. The average rainfall measured at the town of Ruth, 1 mile away, over the last 20 years has been 11.85 in./yr, with a standard deviation of 3.4 in./yr. This figure is useful, but of greater importance is the maximum inflow during a short period of time.

During the month of May 1977, 3.87 in. of moisture fell. At the end of this wet period, the usually dry bottom of the Tripp Pit, which is at an elevation of 6,670 feet, has a small, 5-foot-deep lake in it. For slope stability considerations, the maximum expected water pressure is

more important than the average pressure. Reviewing the rainfall record revealed that this event had occurred during the following periods: March 1958 (3.07 in.), June 1963 (4.94 in.), April 1967 (3.75 in.), February 1969 (3.95 in.), May 1971 (3.33 in.), June 1967 (4.43 in.), and May 1977 (3.87 in.). Thus over the last 20 years there were seven large influxes of water over comparatively short periods. In other terms, if a future mine was to last 5 years, there would be an 88 percent probability that a large influx of water greater than 3 inches in one month would occur.

For the poorly drained north side of the Tripp Pit, the maximum amount of water over a period of a year may also be important. During 1969, 16.35 inches of precipitation were recorded. Then in 1970 the largest of the north-wall slides became noticeably active (Dimock, 1970). Although many other factors, such as mining activity around the toe of the slide, may have been the main cause for this failure's occurring at this time, the large amount of precipitation the previous year cannot be ignored.

There are not enough snowpack data for the Tripp area to evaluate the combined effect of snowpack melting with a large amount of rainfall in the month of May. For some unknown reason, this combination of a wet winter and a very wet May has not occurred in any other of the 50 years of records reviewed. The closest case was in 1967 when from December 1966 to April 1967 8.64 inches of precipitation fell and May 1967 had 1.41 inches of rain.

For the more critical north-side area of the Tripp Pit, the surface area of the basin above the Northeast Tripp slide is  $1.2 \times 10^6 \text{ ft}^2$ .

(27.6 acre-ft). A wet May could generate 35 million gallons of water in this area, only part of which could be drained off in a short period of time.

#### Ground Water in the Tripp Pit Area

The region south of the footwall fault is composed mainly of high permeability rocks (sandstones, limestones). In addition, these rocks are highly jointed and faulted. The water table is usually below the bottom of the Tripp Pit, which is at an elevation of 6,670 feet. The nearby Veteran Pit, 1,000 feet to the west, has a small lake in it at an elevation of 6,600 feet. The water table below the bottom of the Tripp Pit can therefore be estimated at 6,600 feet elevation. After the high amount of precipitation during the month of May 1977, the bottom of the Tripp Pit filled with 5 feet of water, which remained for approximately one month. Thus the estimated maximum elevation for the water table at the bottom of the pit would be 6,675 feet.

North of the Footwall fault, a totally different ground-water environment exists. The rocks change abruptly to low permeability shales or hornfels in which water must flow across the bedding. In addition, the basement rock below the Kimberly, Pilot Knob, and Morris faults is a monzonite porphyry, which can be expected to have a low permeability. The water level in three cased drill holes in this area was measured in July 1977. Two of the holes, which were approximately 1,200 feet northeast of the center of the Tripp Pit, had water at an elevation of 6,930 and 6,954 feet. The third hole, 1,550 feet northeast of the center of the pit, had water at an elevation of 7,078 feet (Fig. 8, in

pocket). The water was measured in these three holes after a period of high water influx, thus it should be an estimate close to the maximum height of the water table for the region. The projected water table on the north side is shown on the cross sections in Figure 9 (in pocket). The water table is perched above the basement monzonite and the low-permeable, clay-filled fault zones, with the only drainage across the bedding in the low permeable shales and hornfels.

This assumption of low permeability for the north side is supported by data from two premining churn drill holes in which the water level was recorded (Fig. 8). Both holes indicate that the water table was higher in July 1977 than it was before mining began in the area.

An interesting historical note should be mentioned before ending this chapter. The large 33-million-ton Northeast Tripp slide (NETS) had the pit repair shops above it (Fig. 8). These shops included a wash rack for cleaning the pit trucks. The waste water from the wash rack was conveniently disposed of by dumping it down one of the tension cracks that had developed behind the slide (Smith, 1977). The shops were abandoned in 1970 when movement from the slide made them unsafe.

## SLIDE MORPHOLOGY, MOVEMENT, AND MECHANICS

This section will take the information discussed in the previous sections and add to this observed evidence on the morphology and available evidence of the failure movements. Then all these data will be used to give some insight into the mechanics of the slope failures in the Tripp Pit. The word "mechanics" is used here to mean how the failures developed into the type of slide observed in the pit today.

### Morphology of the Tripp Pit and Slide Locations

The Tripp Pit is approximately 2,500 feet long, 1,600 feet wide and has its long axis oriented northwest-southeast. The elevation of the pit rim averages around 7,240 feet but ranges from a low of 6,920 feet at the saddle separating the Tripp from the Veteran Pit on the northwest to a high of 7,360 feet on the southwest side. The center of the pit is at an elevation of 6,670 feet, which gives the pit an average depth of 570 feet. Approximately 70 million tons of rock have been removed to create the pit. The topography of the area was used as a base for Figures 3 and 8.

Before discussing each of the slides individually, a brief review of the slides with respect to each other and the Tripp Pit in general will be made. Figure 8 shows the location of the slides. Almost the entire north wall of the pit is involved in some sort of slope failure. These failures have been divided into two main slides: the Northwest Tripp slide (NWTS) on the west and the Northeast Tripp slide (NETS) on the east. The area between the two main slides is a transition zone, which runs

roughly between 95,000 E. and 94,700 E. One small slide, the Morris, exists on the extreme eastern end of the north side. It was the Morris failure that finally forced the mining in the Tripp Pit to be abandoned.

The eastern corner of the pit has been backfilled and has no failures in it. The south side has two distinguishable failures. On the far eastern side just before the backfilled material is the Richards slide, and on the western portion of the south side is the Southwest Tripp slide (SWTS), which has involved about 800 feet of the pit rim. Between these two slides is a relatively stable section of pit wall that has a few small (less than 50,000 tons) failures, which involve only a few benches. Table 9 lists the important features of each of the main identifiable failures, and the failures are shown on Figure 2.

### Northwest Tripp Slide

#### Morphology

The Northwest Tripp slide has involved approximately 800 feet of the pit rim. Above the saddle going to the Veteran Pit, the slide has a vertical relief of 370 feet and a little further to the east above the main Tripp Pit, the vertical relief increases to 580 feet. Tension cracks can be found 450 feet behind the pit rim.

The failure can be subdivided into two parts. Above the saddle failure has not totally developed and much of the pit wall is intact. Just east of this, where the vertical relief is greatest, the failure is now a rubble slope standing at 29 degrees. The difference in the current physical nature of the two parts is believed to be a function of the vertical relief.

Table 9. Features of the Tripp failures

Failure	Controlling Structure	General Type of Failure	Size (tons)	Present Form of Failure	Present Angle of Pit Slope (degrees)
NWTS	Pilot Knob and Footwall	Wedge and complex	$4.0 \times 10^6$	Partially intact wedge and rubble slope	30
Transition Zone	Footwall and Kimberly	Wedge and complex	2.0	Rubble slope	29
NETS	Kimberly and Morris	Wedge	33.0	Intact wedge	
Morris	Morris and Footwall	Wedge	0.35	Intact wedge	32
Richards	Fault and joint	Wedge	0.40	Rubble slope	22
SWTS	Soil type?	Circular	2.5	Shallow rubble slope	36

### Structure and Rocks

Identifying the geologic structure controlling this slide is difficult because of a general lack of drill-hole information. All drilling was confined to the ore zone south of the Footwall fault. From the surface cracks and old surface mapping (Fig. 3), a wedge-type geometry is indicated. A straight-line projection of the Pilot Knob and Footwall fault system (as was done in Figure 4) from where the faults are better delineated does not yield a satisfactory wedge geometry that would account for the failure. To explain the slide, one or both of the faults would have to flatten out. The angle from the tension crack furthest from the rim to the center of the pit where mining ceased is 26 degrees. This angle is probably close to that of the plunge of the intersection of the controlling faults.

The material involved in the slide consists of calc-silicate skarns, altered porphyry, and some sulfide skarns. Above the 7,000-foot elevation, the rock becomes increasingly oxidized and weathered. Below the Pilot Knob fault is marble and at depth monzonite porphyry. On the surface, old geologic mapping showed shale below the Footwall fault. This information is strengthened by the fact that one large zone within the rubble slope on the far eastern portion of the slide consists of rubbleized shale and hornfels (Fig. 3). Somewhere around the 6,900-foot elevation monzonite porphyry underlies the Footwall fault.

### Movement

This section of the Tripp Pit has exhibited slope instability since open-pit mining first began in the area. Two areal photographs,

one taken for Kennecott in 1955 and the other in 1966, show slides similar to the NWTS and in the same relative position. A 1970 mine map of the pit topography shows the eastern portion of the present slide fully developed as it is today. Since 1970 most of the movement within this part of the failure has apparently been the rubble slope itself and has not involved any new material.

The western portion above the saddle is a different story. Just before mining was abandoned, the saddle was deepened by 80 feet. Comparing the 1971 and current topography reveals that most of this part of the failure has developed since 1971 and the deepening of the saddle. The movement includes the development of tension cracks behind the pit rim. These cracks generally parallel the Footwall and Pilot Knob faults (Fig. 8). On the main crack furthest to the north, the pit side has dropped 25 feet. Comparing 1970 and 1975 topography contours indicates that the pit face here has moved out and to the south between 20 and 35 feet. The saddle at the toe of the failure shows signs of being under compression. For a flat area 60 feet north of the saddle has been "bulldozed" 40 feet to the south by the pressure exerted by the slide.

### Slide Mechanics

By comparing the two parts of the NWTS, a model for the development of this slide can be made. The western portion was stable until the saddle was deepened, increasing the vertical relief to 440 feet. At this depth the controlling structure was close enough to being daylighted that the slope began to fail and move toward the pit on this structure. This movement caused the crest to develop tension cracks and

drop 25-40 feet, the pit face to be pushed out, and the toe area of the slide to be "bulldozed" similar to toe heave. The material within the slide at this stage has begun to rubbleize but is still in its approximate relative position before the failure began.

Both the Footwall and Pilot Knob are part of fault systems with many parallel faults and joints. As mining progressed below a 440-foot vertical relief, so did the extent of the failure. The main change in the nature of the slide during this second phase is its gradually beginning to resemble a circular-type soil failure rather than a structurally controlled wedge failure. Further movement appears to cause the sliding wedge to break up. This is shown by either toppling or sloughing of the pit rim and continued downdropping of the material behind the rim. The pit face has become so raveled that the mining benches can no longer be identified. Figure 10 illustrates the development of the NWTS.

#### Effective Rock Mass Strength

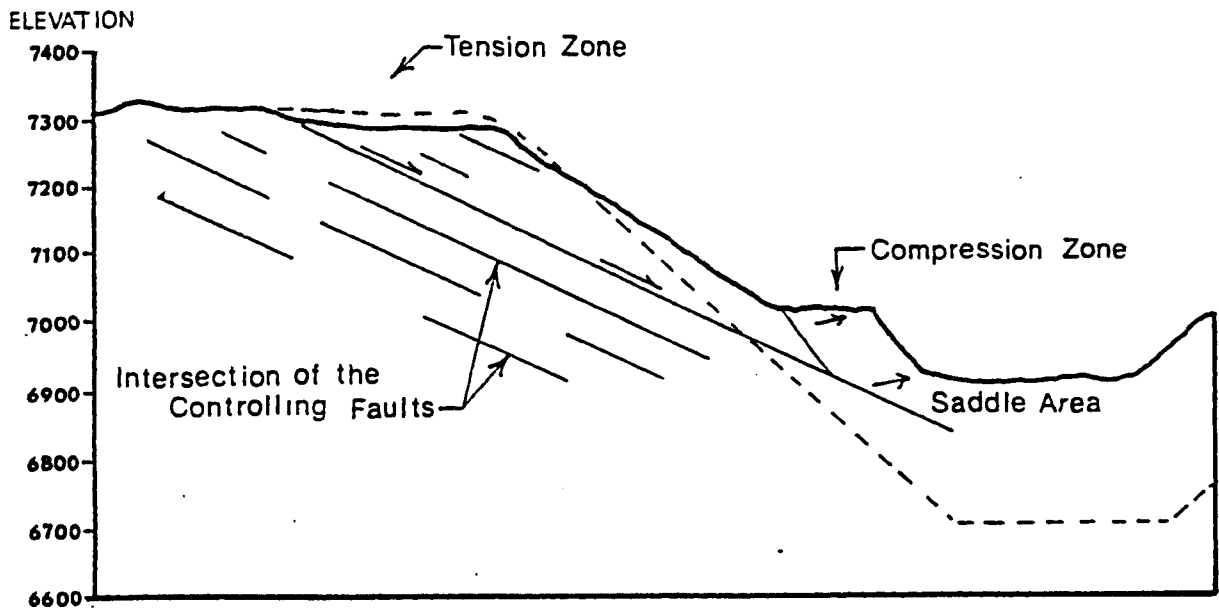
Unfortunately, there is not enough structural data to adequately delineate the position of the two controlling faults. Because of this, back-calculating the shear strength of the failure surface by using a limiting equilibrium analysis is not possible.

#### Transition Zone

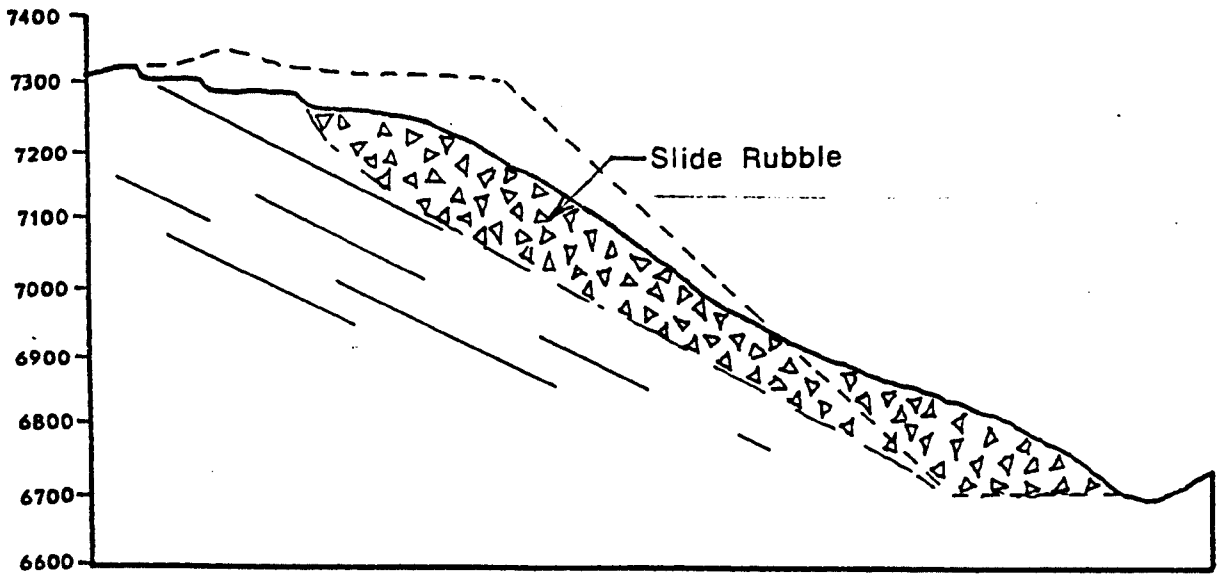
#### Morphology

The transition zone is the region between the Northwest Tripp slide and the Northeast Tripp slide. Approximately 600 feet of the pit rim falls into this zone. The crest of the pit here lies at an elevation of

INITIAL STAGE , 400 ft VERTICAL RELIEF



SECOND STAGE , 600 ft VERTICAL RELIEF



CROSS SECTIONS LOOKING EAST , SCALE 1 in. = 300 ft

Figure 10. Schematic cross section of the Northwest Tripp slide illustrating slide development

7,280 feet and the pit center at 6,670 feet, making the vertical relief 610 feet. The pit slope in this zone ranges from a high of 35 degree on the eastern end to a low of 22 degrees for the center area.

### Structure and Rocks

Three major faults (the Pilot Knob, Footwall, and Kimberly) and their related systems exist in this zone. The region between the Pilot Knob and Kimberly faults can be expected to have many parallel smaller faults and joints that would behave like the large faults. The Footwall fault structure here consists of the main fault plus all the discontinuities related to the bedding and bedding-plane faults.

The intersection of the Pilot Knob and Footwall fault systems would be the same as already discussed for the NWTS. The intersection of the Footwall and Kimberly faults plunges approximately S. 15° E. at 32°.

On the south side of the Kimberly fault are two types of rock. Above the 6,900 elevation are mainly shales with a strike and dip parallel to the Footwall system and below this depth is monzonite porphyry. On the pit face the slide material appears to be mainly marble or calc-silicate skarns with varying degrees of oxidization and weathering (Fig. 3), but underlying this surface rubble there may be mostly shale. One pressure ridge resulting from differential movement within the rubble in this zone has pushed up a finely rubbleized (1-6 in.) shale, supporting the conclusion that shale underlies most of the rubble.

### Slide Movement

The transition zone contains remnants of slides, which resembled the NWTS in 1955 and 1966. These remnants are now the very low angle rubble material just west of 95,000 E. Since 1970, the movement here has been a further sloughing of the rubble material itself. It appears that very little new rock has been incorporated into the slide. The toe has been pushed 70 to 90 feet into the pit, while the crest and upper slope appear to have dropped vertically (Fig. 8).

Just west of 95,000 E. is a different story. In this area of the slide it appears that a considerable amount of new material mainly from the upper portions of the pit has been incorporated (Fig. 8). Along the rim one large block has moved as much as 120 feet toward the pit. Similar displacement can be found in the toe of the transition zone.

### Slide Mechanics

In this zone there is a transition from the NWTS mechanics to a new type of wedge failure caused by the Footwall, Kimberly, and Morris fault systems. The remnant of the NWTS is now a rubble zone that can be expected to behave like a circular failure. The weakest material in this slide is a shale, which may underlie the area. The very low angle of repose ( $22^{\circ}$ ) for this rubble material tends to support this.

The area just west of 95,000 E., which has been very active in the last 7 years, has a very complex failure mechanism. The two block diagrams in Figure 11 illustrate two possible mechanisms.

Mechanism A is the intersection of the Kimberly fault and the Footwall fault system, which plunges S.  $15^{\circ}$  E. at  $32^{\circ}$  but does not

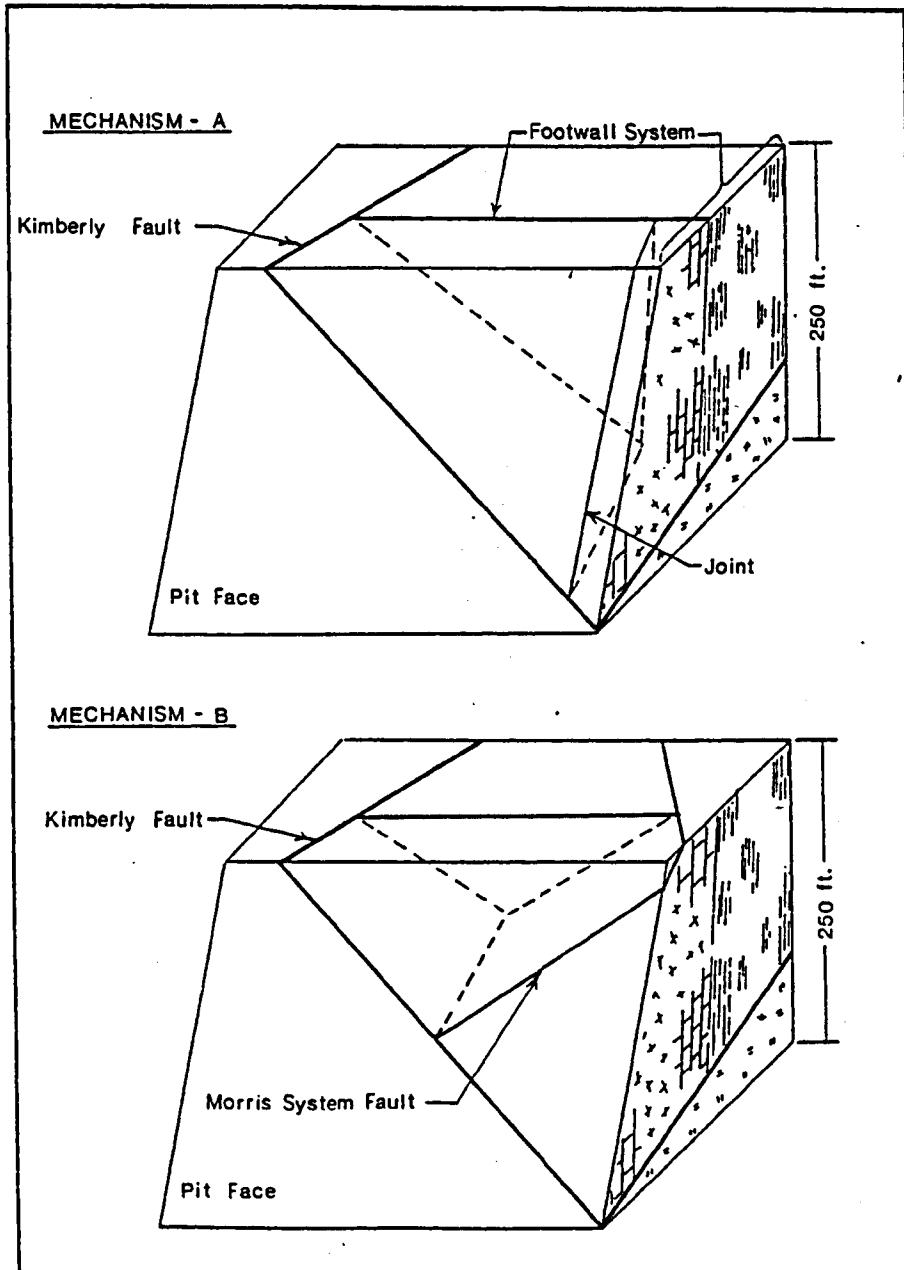


Figure 11. Block diagrams showing possible failure mechanisms for the transition zone.

intersect the pit face. To fail, one of the many steeply dipping, northeast-striking joint sets needs to be included in the mechanics. In the Tripp Pit the failure that is believed to be caused by this mechanism resembles a toppling failure. As the block started to move a graben formed behind it on the footwall system. This graben, acting as a nearly vertical, gravity-driven wedge, would force the upper portion of the block to move faster than the lower portion. Another explanation could be that as the block moved past the pit face its leading edge became supported by only the rubble material already on the face. The tension caused by this broke off the leading edge, which was rotated forward by additional rubbleized rock falling in behind the break. This is similar to the overturning failure of a retaining wall.

Mechanism B is a wedge-type failure caused by the intersection of the Kimberly fault and one of the parallel faults in the Morris fault system. One of these parallel faults was mapped in the area (Fig. 3). The intersection of the mapped Morris fault system and the Kimberly fault plunges into the pit at  $17^{\circ}$ , S.  $40^{\circ}$ W. This combined with a low friction angle for the two faults (around  $10^{\circ}$ ) caused the wedge to slide into the pit.

#### Effective Rock Mass Strength

A Hoek wedge failure analysis was run on both mechanisms illustrated in Figure 11. For mechanism A the input data were:

1. Plane A (Kimberly fault): strike, N.  $70^{\circ}$ E.; dip,  $33^{\circ}$ SE; friction angle,  $12.7^{\circ}$ ; cohesion, zero.

2. Plane B (joint in limestone): strike, N. 10° E., dip, 60° NW.; friction angle, 28°; cohesion, 1,000 lb/ft<sup>2</sup>.
3. Tension crack: 250 ft behind rim; strike N. 40° W.; dip, 70° SW.
4. Pit face: strike, N. 50° W.; dip, 40° SW.
5. Wedge above water table: rock density, 160 lb/ft<sup>3</sup>.
6. Other external forces: none.
7. Vertical relief: 225 ft.

This analysis yielded a safety factor of 1.00.

For Mechanism B the input data were:

1. Plane A (Kimberly fault): strike, N. 70° E.; dip, 33° SE.; friction angle, 12.7°; cohesion, 150 lb/ft<sup>2</sup>.
2. Plane B (Morris fault system): strike, N. 05° E.; dip, 25° NW; friction angle, 12.7°; cohesion, 150 lb/ft<sup>2</sup>.
3. Tension crack: 250 ft behind rim; strike, N. 40° W.; dip, 70° SW.
4. Pit face: strike, N. 50° W.; dip, 40° SW.
5. Wedge above water table: rock density, 160 lb/ft<sup>3</sup>.
6. Other external forces: none.
7. Vertical relief: 225 ft.

This analysis yielded a safety factor of 0.92. Thus both proposed failure mechanisms yielded a safety factor of one or less and are therefore valid mechanisms.

#### Northeast Tripp Slide

The Northeast Tripp slide (NETS) failure is one of the most interesting in the pit. Its shear size, 33 million tons, makes it one of the largest slope failures attributable to open-pit mining. The NETS has

been and will be a major consideration in evaluating future mining in the Tripp Pit.

When in 1970 the extent of the failure was recognized, four diamond drill holes were placed to obtain more information about the controlling faults under the slide. These data and data from 22 older churn drill holes, underground geologic mapping of the Morris workings, which lie at the toe of the failure, and some recent surface geologic mapping have made it possible to make a fairly accurate determination of the geologic structure controlling the failure. In addition, fault gouge testing was done specifically to yield strength data relevant to the NETS.

During the failure's most active period (first half of 1970), the Bureau of Mines initiated a microseismic investigation (Merrill and Stateham, 1970). The highest seismic noise rate was recorded in April 1970, which corresponded to the failure's highest velocity. After May 1970, both the noise rate and the velocity decreased rapidly (Fig. 12).

The overall movement of the NETS and the differential movement within the slide can be better understood than movement in other failures in the Tripp Pit because a survey net consisting of 27 stations was established. These points were monitored bimonthly from February 1970 to February 1971 during the slide's most active period. For my study, the survey net was resurveyed in July 1977 and the total movement to date determined. The data have been presented in vector form on Figure 3 for the first year (February 1970 to February 1971) and on Figure 8 for the accumulated movement to date (February 1970 to July 1977).

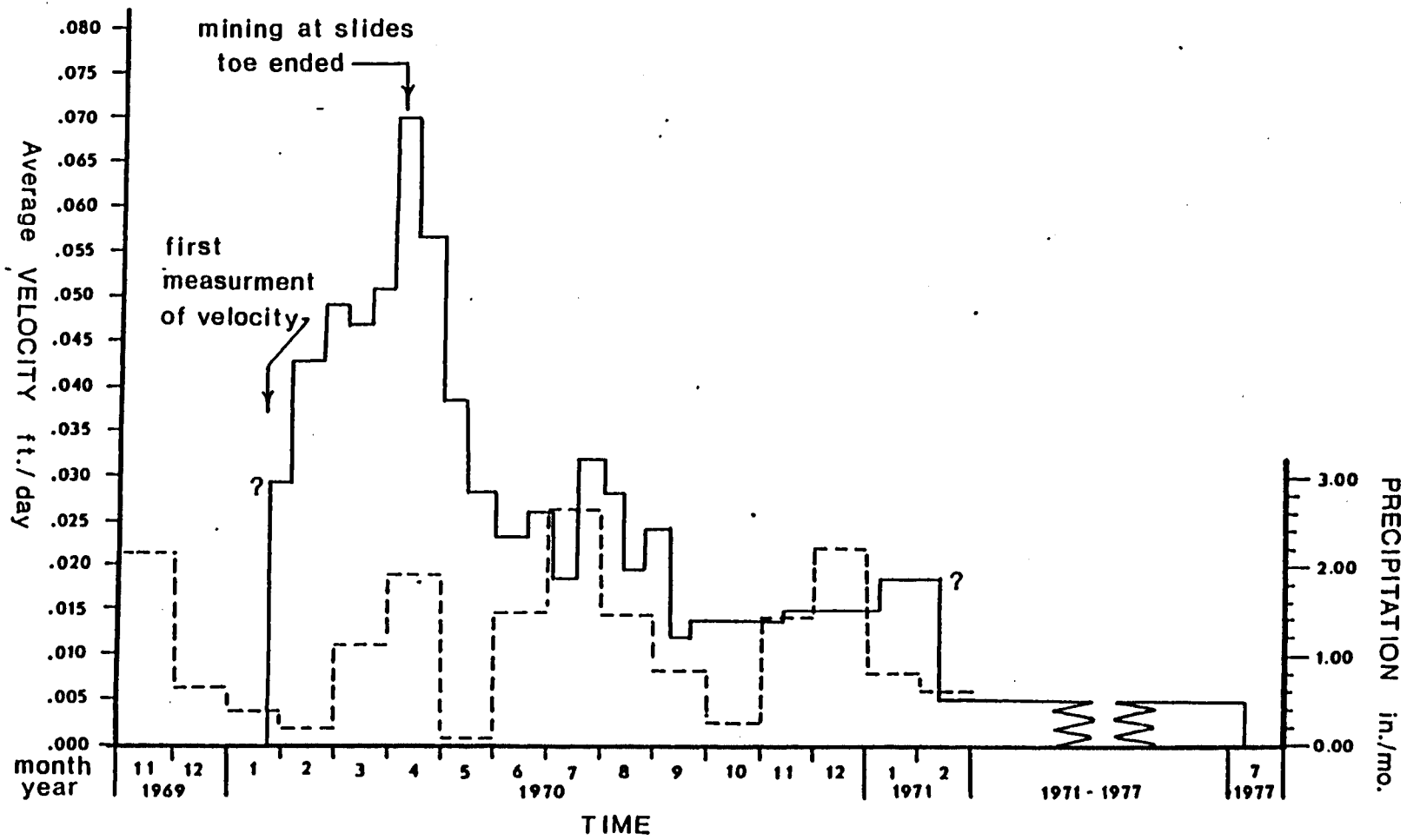


Figure 12. Precipitation and wedge velocity of the Northeast Tripp slide over time

### Morphology

The NETS is still basically intact and only the northwestern portion of the pit rim has begun to rubbleize. This section has been included in the transition zone, and the rubble material in the transition zone has an angle of repose between 27 and 35 degrees. The southeastern portion of the pit face in front of the slide shows only a few signs that it has been involved in a major failure. The mining benches show the effects of weathering but are basically intact. If it was not for the four survey monitoring stations along this section of the pit face, it would be hard to prove by morphological evidence that the entire face has moved an estimated 28 feet toward the pit.

The failure has involved approximately 1,500 feet of the pit rim. The rim ranges in elevation from 7,280 to 7,180 feet. The vertical relief in front of the slide averages 550 feet. Behind the rim two main tension zones have developed. The first, 600 feet behind the rim, has resulted in the formation of a graben, which is 25 feet wide and 8 feet deep. The second major crack is 1,000 feet behind the rim. The tension cracks and zones strike N. 40-45° W., which is the same strike as that of the Footwall structure throughout the area.

The southeastern side of the failure has developed a large scarp created by the slide's 28 feet of displacement. This crack, which is comparable to a left-lateral strike-slip fault, strikes N. 38° E. and roughly parallels the Morris fault. On the northwestern side of the failure, the strike-slip nature of the movement is masked by 120-foot-thick mine dumps. Here the cracks strike N. 68° E., roughly parallel to the Kimberly fault.

### Structure and Rock Types

The Kimberly and Morris faults are the controlling structures underlying the NETS. Their intersection plunges S.  $48^{\circ}$ W., at  $13^{\circ}$ . It is this shallow intersection that has created the unusually large, 33-million-ton wedge.

The two cross sections shown on Figure 4 illustrate the controlling structure and rock types in the NETS. Almost the entire area is underlain by weakly propylitically altered monzonite porphyry (can be considered "fresh" porphyry). It is this low-permeability rock that is partially responsible for the high perched water table within the slide. All the rocks above the Morris and Kimberly faults can be considered part of the Footwall system. Basically they are interbedded skarns, hornfels, shales, and marbles, which are generally separated by bedding-plane faults that strike N.  $35-45^{\circ}$ W. and dip steeply ( $40^{\circ}$  SW.-vertical). Starting from the toe of the failure, which is also the location of the main Footwall fault, and working back to the northeast into the pit face and failure, the rock types change as follows:

1. Marble and skarns, 200-400 feet thick, locally intruded by small plugs of rhyolite breccias and small dikes of highly altered monzonite porphyry.
2. Chainman Shale, 300 feet thick, generally altered to a hard hornfels.
3. Marble, 0-200 feet thick, with some skarns. These were probably thrust into the center part of the Chainman Shale.
4. Shale, up to 1,000 feet thick, generally fresher than the hornfels on the western side of the marble lens.

Within 100 feet of the surface, all rock types become weathered and oxidized. The surface area is covered by a shallow alluvium or on the northwestern side of the slide by up to 120 feet of mine dumps.

### Slide Movement

The Kimberly repair shops are a striking example of what slide movements can do to structures above them. The concrete floors are extensively cracked with some of the cracks having several feet of both vertical and horizontal displacements. The buildings themselves, being constructed of steel, have not collapsed, but several have walls leaning 15 degrees from the vertical. The shops were abandoned in 1970 because of the movement of the NETS.

Velocities recorded at 13 of the central points of the 27-point survey net established to monitor this slide were averaged for each of the bimonthly period. These data are presented in Figure 12. Based on the changes in velocity, movement of the NETS has been divided into three periods.

The initial period is from January 26, 1970, when the net was established, to April 18, 1970. During this period, and probably for several months before, the failure was accelerating. The average velocity increased from 0.029 ft/day during the period from January 26 to February 9 to the maximum recorded average velocity of 0.070 ft/day during the period between April 4 and April 18. One station recorded a velocity as high as 0.091 ft/day during the latter measuring period. Two historical events, which will be discussed more extensively, happened during this time: the bottom of the pit at the toe of the failure was being

actively mined, and 1.10 inches of precipitation in March and another 1.19 inches in April were added to the spring runoff.

The second period is from April 18, 1970 to February 14, 1971, when the monitoring was abandoned. This was a period of deceleration during which the average velocity dropped as low as 0.012 ft/day. There was no significant mining around the toe during this period, and after October 1970 most mining was done 200 feet northeast of the toe area. The general deceleration had two subperiods marked by a slight acceleration (Fig. 12). Both of these subperiods corresponded roughly to the periods of high precipitation during June and July, 1970 and again in November and December, 1970.

The third period extends from the time when the last measurements were made for the slope stability monitoring program on February 14, 1971 to July 1977, when the survey net was resurveyed for this study. No mining was done in the pit during this period, and the most significant period of rainfall was in May 1977, when 3.87 inches of precipitation fell. The average velocity over this 6.5-year period was 0.005 ft/day. This indicates that the failure had continued to decelerate and may be moving at a much slower velocity today (in the range of 0.0 to 0.002 ft/day).

The total displacement recorded by the survey net averaged 23.2 feet for the 12 central stations with a standard deviation of 2.8 feet. Assuming a constant acceleration and the velocity changed from 0 to 0.028 ft/day over one year, 5 feet of movement can be estimated prior to the establishment of the survey net. This makes the total displacement to date for NETS wedge of the order of 28 feet.

The direction of the movement is also important. To show this, the displacement of each individual station has been reduced to a directional vector with a specified plunge. Vectors for motion during the first two periods (February 1970 to February 1971) are shown on Figure 3, and the ones for the entire period of monitoring through July 1977 are shown on Figure 8. Except for two anomalous vectors, which can be explained by either proximity to the edge of the slide or an unusual tension crack nearby, the directions of the vectors parallel the proposed intersection of the two controlling faults. The increase in the vertical components (the plunge) of the vectors during the third period of movement will be discussed in the section on failure mechanics.

### Effective Rock Mass Strength

Back-calculated Strength. Before the slide mechanics can be investigated, the strengths of the controlling fault zones need to be established. When the failure first began, the forces acting on the wedge changed so that the sliding forces were slightly greater than the forces resisting the sliding. The safety factor changed from greater than one and given the forces resulting from the geometry of the wedge and the water within the failure, the strength of the controlling faults can be back calculated. Such a wedge failure analysis was done on the NETS using the method outlined by Hoek and Bray (1977). Following are the input parameters for that analysis:

1. Plane A (Kimberly fault): strike, N. 69° E.; dip, 33° SE.
2. Plane B (Morris fault): strike, N. 24° E.; dip, 31° NW.
3. Pit face: strike, N. 50° W.; dip, 37° SW.

4. Top of wedge: flat, at 7,200-foot elevation.
5. Toe of wedge: at 6,600-foot elevation.
6. Tension crack: 1,000 feet behind rim; strike, N. 50°W.; dip, 70°SW.
7. Water table: as shown on Figure 9.
8. Rock density: 160 lb/ft<sup>3</sup>.
9. Wedge weight: 33.0 million tons (from planimetry).

Details of this analysis can be found in Appendix B. One way of representing the possible solutions is to assume that the two faults have the same strength. The solutions can be represented by a line on a graph of cohesion vs. friction angle as was done for Figure 13. Thus, if the cohesion was 1,000 lb/ft<sup>2</sup>, the friction angle would be 10.7 degrees; and if the cohesion was zero, the friction angle would be 12.8 degrees.

Another aspect of this wedge failure analysis is how the friction angles of the two faults interrelate. If one plane was tested and found to have a friction angle greater than 12.8 degrees, the other fault plane would have to have a lower friction angle. Goodman (1976) presented a method for determining this by using a stereographic project and the friction circle concept. This can also be determined by assuming equal cohesions in the two fault planes in the Hoek limiting equilibrium analysis. Such an analysis with zero cohesion yields the equation:

$$2.10 \tan \phi_A + 2.28 \tan \phi_B = 1.00$$

From this, if plane A (Kimberly fault) was found to have a friction angle  $\phi_A = 14.5^\circ$ , plane B (Morris fault) would have to have a friction angle of  $11.3^\circ$  to keep the safety factor equal to one. This analysis was

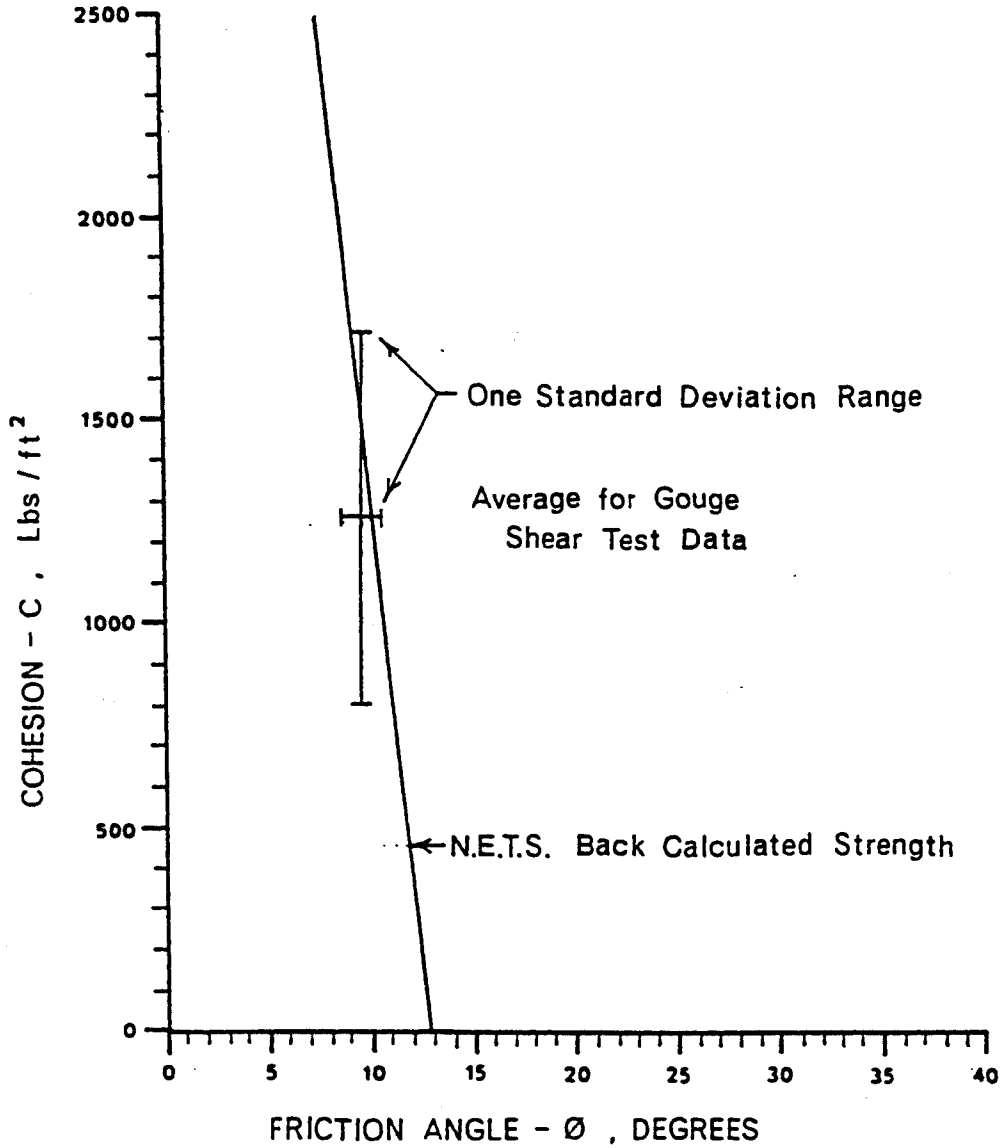


Figure 13. Back-calculated and tested shear strength for the Northeast Tripp slide

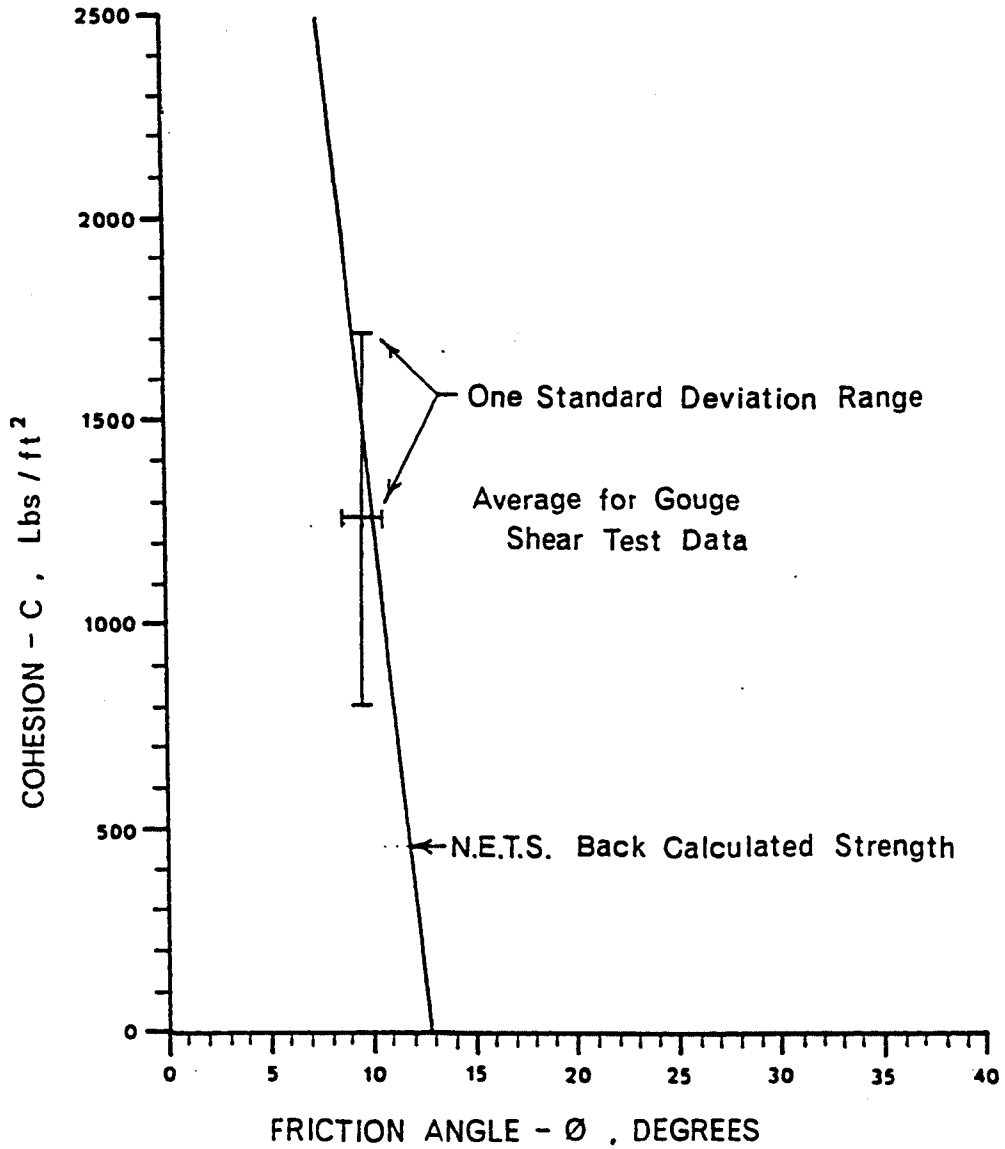


Figure 13. Back-calculated and tested shear strength for the Northeast Tripp slide

repeated for various cohesions between zero and 2,000 lb/ft<sup>2</sup> and the results plotted in Figure 14.

Back-calculated vs. Tested Strength. On Figure 13 both the back-calculated strength (assuming equal friction angles and cohesion for the two controlling faults) and the average strength calculated from the direct shear testing of the clay fault gouge are plotted. As can be seen, both strengths compare very favorably, especially when the standard deviation statistics of the shear data is considered. In addition, the back-calculated strength is very sensitive to the orientations of the two controlling structures. Changes in the strike or dip of either fault could change the back-calculated friction angle. The accuracy of the structural interpretation for the Kimberly and Morris faults is believed to be good but not to within one or two degrees of either strike or dip.

The question arises as to why the tested residual strength of a thick fault zone should be more representative of that zone's effective strength than the tested peak strength of the fault gouge. As shown in Figure 5, the gouge is far from homogeneous. Within the zone there can be expected to be subzones in which the gouge is weaker. This could be where movement last occurred on the fault. For most of the test samples, the peak shear force was roughly twice the residual strength. The exception was sample 2-6 (tested at 227 psi normal pressure, see Appendix A). The peak and residual strengths of this sample were almost equal, suggesting that subzones existed within the tested samples where this was true. Skempton (1964) came to a similar conclusion.

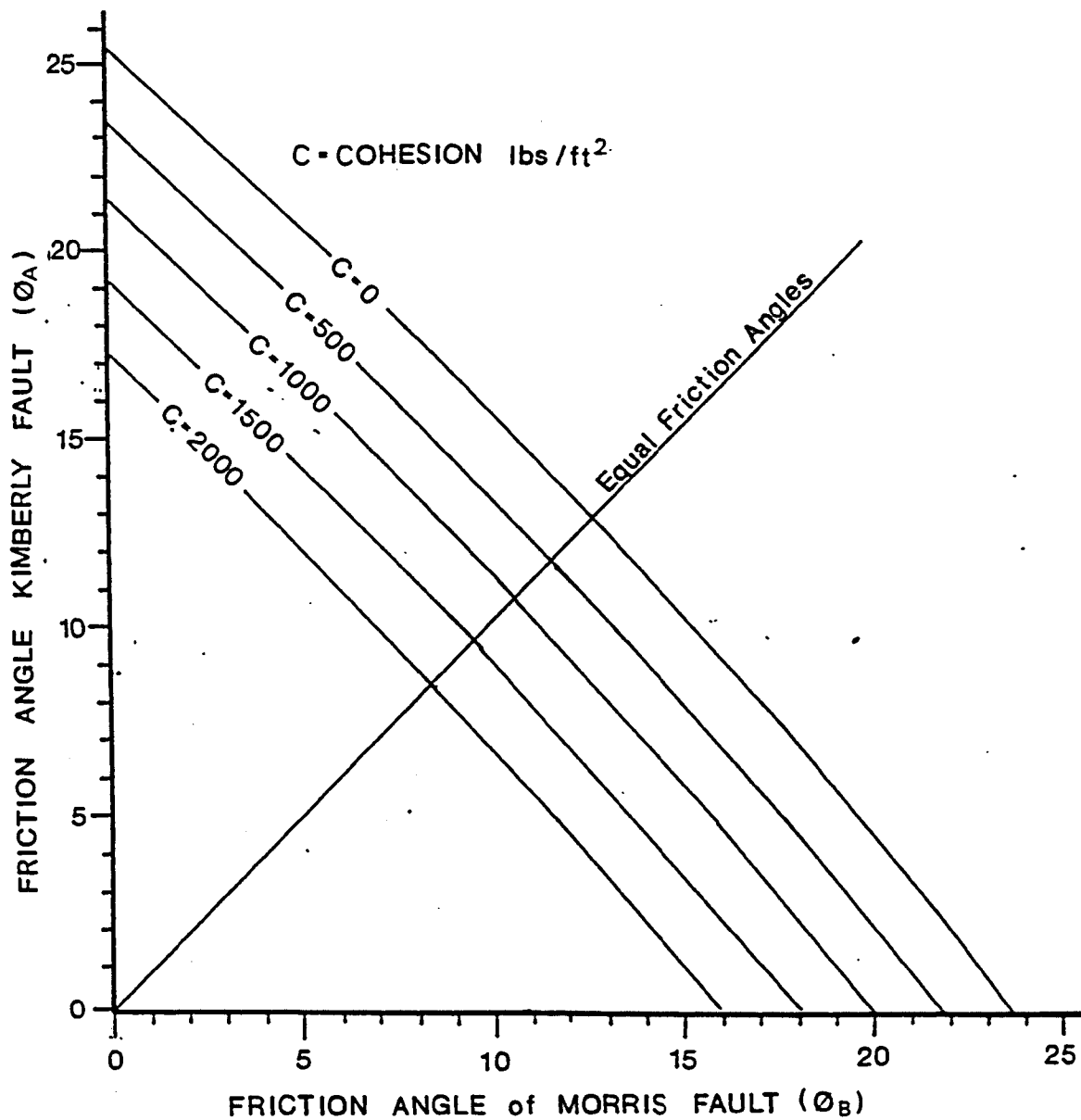


Figure 14. Effective strength of faults controlling the faults for the Northeast Tripp slide

### Slide Mechanics

Although the NETS can be considered an intact wedge, it is actually dissected into many parts, all behaving differently. As can be seen from the vector movements (Figs. 3 and 8) within the wedge there has been noticeable differential movement. In discussing the slide mechanics, first the complete wedge then the mechanics within the failure will be discussed.

The Complete Wedge. The movement of the wedge can be closely correlated with mining activity in the Tripp Pit. The wedge could not fail until mining had deepened the pit to the depth where the controlling structure was almost daylighted. The first movement on the slide appear to have occurred in July 1968 when some cracks were noticed in the concrete foundations of one of the buildings in the Kimberly repair shops (Ko, 1970). At this time, the cracks were attributed to settling. The first significant movement began a year and a half later when "in January 1970 large cracks in the shop floors began to enlarge and it became obvious that the buildings were being pulled apart" (Dimock, 1970, p. 6). By January 1970, mining had deepened the pit to its present depth thus daylighting all except the very toe of the wedge. Without the external forces exerted by the toe constraints, the wedge was at a safety factor less than one.

When the failure began not all of the toe constraint was removed. The effective strength of the remaining constraint may have been partially destroyed by the swelling pressures exerted by the montmorillonite in the controlling faults, thus allowing the failure to begin. When

the rock above such a fault zone is removed so that the normal pressure is less than the swelling pressure of the saturated clay, the clay in the fault zones swells until the pressures are returned to equilibrium (Barton, 1974). In the case of the remaining material in front of the NETS, the swelling may have caused a considerable loss in the effective strength of this buttress. Once the failure started, it accelerated until mid-April 1970. Such an acceleration would be expected if the sliding forces due to gravity are greater than the resisting forces. After April 1970, the motion of the wedge decelerated. The biggest single factor appears to be that mining at the toe of the slide ended in April (Fig. 8). Following this the weight of the toe constraint was increased by rubbleized rock that sloughed onto the toe area from transition zone slides. Only a few thousand tons of this rubble material appear to have brought the wedge back into equilibrium. Another explanation of this rapid deceleration arises from the plastic nature of the gouge. Where exposed by open-pit mining, the gouge could have conceivably started to flow out of the fault zone. This flowage would not have been observable by the engineers at that time due to the fact that most of the slopes were covered by rubble material. This could continue until the sides of the fault zones near the pit face come into contact with each other, which would raise the effective strength of the overall zone. With the apparent slight difference between the resisting forces and the sliding forces, there are many other possibilities for explaining why the slide returned to equilibrium.

Mechanics within the NETS. Different parts within the wedge have behaved slightly differently than the overall wedge. The individual

failure mechanism within these parts is important to understanding the overall nature of the NETS.

Walking from the furthest tension crack toward the pit rim, many tension cracks are observed between the rim and the furthest tension crack. On most of these, the pit side has been downdropped anywhere from a couple of inches to 2.5 feet. These tension cracks generally parallel the strike of the Footwall system, and it would seem highly unlikely that the cracks not follow the bedding and bedding-plane faults of this system at depth.

Based on the nature of the tension cracks and the vector movement data, the mechanics within the slide has been divided into two stages, which are illustrated on Figure 15. The change from the first stage to the second stage was gradational and probably occurred in the 1st half of 1970. The first stage can be characterized by limited differential movement within the Footwall system and by the displacement vectors' paralleling the intersection of controlling structures. The failing wedge was basically behaving as a single mass.

The second stage can be characterized by the breakup of the wedge. Dip-slip movement along the Footwall structure began as the bottom of the blocks within the wedge moved further toward the pit than the top portions. This rotation would explain why the vertical components of the movement vectors greatly increased during this period and also the dip-slip movement on the pit side of most of the tension cracks. During the second stage, the rotation of the blocks could have been aided by plastic flow within the fault zones. There exists the possibility that the gouge has been totally squeezed out in places but to prove such a theory

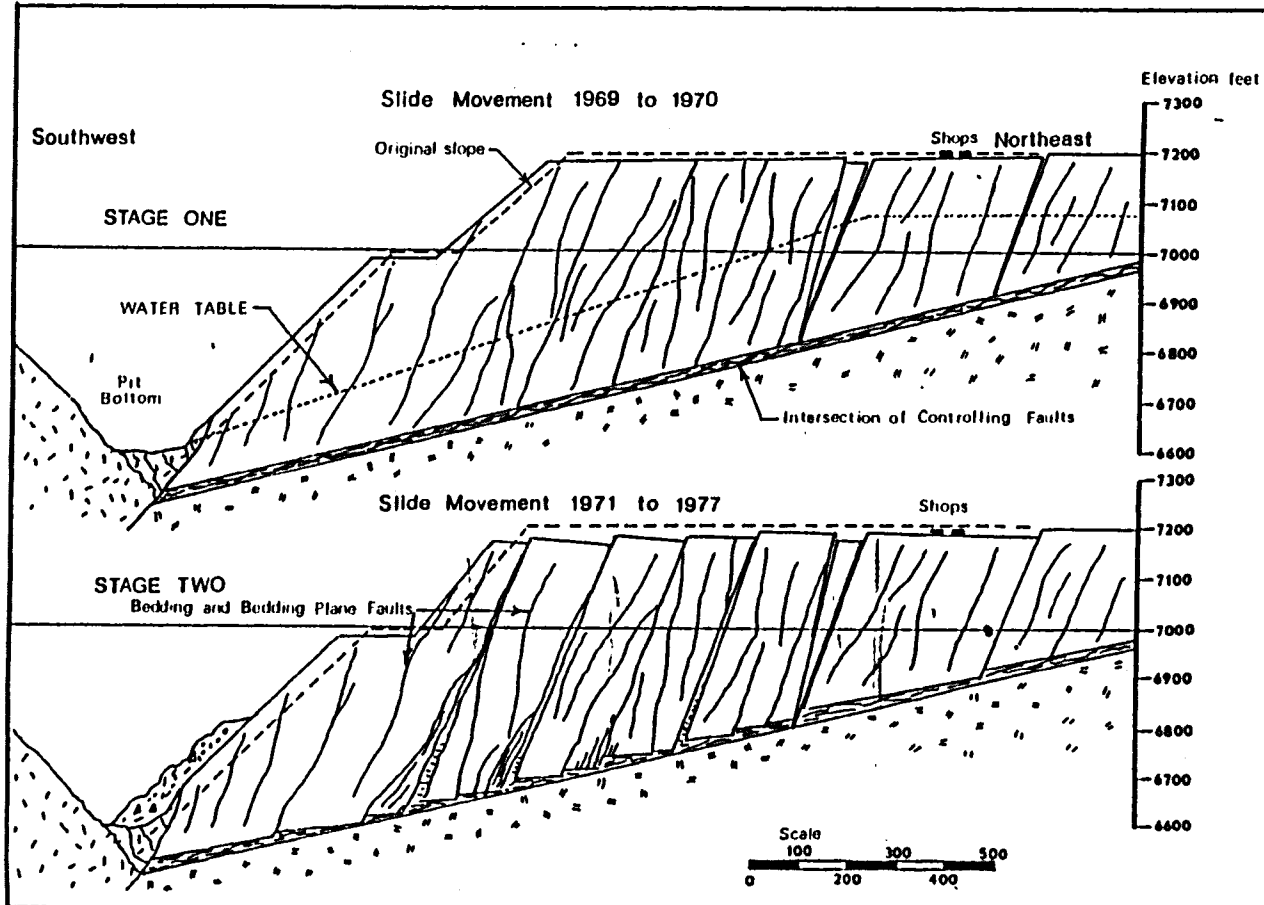


Figure 15. Cross section of the Northeast Tripp slide illustrating its failure mechanism

would involve drilling several diamond drill holes to see if the width of the fault has changed.

Apparently the northwest half of the pit side moved faster and entered this second stage earlier than the southeastern half. One possible explanation for this is that the Morris fault has a slightly higher effective strength than the Kimberly. Another is that near the surface the Morris fault has not controlled the failure. Instead, a much smaller fault zone or shear zone that dips  $50^{\circ}$  NW. has caused the strike-slip movement of this half of the failure to occur in front of the probable surface exposure of the Morris fault. Whatever the reason, the northwest half of the slide has moved 3 to 5 feet farther than the southeast half. Many tension cracks in the northwestern half strike 5-10 degrees more to the northwest than in the southeastern half. This may also be a result of the different amounts of movement between the two halves.

The pit face and the first 600 feet behind the face have moved the most. Then starting with the first tension zone and going farther behind the pit face, the amount of movement decreases. A monitoring station 840 feet from the rim has a recorded movement of 3.9 feet during the first year and a total movement to date of 4.5 feet. One possible explanation for this may be that the effective friction angle of the fault zone increases at lower normal stresses. The fault gouge tested in this study did show such a characteristic. Another explanation is that the two controlling faults are not planar. In the back part of this failure there could easily be large undulations in the fault zones. With only one diamond drill hole in the area placed almost directly over the intersection of the faults, this possibility can neither be proved nor disproved.

Today the overall motion of the wedge is believed to have nearly stopped. The same is true for the parts within the slide. Even after the heavy rains in May 1977, no rejuvenation of any of the surface cracks was observed. The one exception to this is in the northwest corner that is in the transition zone.

#### Estimation of the Net Driving Force

Two approaches will be used to make this estimation. During April 1970 the failure started to decelerate when mining at the toe of the failure ceased. From the October 1970 topographic map of the pit was estimated that roughly 15,000 tons of rubbleized rock had sloughed onto the northwest side of the toe area. If only half of this October tonnage had sloughed in April 1970, 8,000 tons of increased weight in the toe constraint may have stabilized the failure. In order to analyze how this increase in weight affected the net driving force a very complex analysis would be necessary. Ko (1970) in his analysis of the problem decided to assume a frictionless wedge as representing the toe constraint. A similar analysis, using a slightly different geometry, yielded half the increased weight of the toe constraints as working against the sliding force of the failure. Thus a roughly 4,000 tons ( $8 \times 10^6$  lb) decrease in the net driving force may have caused the slide to stabilize.

The second approach used the observation that changes in the water height in the tension crack behind the failure may have caused the failure to briefly accelerate after April 1970. A 20-foot increase in the height of the water in the tension crack would cause a  $100 \times 10^6$  lb increase in overall driving force. The proportion of this change which

actually caused the acceleration is uncertain. However, it does indicated that the figure obtained in the first analysis is not unreasonable.

### Morris Failure

#### Morphology

The Morris failure is situated high on the northeastern end of the Tripp Pit. The rim of the pit in this area is at an elevation of 7,230 feet. The failure is not believed to extend below the 6,800-foot elevation on the pit face, which would give the failure a vertical relief of 430 feet. The intermediate slope in front of the slide is now in places as steep as 39 degrees but averages 32 degrees.

#### Structure and Rocks

The failure is a classic wedge failure. On the southeast it is controlled by the Morris fault, which in this area strikes N. 74° E. and dips 31° MW. The northeast side is controlled by an unnamed fault probably in the Footwall system, which strikes N. 39° W. and dips 33° SW. The intersection of these two faults plunges 29° at S. 83° W. and daylights into the pit at an elevation of 6,800 feet. The geometry of this failure is shown on Figure 16. At a rock density of 160 lb/ft<sup>3</sup>, the failure has involved 350,000 tons of rock.

Below the unnamed fault in the Footwall system are oxidized skarns and directly above this fault is an altered quartz sericite porphyry. Below the Morris fault are steeply dipping marbles and above the fault are oxidized skarns and the altered porphyry.

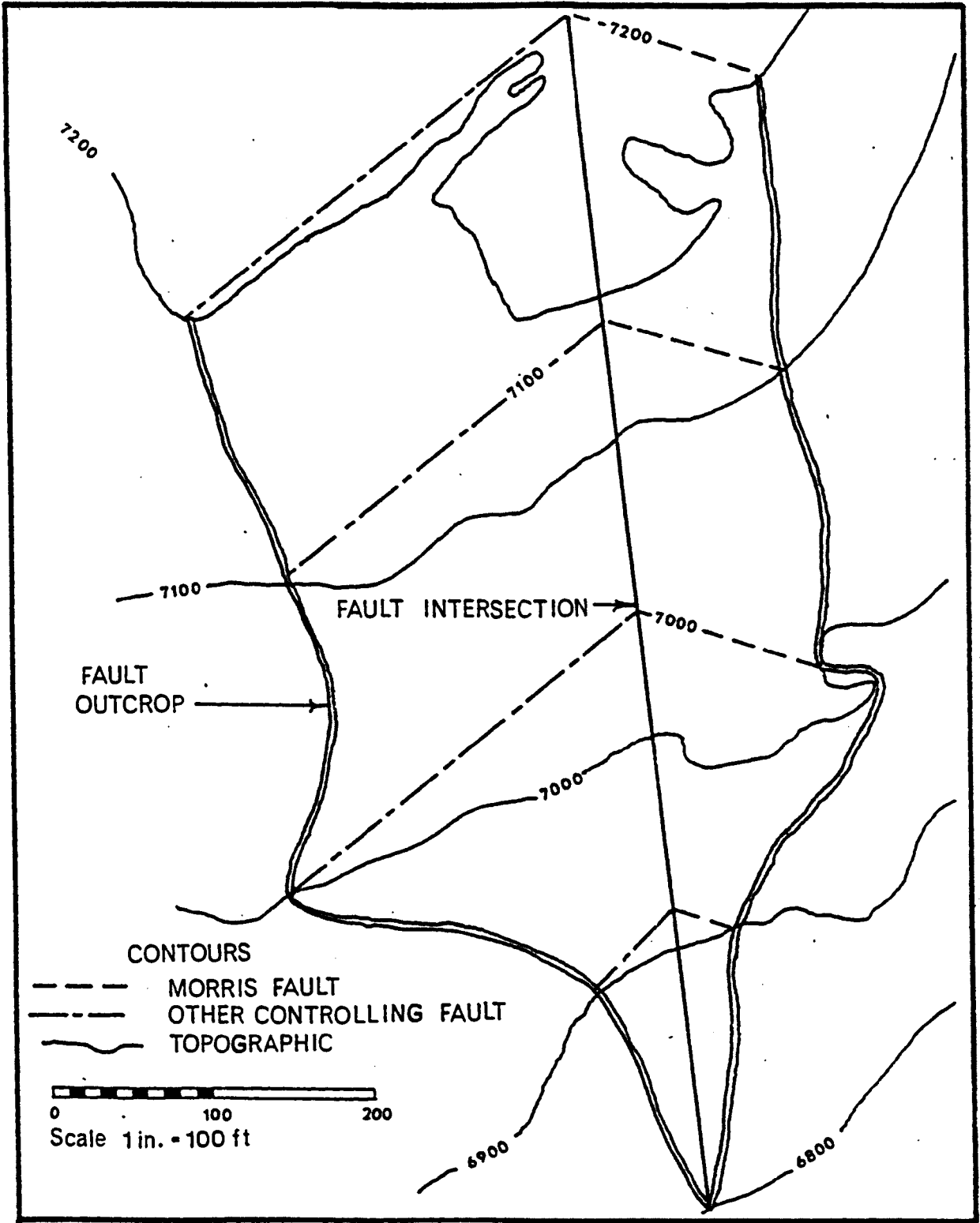


Figure 16. Structural and topographic contour map of the Morris slide area

### Slide Movement

The Morris failure began in late 1970. Since then the pit face has pushed out 20-30 feet and the top has dropped a similar amount. Scarps made by the movement show excellent exposures of both the controlling faults. The movement has opened many of the discontinuities in the pit face, but in general the failure has not rubbleized.

### Slide Mechanics and Effective Rock Mass Strength

This failure may be tied to the Northeast Tripp slide. Although the southeast scarp of the NETS did not form along the Morris fault, a shear zone above the Morris seems to have controlled the scarp. This area, or island, between the shear zone and the Morris fault is where the Morris failure is located. Except for the Morris failure, this island has been relatively more stable than the NETS. Data from the only survey monitoring station in the area indicates that up to 1.5 feet of movement did occur.

The Morris failure did not begin until significant movement had already occurred on the NETS. This suggests that the stress and strain exerted by the NETS on the Morris area were key factors in initiating the Morris failure. Once the peak strength of the Morris was overcome, the failure developed rapidly.

Why the wedge eventually stopped is not known. Possibly as it slide toward the pit its leading edge moved off the gouge-filled fault zones and onto either a marble or skarn surface. The higher amount of resisting frictional force on these rock surfaces could have caused the failure to stop. Another possibility arises from the gouge in the faults

being only 1-2 feet thick. This thickness may not have been enough to keep the sides of the faults from eventually coming into contact with each other, thus increasing their effective strengths.

In order to estimate the strength of the two controlling fault zones, a limiting equilibrium wedge analysis was performed on the wedge and the strength back calculated. Following are the input data used for this back calculation:

1. Plane A (Morris fault): strike, N. 14° E.; dip, 31° NW.
2. Plane B (part of the Footwall system): strike, N. 39° W.; dip, 33° SW.
3. Tension cracks: none behind the failure.
4. Pit face: N. 22° W.; dip, 33° SW.
5. Vertical relief: 430 feet.
6. Wedge above water table.
7. External forces: none.

Assuming that both faults had equal strength, this analysis yielded an effective friction angle of 27.2 degrees for zero cohesion, 20.7 degrees for 500 lb/ft<sup>2</sup> cohesion, and 13.0 degrees for 1,000 lb/ft<sup>2</sup> cohesion.

Based on the previous testing of fault gouge similar to that in the Morris, the friction angle for this zone was estimated at 12.7 degrees. Because the gouge in the Morris fault was not nearly as thick as it is at depth beneath the NETS (1-2 feet vs. 20-40 feet), the cohesion was estimated to be 500 lb/ft<sup>2</sup> for the Morris fault under the Morris slide. If the other controlling fault also had 500 lb/ft<sup>2</sup> cohesion, it would have to have a friction angle of 23.7 degrees for the failure to occur. Both these estimates of the effective strength for the two controlling

faults are within the range of strengths reported for filled discontinuities by Barton (1974).

### Richards Failure

#### Morphology

The Richards failure is located in the far southeastern corner of the Tripp Pit. Unlike the Morris failure, which starts at the pit rim and ends part way down the pit face, the Richards starts on a haul road at the 6,970-foot elevation and ends in the bottom of the pit at an elevation of 6,700 feet. The width of the failure ranges from 300 to 500 feet. The slide is now a rubble slope.

#### Structure and Rock

The structure controlling the Richards failure is not as well understood as those for the NETS or Morris. What structural information is available comes from the pit face just above the failure. The biggest problem with these data is that there is a major south-dipping thrust between the failure and the area above the haul road where the structure was derived. The east side of the slide may possibly be controlled by a fault that will be referred to as the Richards fault (Fig. 3). Above the failure this fault strikes N. 24°E. and dips 53-65°NW. Based on the east-side scarp created by the failure, the dip of the Richards fault flattens out to 38 degrees under the failure. Where exposed, the fault gouge in the Richards fault is oxidized and weathered and appears to be from 1 to 6 inches thick.

On the southwest side, the controlling structure may have been a joint. A detailed line completed just above the failure showed a prominent joint set that strikes N.  $65^{\circ}$ W. and dips  $40^{\circ}$  NE. The intersection of the Richards fault and this joint set plunges  $30.5^{\circ}$  N.  $21^{\circ}$ W. and would daylight into the pit. This possible controlling structure is based on the shaky assumption that the structure can be projected across the thrust.

The rock types in this failure cannot be determined because of a lack of data. Generally, the rocks involved in the failure appear to be rhyolite and rhyolite breccias, oxidized sandstone, oxidized altered porphyry, and some oxidized skarns.

### Slide Movement

The movement of this failure can be estimated by comparing the 1970 and 1975 topographic maps of the Tripp Pit (Fig. 8). At the toe, the slide has pushed 120 feet into the pit. Above the rubble material, a 100-foot-wide haul road has completely failed and slid down the failure. Roughly 400,000 tons of rock are involved in this slide.

### Slide Mechanics and Effective Rock Mass Strength

Because there are many uncertainties about the structure controlling the failure, the strength of the original wedge was not back calculated. Once failed, the wedge appears to have quickly rubbleized and now has an angle of repose of 23 degrees. The effective strength of the rubble material can be estimated using Hoek and Bray's (1977) circular failure charts. The rubble would have a friction angle of 25 degrees, assuming cohesion to be zero and the vertical relief at 180 feet.

### Southwest Tripp Slide

Of all the slides in the Tripp Pit, the least is known structurally about the Southwest Tripp slide. The failure is presented here because it may have involved a different mechanism than the other failures already discussed.

#### Morphology

Roughly 800 feet of the pit rim are involved in the SWTS. The elevation at the rim ranges between 7,280 and 7,389 feet, and the toe of the failure is at 6,690 feet. The average vertical relief is 630 feet. The slide is now a rubble slope with an angle of repose between 35 and 37 degrees.

#### Structure and Rocks

Prior to the failure, several benches were mapped and the resulting geology is shown on Figure 3. The area is highly faulted, but with only a few churn drill holes and one diamond drill hole in the area the structure could not be delineated. From the pit geologic mapping, the rock types involved in the failure are mainly rhyolite breccias, skarns, and altered porphyry. In the upper portions of the slide area, these rocks are increasingly oxidized. The upper 250 feet of the slide area consist of a mine dump containing highly oxidized material.

#### Slide Movement

The movement history of the SWTS can be estimated by comparing the October 1970, October 1971, and the most recent 1975 topographic maps of the Tripp Pit. During October 1970 the failure had just begun

on the eastern portion of the present failure. The failure was 300 feet wide, 0-100 feet deep, with a vertical relief of 475 feet and an angle of repose of 35 degrees. The lower rubble material from the failure appears to have just pushed across the bottom haul road at an elevation of 6,800 feet. By October 1971, the failure had nearly attained its present size. The slide had buried the lower haul road and had extended to the pit bottom 125 feet lower. Since then the slide has changed very little.

#### Slide Mechanics and Effective Rock Mass Strength

The failure appears to have involved only the upper 250 feet of the pit face, which consists mostly of mine dumps and highly weathered rhyolite and altered porphyries. It appears that the SWTS is a result of a soil-type circular failure caused by oversteepening the pit face. From the October 1970 topography of the western portion of the slide, it can be determined that the overall mining slope was 45 degrees and the slope for the upper 200 feet was 43 degrees. The strength of this upper material is unknown, but most mine dumps in the area are known to stand at an angle of repose of 37 degrees.

One problem with the soil circular failure theory is the timing. The failure occurred only after mining had deepened the pit from 200 to 400 feet below where most of the failure occurred. Ideally, a soil failure should have occurred as soon as the face was mined down the upper 250 feet. One possible explanation could be that initially the upper 250 feet were strong enough to stand at 43 degrees. Then after several years' exposure to weathering and the vibration from pit blasting, the strength deteriorated until the area was no longer stable.

The material in the failure continued to move until the overall slope of the entire failure has changed from 45 to 36 degrees. The final angle of repose is very close to the natural angle of repose for this type of rubble material. If this proposed mechanism is correct, the SWTS would be the only failure in the Tripp Pit that is not structurally controlled.

## SLOPE DESIGN

The potential ore in the Tripp Pit is marginal, and the slope design will be a critical factor in determining the ore's economic viability. A review of the slope design factors should be considered before the final (optimum) slope is decided on. For several areas in the pit there is not enough geotechnical data to determine an optimum slope design. In other areas the determination of the optimum slope will be a lengthy and time-consuming process, and it was believed that this final step goes beyond the scope of this thesis.

To avoid unnecessary repetition, only the slope design for the NETS will be dealt with at length. The other failures will be considered only if they require different factors than the NETS.

### Overview

#### Safety Factor Approach

Recently the concept of optimum pit slope design has changed. Not too long ago the ideal pit design was "the one that failed the day after mining ceased." This design method attempts to minimize the safety factor. Ideally, the engineers have at hand all the input parameters needed to determine all the forces that either produce or resist the failure. If the parameters are precisely known, the ideal slope designed would have a safety factor of one.

A major problem with this method is the inherent uncertainties in estimating the geologic parameters affecting slope stability (Cassun,

1976). To allow for this, the engineer uses a higher safety factor usually based on his judgment and experience.

The safety factor may also be raised by management to allow for the economic risk involved if the design should fail. For example, if the mill is sitting on the pit edge, a slope failure would be very costly and could even put the future of the mining operation in jeopardy and a much higher safety factor would be required to protect the investment.

### Probability of Failure

The first step in getting away from the problems with the safety-factor approach is the recognition that many geologic and engineering parameters are variable and can be better represented by statistical functions. By using the computer and the Monte Carlo overlay system, these statistical functions can be used to obtain a probability of failure schedule for a given slope. Coates, McRorie, and Stubbins (1963) were probably the first to recognize the need for a probabilistic approach in slope design.

### Benefit-Cost and Risk Analysis

Even with the probability-of-failure schedule, the engineer is still faced with the problem of deciding on the optimum slope design. Using the benefit-cost approach, the optimum slope is the one in which the incremental benefits of that design are greater than the incremental costs associated with its probability of failure. The benefits of a particular design are usually tied closely with the cash flow derived from the mined ore. The costs of failure may be just those associated with

the removal of the failed material from the pit but can also include increased operational expenses.

At this point, the optimum slope design may be obvious, but if not, the tax and capital investment effects must be considered. A risk analysis program, INRISK, has been developed by Kim, Cassun, and Hall (1977) that simulates the operating economics and capital investment characteristics of each alternative slope design to develop a probability distribution of appropriate financial decision criteria described by Cassun (1976).

Such an approach is called probabilistic slope design and was used by Cassun. The method is also discussed in depth by Kim, Cassun, and Hall (1977).

### Northeast Tripp Slide Slope Design

#### Scope of Design Problem

The probability of the Northeast Tripp Slide's failing during future mining is very high. The cost associated with such a failure is also very high. Even if only half of the 33-million-ton wedge slide into the pit, it would be more than enough to make the mining venture unprofitable. For the same reason, the design option of removing the entire NETS failure would be an unacceptable \$16.5 million solution to the slide.

The problem is to decide on a stabilization technique. This technique should be able to reduce the probability of failure to an acceptable level and yet be reasonable enough in cost so as not to adversely affect the marginal mining economics.

## Design Method

Probability of failure curves can be a function of slope height and slope angle. It will become evident that this is only partially applicable to the NETS.

Slope Height. The critical slope height here becomes the one at which the two controlling faults become daylighted. At this point the probability of failure goes from near zero to very close to 100 percent. Since future mining must daylight these faults to get at the remaining ore in the Tripp Pit, the future stability of the area is nearly independent of the slope height.

Slope Angle. The design is also very insensitive to changes in the slope angle. If a 37-degree slope was found to be the optimum angle for dealing with the secondary failures along the pit face, a sensitivity analysis was run between the pit slope, the resulting safety factor, and the back-calculated strength for the NETS, assuming this pit slope as a maximum. This analysis used the limiting equilibrium technique of Hoek and Bray (1977) with the following results.

The controlling faults would have a friction angle of 9.6 degrees if the cohesion is zero, and lowering the slope angle actually made the wedge more unstable. This can best be illustrated by giving an example. If the slope were reduced to 30 degrees, an additional 4.95 million tons of rock would be removed from the wedge. At the same time, the water-related forces in the tension crack and the uplift forces in the fault zones do not change. Because of this, the forces resisting the failure

decreased faster than the sliding forces, resulting in a new safety factor of 0.986.

The effect of lessening the slope angle was found to depend on the assumed cohesion of the controlling faults. At a cohesion of 400 psf and a friction angle of 12.01 degrees, it was found that the safety factor was nearly independent of the wedge's weight. At higher cohesions, the resisting forces decreased less than the sliding forces, making the safety factor increase as the weight of the wedge decreased.

The sensitivity of the safety factor to changes in the slope angle and assumed cohesion was found to be very low. For a 30-degree slope, the resulting safety factor, assuming zero and 1,000 psf cohesions, was 0.986 and 1.018, respectively. Because it is difficult to predict the actual cohesion of the controlling faults, the same would be true for predicting the effect of lessening the weight of the wedge by decreasing the slope angle. A probability of failure analysis was not run on the NETS. However, based on the sensitivity of the safety factor to some of the other input parameters, such as the strike and dip of the controlling faults, it can be estimated that the probability of failure associated with a safety factor of 1.018 is still fairly high.

### Dewatering

Piteau (1970) among others has pointed out that water in the controlling structures is a critical factor in slope failure. Without considering the very low permeability of the fault gouge, a stabilization method involving the use of a drainage adit would appear feasible. Removing all the water in the wedge would result in a safety factor of 1.11.

Even lowering the water to just below the tension crack, which would give a maximum head of 150 feet, yields a safety factor of 1.08 (assuming a cohesion of zero and a friction angle of  $12.85^{\circ}$ ). The cost of such a program for the NETS could be less than half a million dollars even using an adit (Miller, 1977).

Unfortunately, if the undrained loading effect, discussed by Lambe and Whitman (1969), caused by the low permeability of the montmorillonite gouge is considered, dewatering does not look nearly as attractive. Drainage of the gouge would take years, and until this is achieved the uplift forces within the gouge will remain. For a cohesion of zero and a friction angle of 12.85 degrees, the resulting safety factor until the gouge is drained is as low as 1.03, which is significantly less than the estimate of 1.11 for total dewatering.

There is not enough ground-water permeability data to determine the feasibility of dewatering the low-permeable shale, which makes up most of the NETS wedge. In addition, the probability of failure associated with a safety factor of 1.03 for the NETS should still be fairly high. Because of this, dewatering will not be considered as a possible stabilization method until the ground-water permeability data can be obtained.

### Catch Bench

Broadbent (1975) suggested creating a catch bench in front of the failing wedge for it to slide onto and eventually to stop upon. This bench would be mined down to the controlling faults and all the gouge removed from the exposed surfaces. Then as the NETS failed, it would move out onto this high-friction surface and stabilize.

To give a one-shot preliminary evaluation of this method, a 200-foot bench was designed (Fig. 17, in pocket) and found to require 12 million tons of additional waste removal. At 50¢/ton (Crawford, 1977) the bench would cost \$6 million. Estimating the friction angle of the bench at 30 degrees, the resulting safety factor was 1.07 by the time the wedge had reached the far side of the bench.

There exists one serious potential problem with this design. If the thick gouge is pushed out onto the catch bench as the wedge fails the resulting friction angle of the bench area could be considerably less than the assumed 30 degrees.

In order to pick the ideal catch bench width, a probabilistic design will need to be used. The engineer will have to weight the cost of each bench width with its associated probability of failure until an acceptable bench design is determined.

### Tension Cables

At present, the best method for applying an outside force to a wedge failure like the NETS is by the use of tension cables. The engineering application of tension cables is discussed at length by Barron, Coates, and Gyenge (1971) and Sage (1977).

The sheer resistance mobilized by the cable forces reaches a maximum if the dip of cables (D) is chosen so that

$$U = \tan(I + D)$$

where  $U = \tan(\text{friction angle})$  and  $I$  is the apparent dip of the plane of weakness under the slope (Barron et al., 1971). For the NETS, values of 0.228 for  $U$  and  $31.3^\circ$  for  $I$  yield an ideal dip of  $-0.5^\circ$  (up dip). From a

practical standpoint only a +10° dip is possible (Barron et al., 1971). The force applied by the tension cables can be resolved into two vector components. First is the component that directly opposes the sliding force,

$$S_t = T \cos (I + D)$$

where T is the effective tension force of the cable.

Second is the vector normal to the intersection of the controlling faults, which is then divided into two additional vectors normal to the controlling faults. For the NETS the total resisting force mobilized by these two normal components is

$$R_t = 1.120 T \sin (I + D) \tan \phi$$

where  $\phi$  is the friction angle for the two controlling faults.

Using these two equations, two possibilities will be discussed for stabilizing the NETS with tension cables. For both cases, a 12-strand-type 270K cable with a manufacturer's recommended capacity of 340,000 lb will be used (Barron et al., 1971). Seegmiller (1974) estimated the cost per 1,000 pounds of force per 12-strand cable to be \$3.19. This would be equivalent to \$4.12 per 1,000 pounds at 1977 costs (using the Marshall-Stevens index for escalation).

The first possibility for using tension cables applies the safety factor approach. For a safety factor of 1.2 it was found that T must equal  $2.56 \times 10^9$  lb. This would mean that 7,518 tension cables would be required at a cost of \$10.6 million. Because of this high cost and infeasibility of installing so many cables in front of the NETS, the safety-factor approach does not appear to be applicable here.

The second possibility arises from the theory of a small driving force causing the failure. This force was estimated to be on the order of  $8 \times 10^6$  lb. If this small driving force theory is correct, twenty-four 340,000-lb tension cables could conceivably stabilize the failure at a relatively low cost. There is also considerable flexibility in this solution. By closely monitoring the slide's movement and the tension in the cables, the theory could be tested. If the actual driving force was several times larger than estimated, the slide would slowly start to accelerate. At this point, additional cables could be added until equilibrium was again obtained. Even if the theory were found to be incorrect, there should be enough time to mine down the 200-foot catch bench or decide that the costs of the other solutions no longer make the Tripp Pit economically feasible.

### The Adit Solution

If the continuity of the fault zones could be destroyed or altered, the effective strength of the zones would increase. One possibility would be to drive a 1,000-foot adit to the zones along with two 400-foot cross cuts along the fault zones. From these cross cuts, by some combination of cut-and-fill mining along with grouting, a key could be constructed.

There are many engineering problems with this solution. The first is how to estimate the effective strength of the key. In addition, driving the adit and cross cuts into the clay-filled fault zone may require an unreasonable amount of support to keep the headings open and safe. Solving these problems goes beyond the scope of this thesis.

### Preliminary Recommendations

At this point, only two of the proposed solutions can be considered until more information is obtained. The high-cost 200-foot catch bench is probably technically feasible, and depending on the mining economics, may be an acceptable method of stabilizing the NETS. Using a small number of tension cables at the toe of the failure is a potential relatively low-cost solution to the failure (\$30-\$40 thousand for the cables). Its biggest drawback is the small driving force theory.

At this point, it is recommended that Kennecott Copper Corporation compare the mining economics of the two solutions. The first possible outcome is that the pit is economically feasible with the high-cost 200-foot bench. Then the very low-cost tension cables can be tried and if they are successful, a larger profit on the pit would be achieved. The second possibility is that only the low-cost tension cable solution is economically feasible. In this case, it may be necessary to install the cables and mine 100,000-200,000 tons of the toe to test the theory. This would also test the possibility that the slide is now stable and may have a safety factor greater than one even with future mining.

Good correlation has been shown between periods of high precipitation and acceleration of the NETS. The importance of this is believed to be secondary to the mining activity at the toe of the failure. Future mining plans should take precautions to keep as much water as possible out of the tension cracks behind the failure. Reducing the water height from 265 to 75 feet could yield a safety factor of 1.3. Such precautions could include drainage alterations and the physical removal of snow before it melts and pumping water from the cracks.

### The Other Slides

The type of slope design methods and their applicability are highly variable for the other failures. To illustrate this, a few of the different possibilities and resulting considerations will be presented.

#### Southwest Tripp Slide

The Southwest Tripp slide appears to involve only the oversteepening of the upper weathered rock and the mine dumps above them. This material is now stable around 37 degree, and the less weathered rock below appears to be stable at 45 degrees. The pit slope design in this area should plan the upper slopes at 37 degrees down to the 7,040-foot elevation, then over the next 100 feet in depth increase the pit slope to 45 degrees.

The SWTS was initially stable and only after several years did the rock strength deteriorate to the point that the slide could occur. One possible slope design consideration should be the possibility of preventing this deterioration. Shotcrete can be used to prevent weathering of the rock and progressive deterioration (Sage, 1977). An estimated cost of reinforced shotcrete was \$2.40/ft<sup>2</sup> in 1974 dollars (Sage, 1977) or \$3.10/ft<sup>2</sup> in 1977 dollars (using the Marshall-Stevens index for escalation). The cost of covering the upper part of the slide with reinforced shotcrete would be on the order of \$1.5 million. The benefit of increasing the slope angle to 43 degrees is a decrease in stripping of 700,000 tons at a cost of \$350,000. Even using unreinforced shotcrete (at roughly a third of the application cost), shotcrete does not pass the benefit-cost test.

### Morris Slide

The solution for the Morris slide appears to be different from the others already discussed. Trying to stabilize the failure does not seem feasible. Tension cables would have difficulty in applying an effective load to the slide due to its degree of rubbleization. In addition, the current mining plans call for the only ore haul road to be placed directly under the failure. A probability design could be carried out for the failure, but with the high cost of such a failure compared to the relatively low cost of just mining out the entire slide (\$175,000 at 50¢/ton) the latter seems to be the logical solution even without a detailed analysis.

### Northwest Tripp Slide

This is the last area of the Tripp Pit that will be discussed. Here the structure is not known well enough to use either the probability or the safety-factor design techniques. Because the failure has already developed, obtaining additional data would be difficult and where possible hard to interpret. For this area, the best mining plan may be to use what I call a dynamic design: first attempt to maintain the slope at 37 degrees, then modify the slope by terracing and unloading as the failures develop. These types of rubble slopes take time to develop and are predictable, hence mining below the failure can be safely done with extensive monitoring. If the mining can be completed before the failure fully develops at its current 30 to 22-degree slope, considerable savings can be made. One possible way to incorporate this type of design into a mining plan and to evaluate the economic feasibility of such a design would be to predict the amount of additional tonnage of slide

rubble that would be removed before mining was completed. A reasonable prediction for the NWTS may be 2 million tons mined from the 6,950 level over a two-year period.

## APPENDIX A

### DIRECT SHEAR TESTING ON THE TRIPP PIT FAULT GOUGE

#### Sample Site

Clay fault gouge samples were obtained from one of the Morris system faults on the north side of the Tripp Pit, near Ely, Nevada. The coordinates of the sample site are 95,500 E., 104,370 N., using the Kennecott coordinate system (Fig. 1). The fault zone averaged 5 feet in thickness where sampled and consisted of mostly black clay with only a few included rock clasts. The rock types surrounding the sample site were mostly weathered Chainman Shale, which prior to weathering had been altered to a hornfels.

After several inches of the outer surface material was removed, the gouge appeared fresh and moist. Samples, approximately 8 inches on a side, were chiseled out of the face, wrapped in a moist cloth and plastic, and transported to the University of Arizona Rock Mechanics Laboratory for testing.

#### Nature of the Gouge

X-ray analysis by the Kennecott Research Center in Salt Lake City, Utah, of similar gouge obtained from diamond drill core in the same area showed the gouge to contain the following minerals: montmorillonite clay (50-70%), kaolinite clay (10-20%), sericite mica (10-25%), and very fine grained quartz (5-10%). Some other properties of

the gouge are a moisture content of 21-31% (drying at 65°C) and an average Atterburg plasticity index of 09.6.

#### Test Sample Preparation

The 8-inch-square field samples were cored using a circular wood saw bit without water. This yielded samples for testing that were 1-2 inches long and 1.3 inches in diameter. The ends of the samples were made planar and perpendicular to the core axis by slipping the metal rings over the core and using a metal blade to plane off the uneven gouge.

#### Direct Shear Testing Procedure

The gouge core and the two testing rings were placed in a Soil-test direct shear machine for testing. Depending on the normal pressure used, the samples were placed under the normal load in a water-filled shear box from 5 to 30 minutes before the actual testing began.

The shear rate used during the tests was 0.8 in./hr, which was the slowest possible rate for the Soiltest shear machine used. The resulting data (shear displacement or strain and shear stress) were plotted on graph paper during the test by an X-Y recorder. The tests yielded a peak shear strength and a residual shear strength.

For several of the samples it was found that additional residual shear strength data could be obtained by increasing the normal stress once the residual strength had been reached. After the test, the amount and nature of plastic flow within the gouge sample were noted. It was also noted whether the top of the sample (not under water) had sweated off water. The results are shown in Table A-1 and Figures A-1-A21.

Table A-1. Gouge test data <sup>a</sup>

Test No.	Normal Force (lb)	Peak Shear Force (lb)	Residual Shear Force (lb)	Range of Residual Force (lb)
4-9	14	27	8	2
1B-10	30		13	2
2B-10	67		25	2
2-9	67	51	25	5
3B-10	121		30	2
1-9	139	60	45	10
4B-10	176		40	5
1-4	192	115	50	2
8-9Z	236	150	60	5
9B-10	267		60	5
3-9	267	106	58	3
3-2	267	105	35	10
2-6	302	100	70	10
1-10	340	140	50	5
8-9B	345		80	5
7-9A	378	135	85	10
11B-10	376		78	5
3-4	400	175	70	3
1-7	427	162	80	3
8-9C	454		103	5
6-9	466	120	70	10
1-2	485	225	100	3
14B-10	485		98	10
7-9B	487		102	5
1-6	540	195	110	3
7-9C	558		115	5
2-1	594	235		
2-7	594	150	95	5

a. Sample diameter = 1.3 in.; sample area = 1.33 in.<sup>2</sup>. Tests were run between 1/10/77 and 10/11/77.

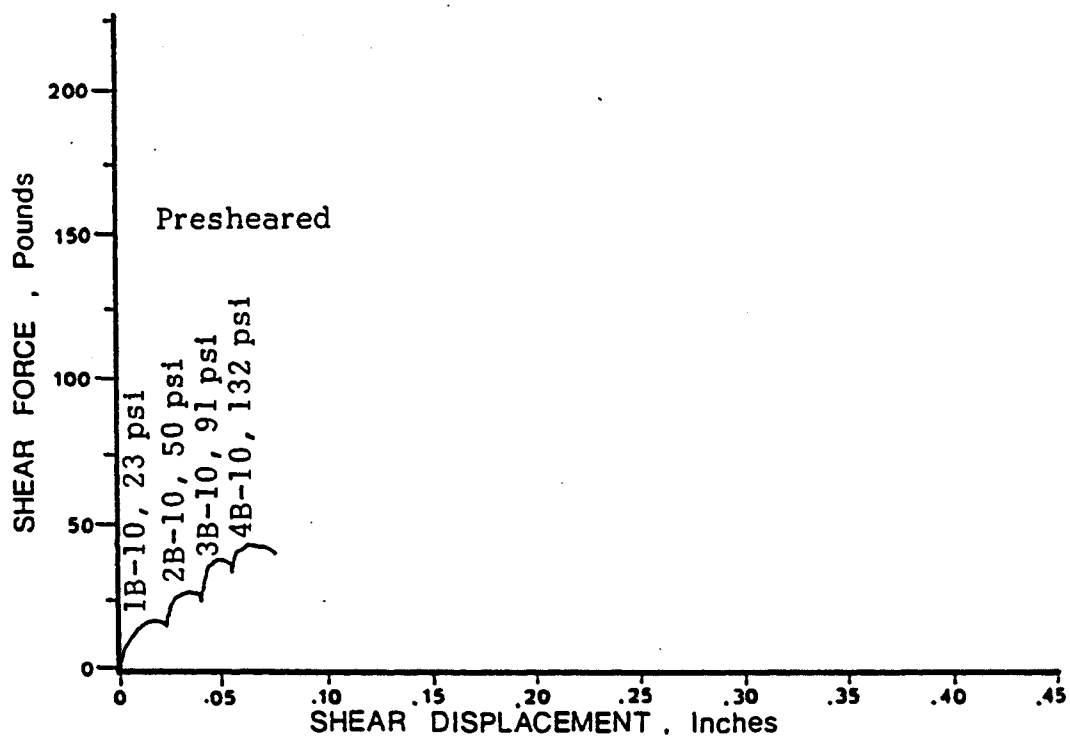


Figure A-1. Shear tests 1B-10, 2B-10, 3B-10, and 4B-10

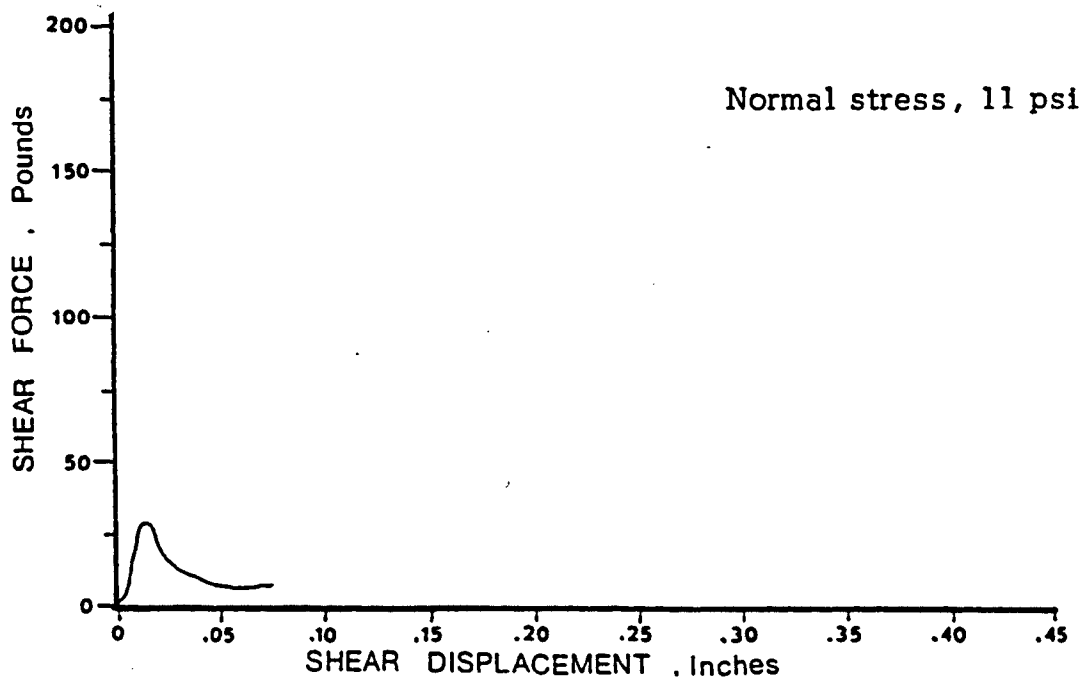


Figure A-2. Shear test 4-9

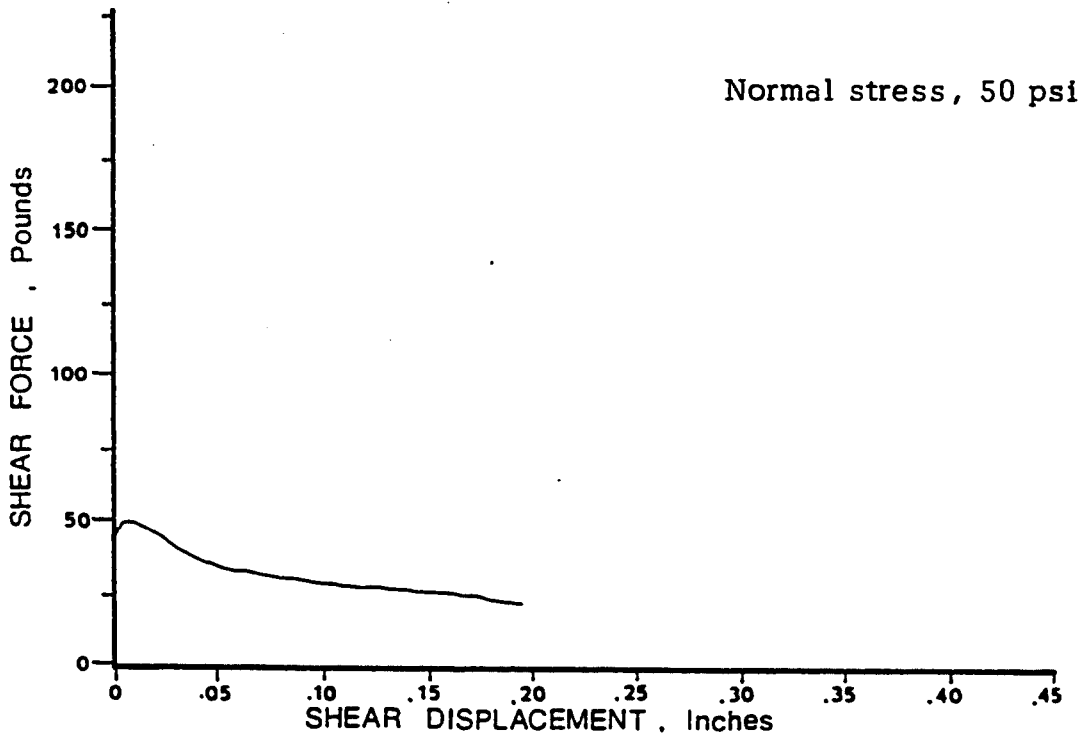


Figure A-3. Shear test 2-9

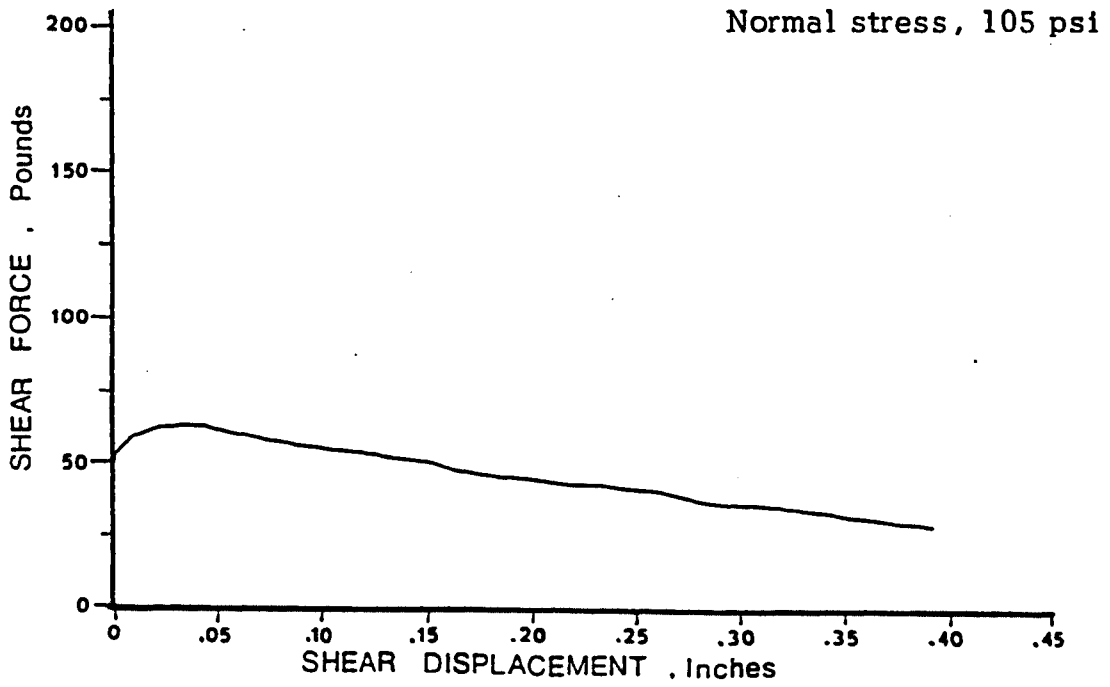


Figure A-4. Shear test 1-9

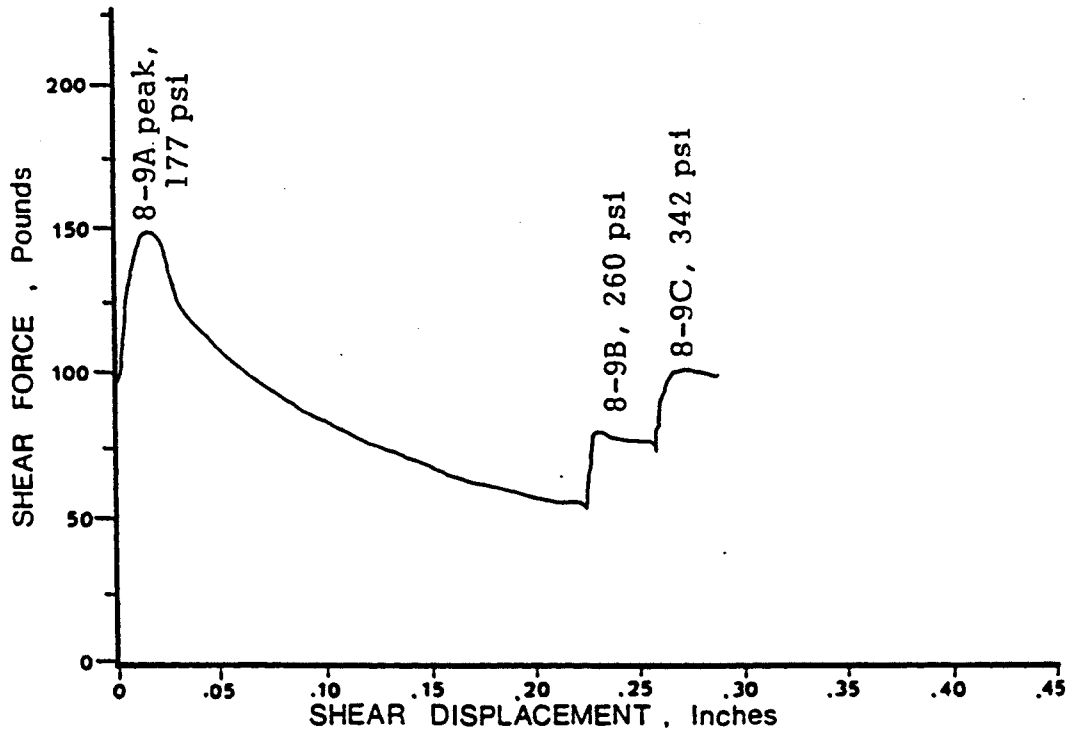


Figure A-5. Shear tests 8-9A, 8-9B, and 8-9C

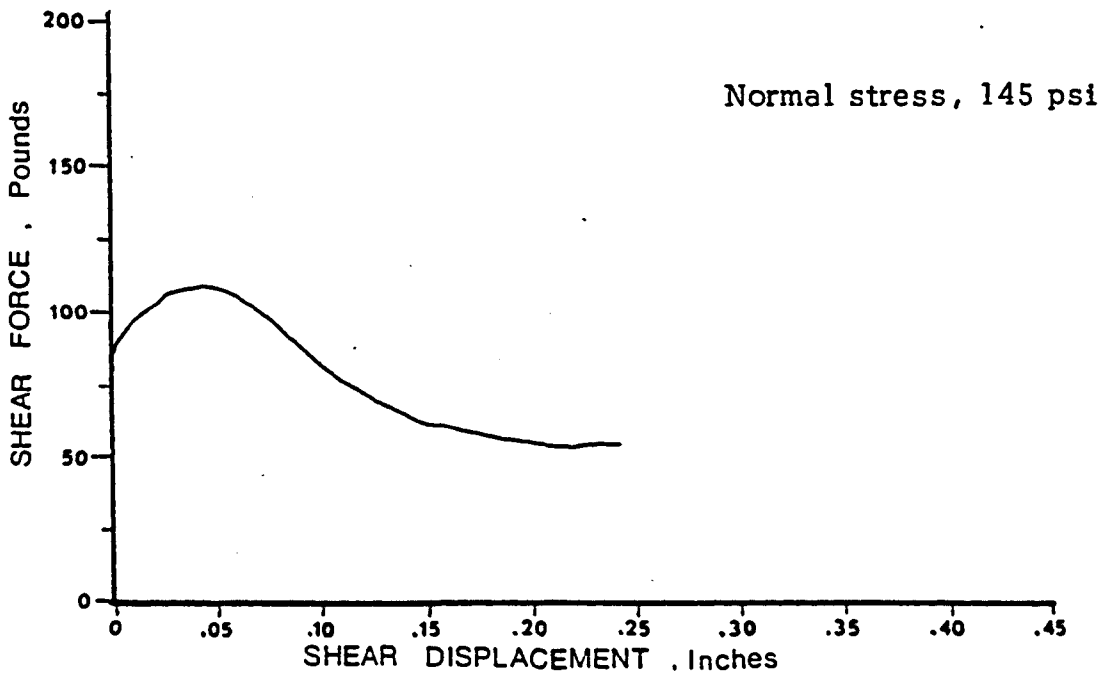


Figure A-6. Shear test 1-4

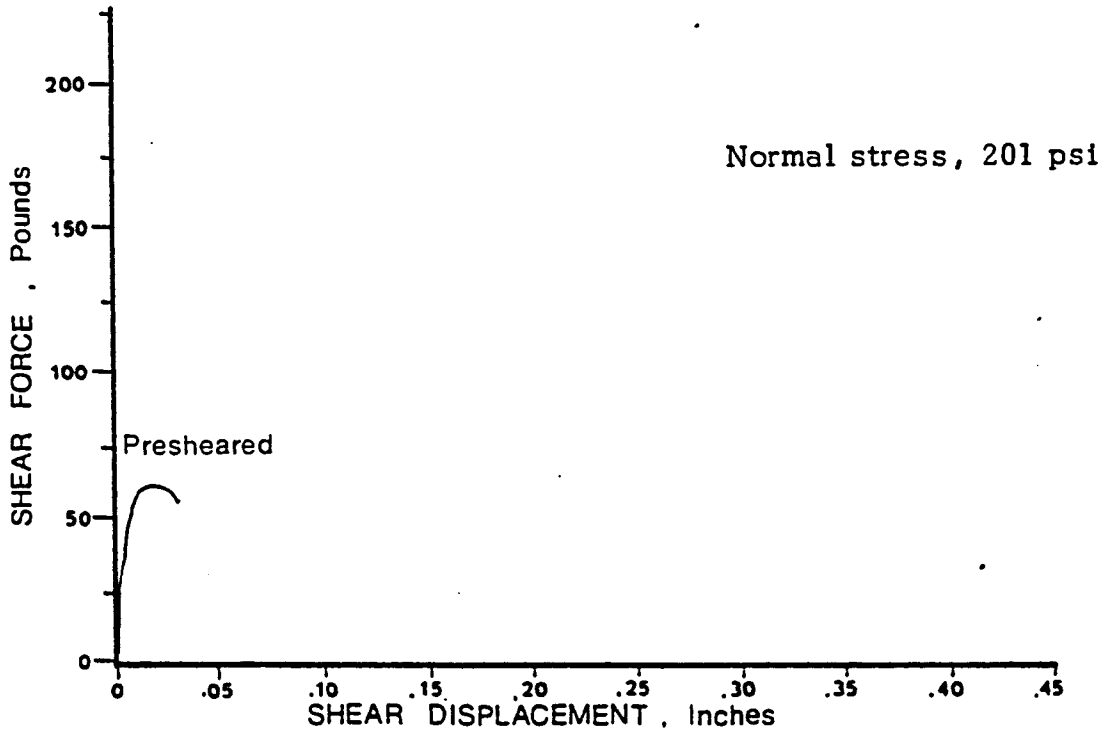


Figure A-7. Shear test 9B-10

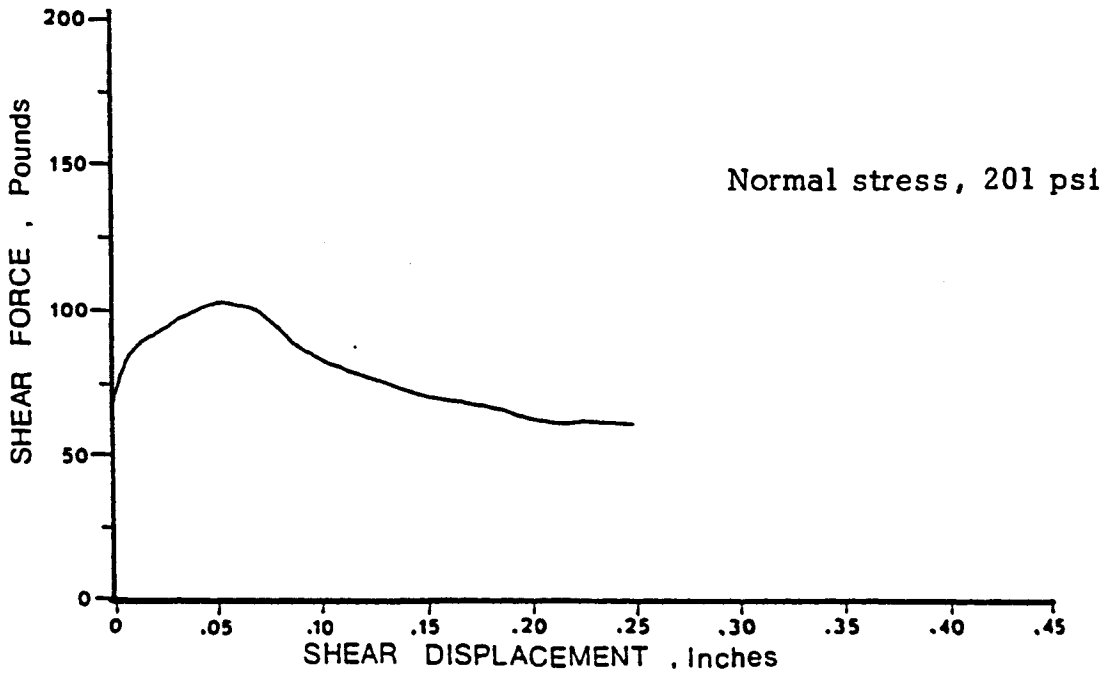


Figure A-8. Shear test 3-9

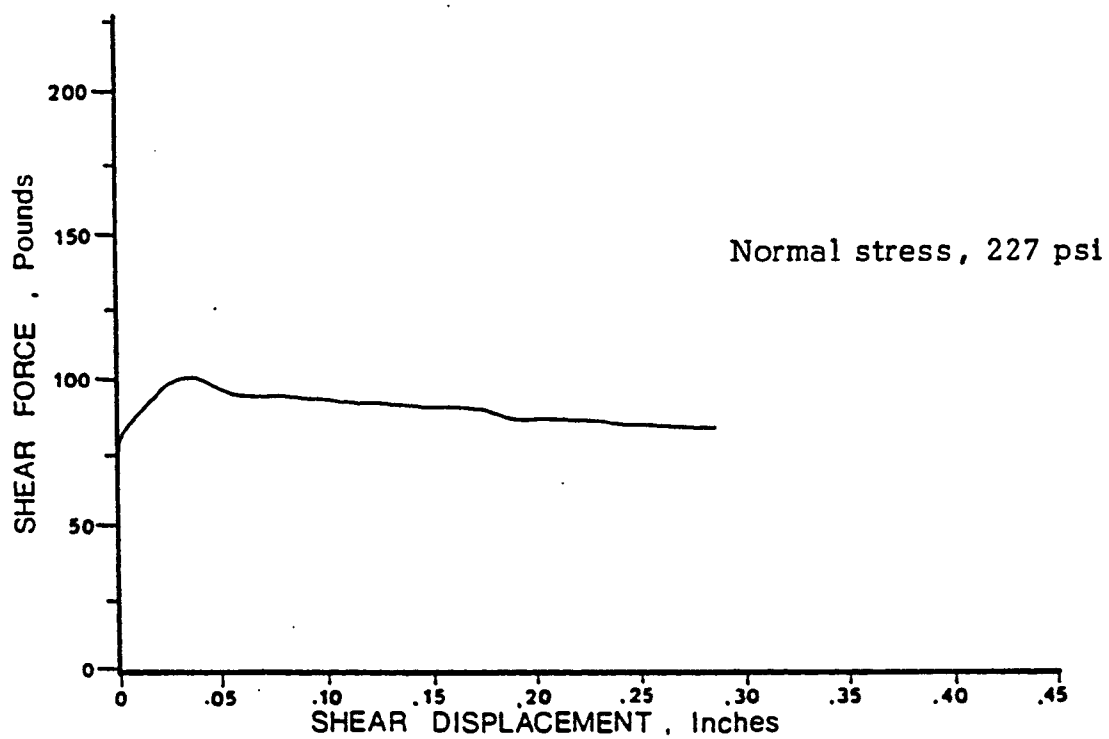


Figure A-9. Shear test 2-6

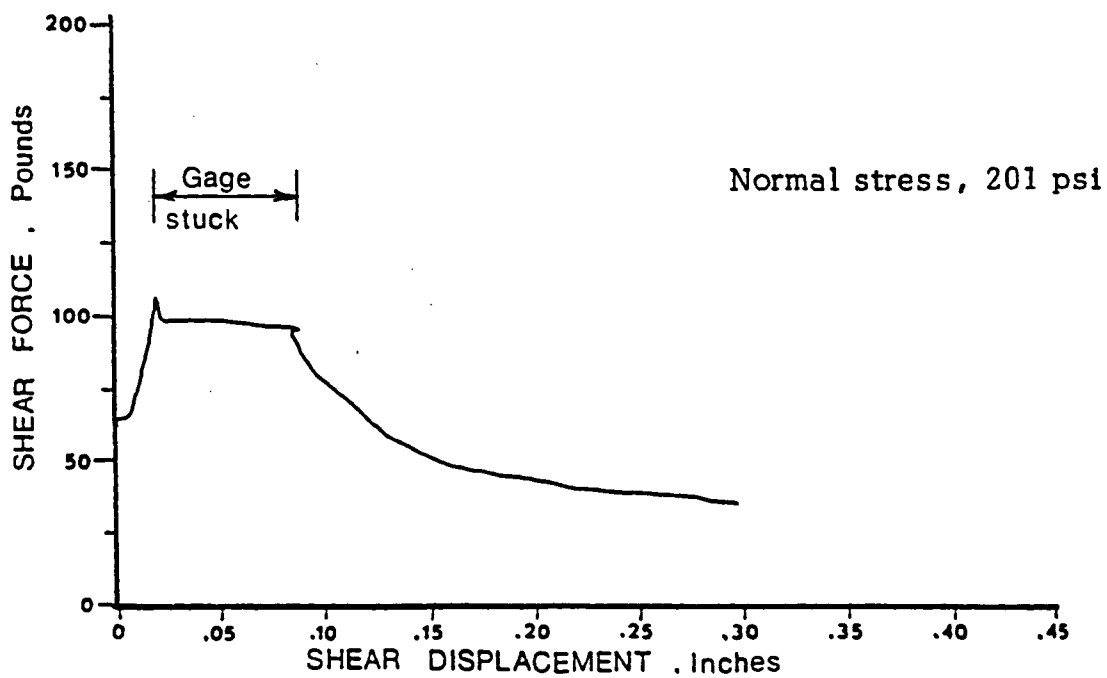


Figure A-10. Shear test 3-2

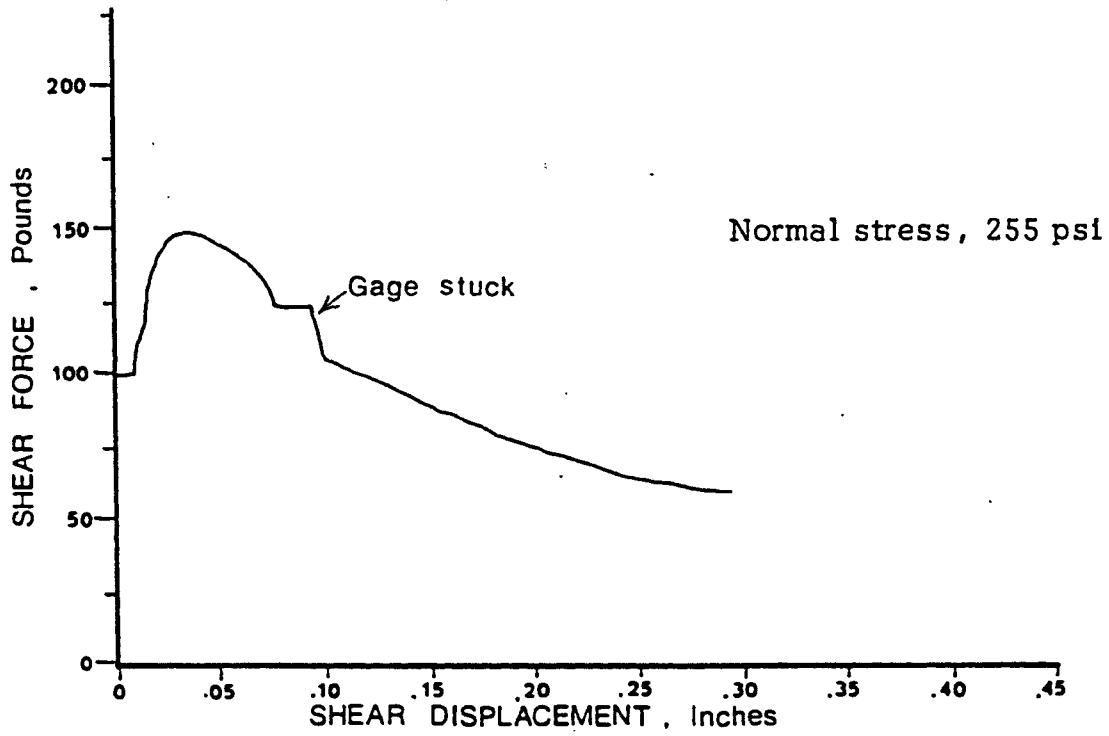


Figure A-11. Shear test 1-10

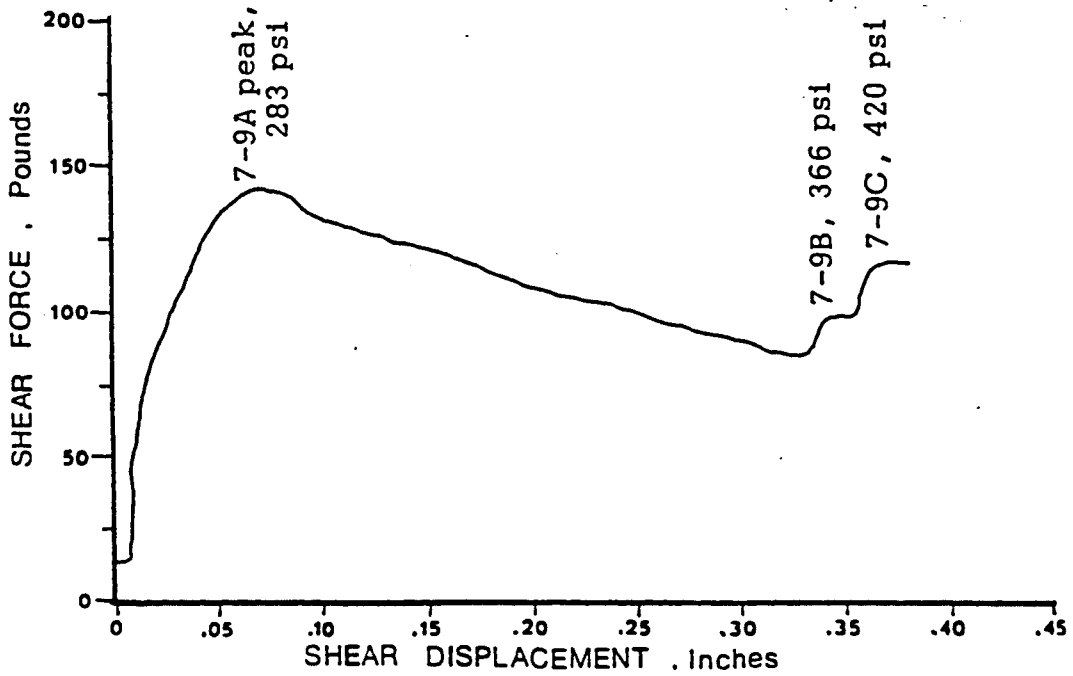


Figure A-12. Shear tests 7-9A, 7-9B, and 7-9C

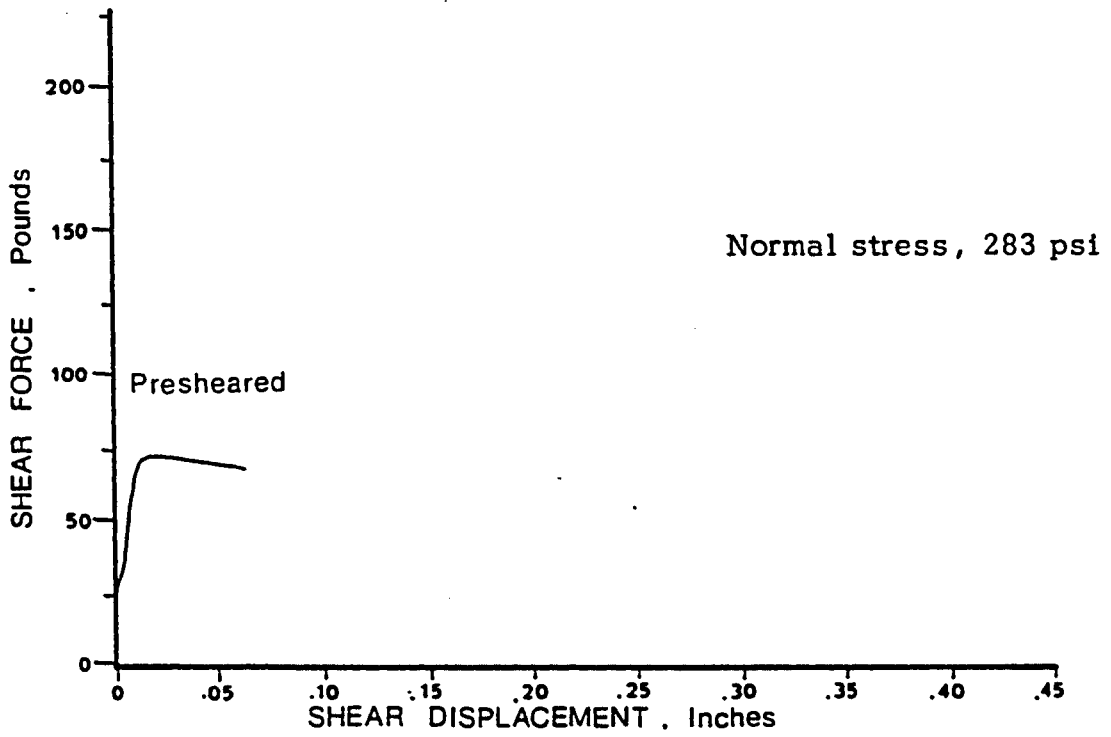


Figure A-13. Shear test 11B-10

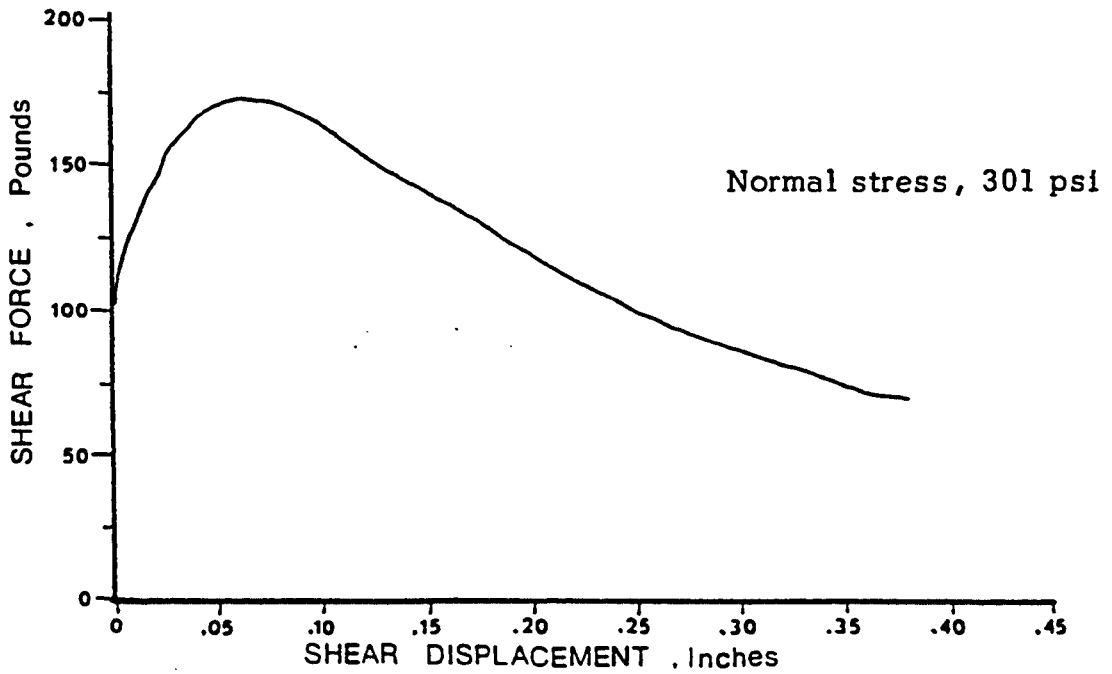


Figure A-14. Shear test 2-4

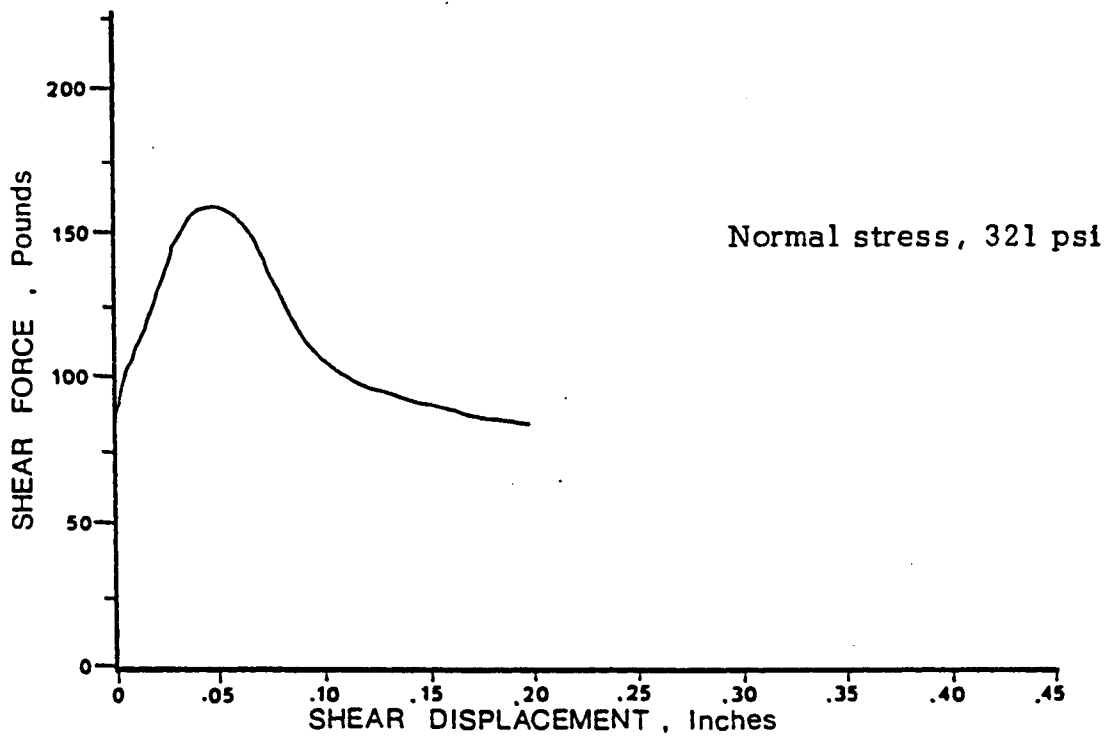


Figure A-15. Shear test 1-7

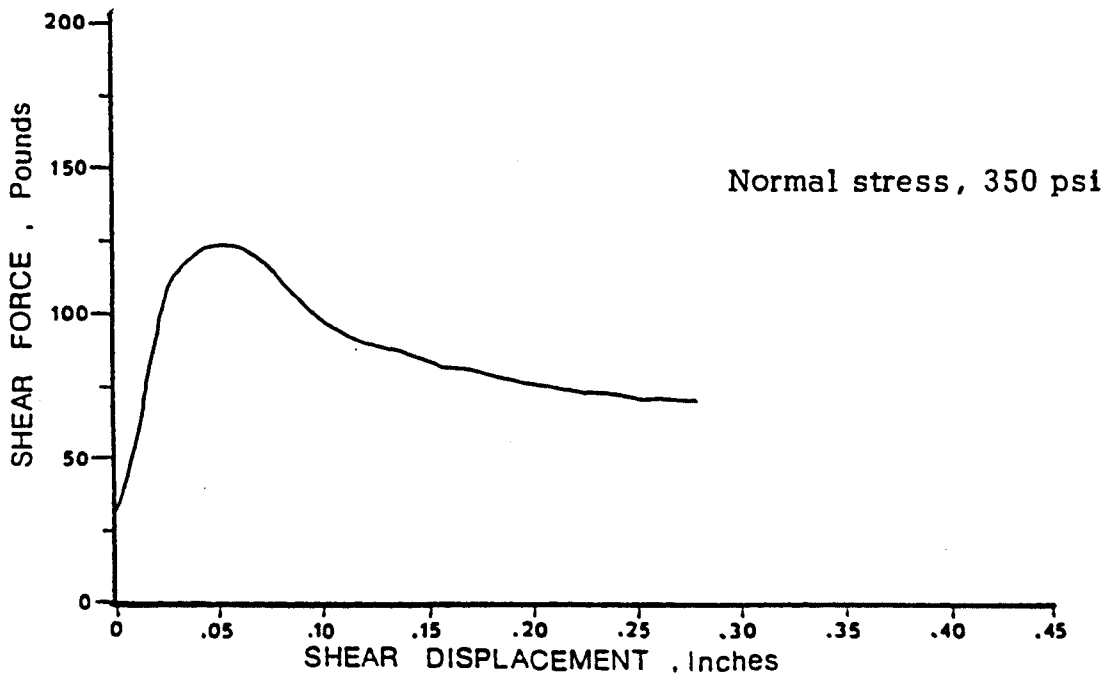


Figure A-16. Shear test 6-9

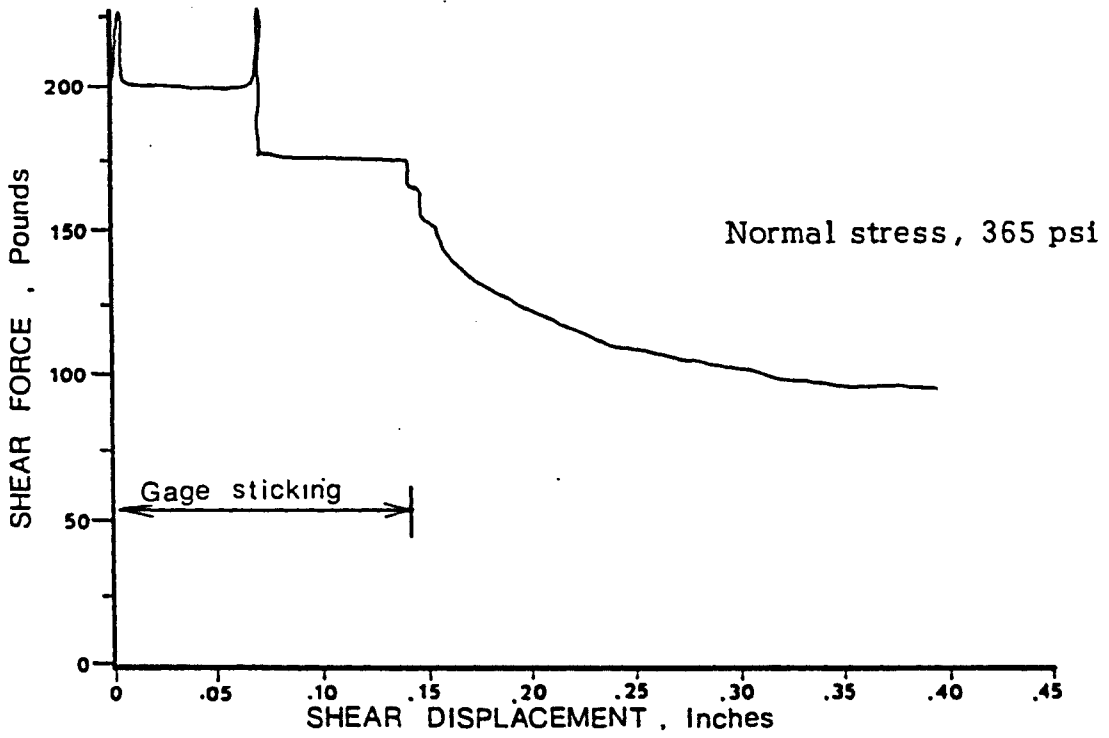


Figure A-17. Shear test 1-2

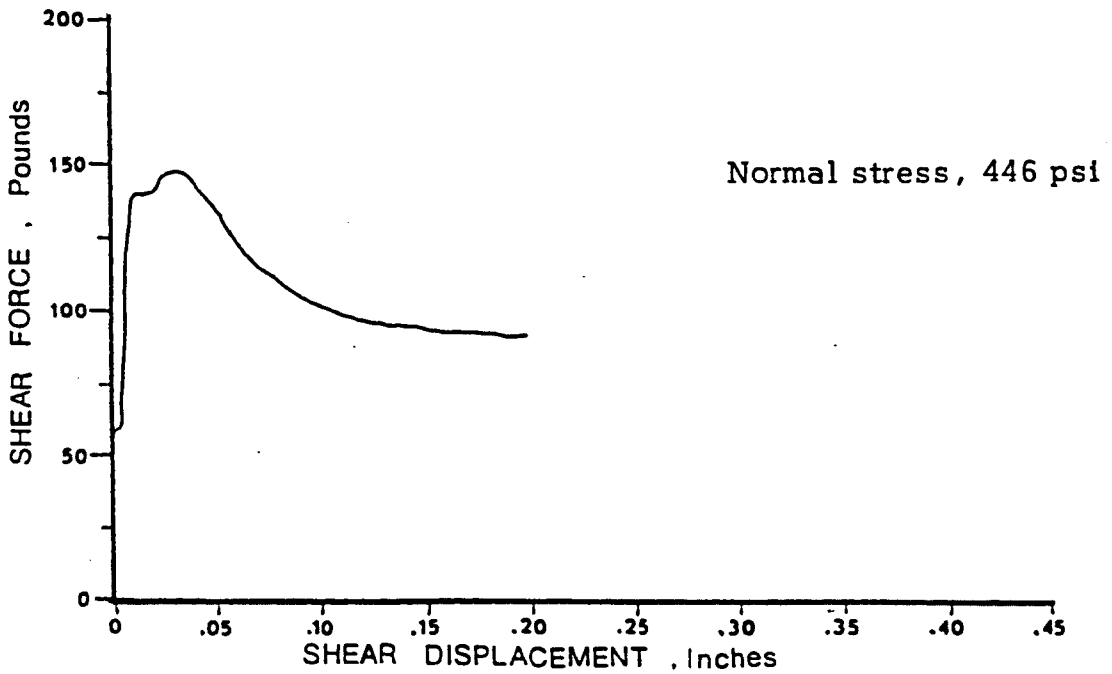


Figure A-18. Shear test 2-7

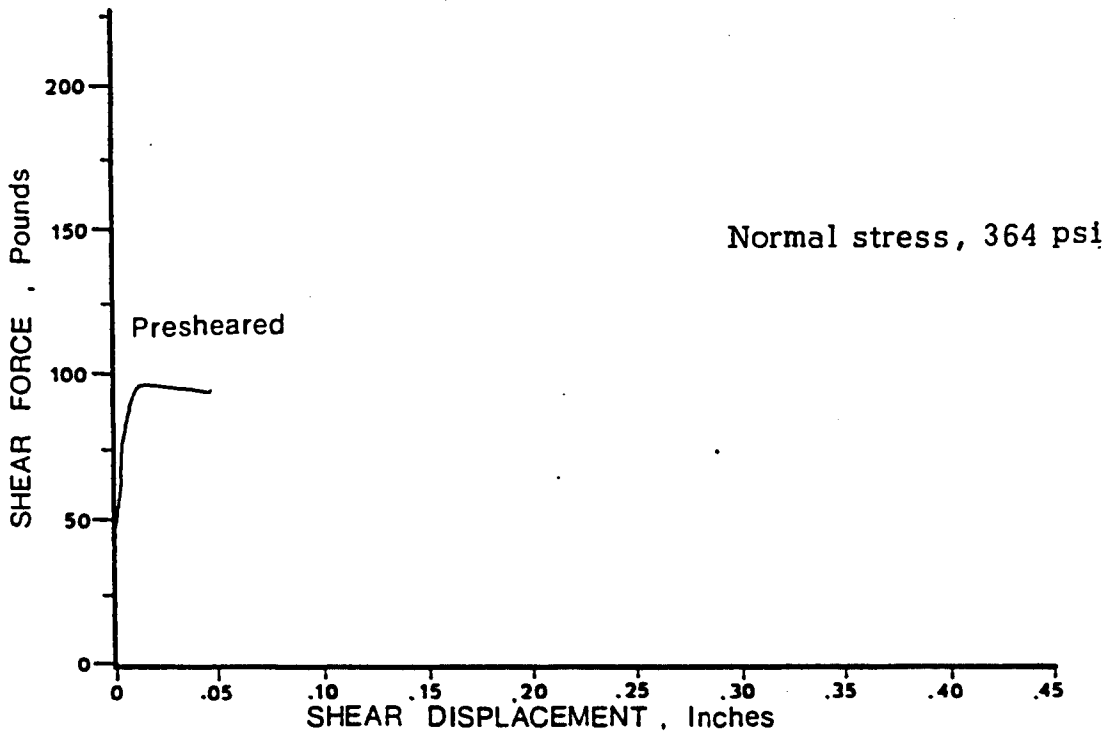


Figure A-19. Shear test 14B-10

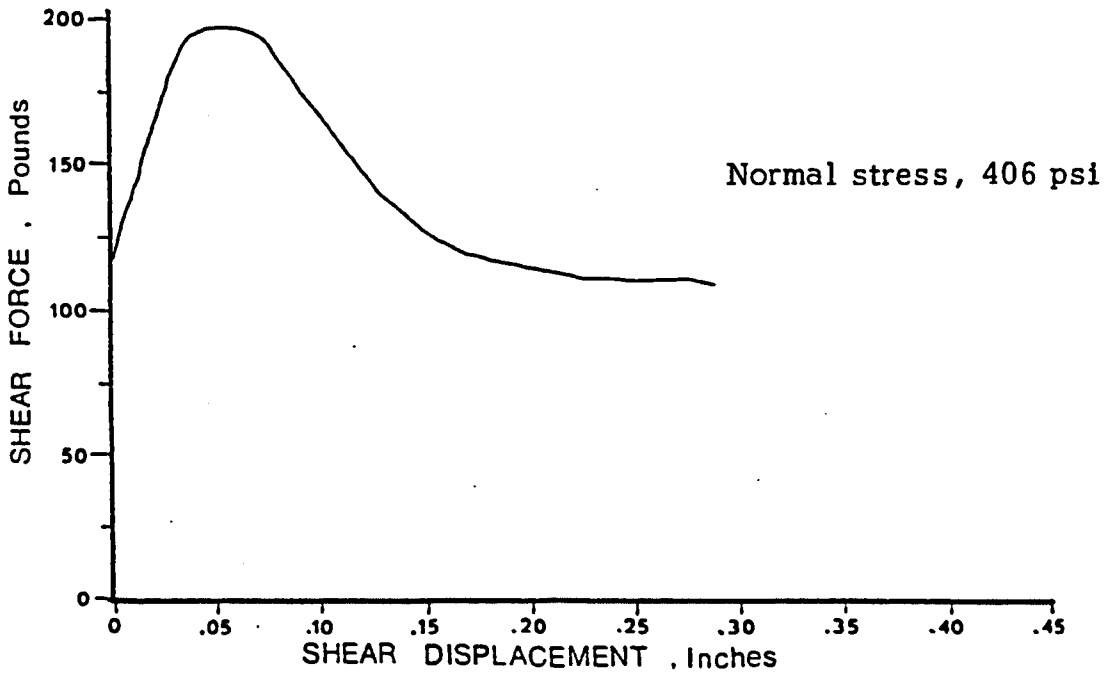


Figure A-20. Shear test 1-6

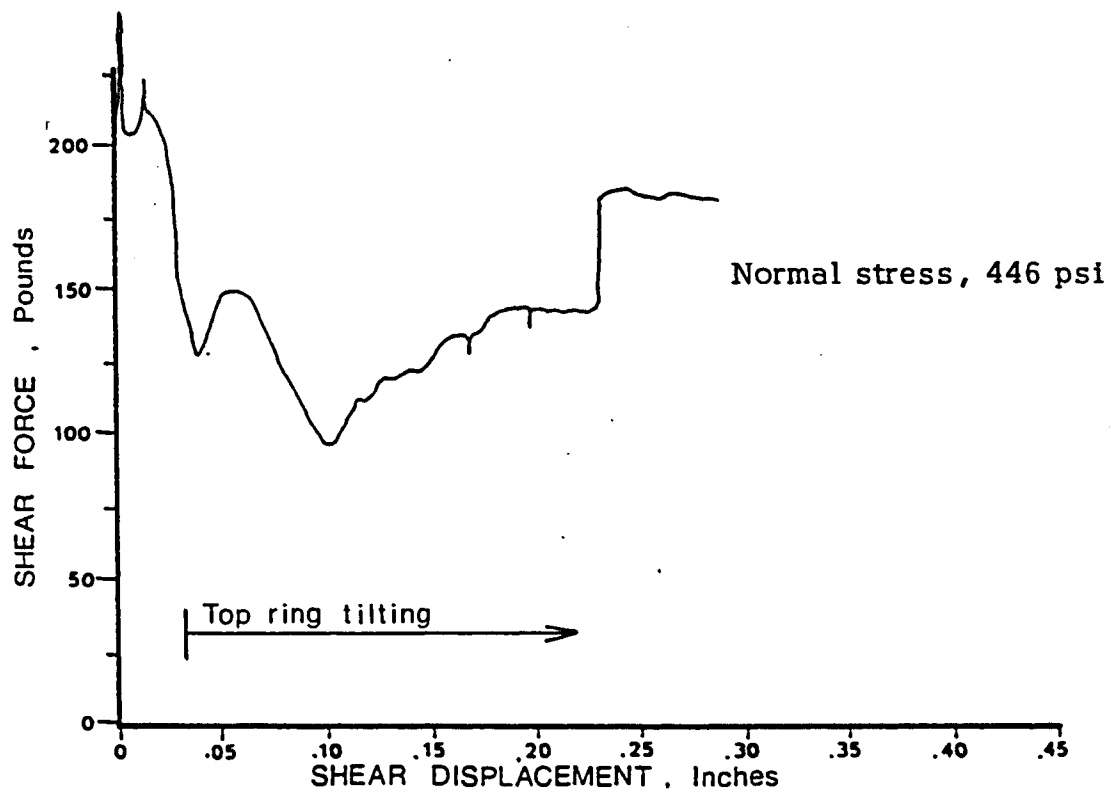


Figure A-21. Shear test 2-1

## APPENDIX B

### BACK CALCULATION OF EFFECTIVE STRENGTH FOR THE NORTHEAST TRIPP SLIDE

Because the Northeast Tripp slide is a wedge failure, its effective strength can be back calculated by using Hoek's limiting equilibrium analysis (Hoek and Bray, 1977, p. 333-348). The geometry of the failure is shown in Figure B-1 (in pocket). The important geometric parameters for the model of this failure are:

1. Plane A (Morris fault): strike, N. 24° E., dip, 31° NW.
2. Plane B (Kimberly fault): strike, N. 69° E.; dip, 33° SE.
3. Pit face: strike, N. 50° W.; dip, 37° SW.; vertical relief, 650 feet.
4. Top of wedge: flat; elevation, 7,200 feet.
5. Tension crack: 1,000 feet behind rim; strike, N. 50° W.; dip, 70° SW.
6. Water table: as shown in Figure 9.

#### Data

Based on the geometry of the wedge as worked out from Figure B-1, the following data were determined:

1. Effective area on plane A of sliding (OATW):

$$A_A = 1.233 \times 10^6 \text{ ft}^2$$

2. Effective area on plane B of sliding (OBVW):

$$A_B = 1.371 \times 10^6 \text{ ft}^2.$$

3. Effective area on plan A below water table (OWIGKM):

$$A_{UA} = 0.515 \times 10^6 \text{ ft}^2.$$

4. Effective area on plane B below water table (OWHFJL):

$$A_{UB} = 0.528 \times 10^6 \text{ ft}^2.$$

5. Effective area of tension crack below water table (HWI):

$$A_{UT} = 0.132 \times 10^6 \text{ ft}^2.$$

6. Plunge of controlling faults:  $13^\circ$ .

7. Angles of controlling faults to horizontal relative to the point view down the fault intersection line (OC):

$$A_{OC} = 28.0^\circ$$

$$B_{OC} = 25.5^\circ.$$

#### Forces Due to Weight of Wedge

1. The planimetric method rather than the Hoek wedge analysis was used to determine the volume ( $V_W$ ) and mass ( $W$ ) of the wedge with the following results

$$V_W = 413 \times 10^6 \text{ ft}^3$$

and, assuming a density of  $160 \text{ lb/ft}^3$ ,

$$W = 66.04 \times 10^9 \text{ lb}$$

$$= 33 \times 10^6 \text{ tons.}$$

2. Weight normal to O-C:

$$W_{OC} = W \cos 13^\circ$$

$$= 66.04 \times \cos 13^\circ$$

$$= 66.35 \times 10^9 \text{ lb.}$$

3. Shear force:

$$S = W_{OC} \sin 13^\circ$$

$$= 66.04 \sin 13^\circ$$

$$= 14.86 \times 10^9 \text{ lb.}$$

4. Forces normal to fault planes:

$$N_A = \frac{W_{OC}}{\frac{\sin A_{OC}}{\sin B_{OC}} \cos B_{OC} + \cos A_{OC}}$$

$$= \frac{64.35 \times 10^9 \text{ lb}}{\frac{\sin 28}{\sin 25.5} \cos 25.5 + \cos 28}$$

$$= 64.35 \times 0.5356 = 34.47 \times 10^9 \text{ lb}$$

$$N_B = N_A \frac{\sin A_{OC}}{\sin B_{OC}} = 34.47 \times 10^9 \text{ lb} \frac{\sin 28}{\sin 25.5}$$

$$= 34.47 \times 10^9 \text{ lb} (1.090) = 37.59 \times 10^9 \text{ lb}$$

Forces Due to Water

1. Water force in tension crack:

$$V = 1/3 (\text{maximum water head}) \times (\text{water density}) \times A_{UT}$$

$$= 1/3 \times 180 \text{ ft} \times 62.5 \text{ lb/ft}^3 \times 132,000 \text{ ft}^2$$

$$= 0.495 \times 10^9 \text{ lb}$$

2. Effective force down fault intersection:

$$V_{OC} = V \cos 13$$

$$= 0.495 \times 10^9 \text{ lb} \times \cos 13$$

$$= 0.482 \times 10^9 \text{ lb}$$

3. Uplift force due to water on fault plane P

$$U_P = 1/3 (\text{maximum water head}) \times (\text{water density})$$

$$\times (\text{effective area on plane below water table})$$

Substituting data for planes A and B,

$$U_A = 1/3 \times 210 \text{ ft} \times 62.5 \text{ lb/ft}^3 \times 0.515 \times 10^6 \\ = 2.25 \times 10^9 \text{ lb}$$

$$U_B = 1/3 \times 210 \text{ ft} \times 62.5 \text{ lb/ft}^3 \times 0.528 \times 10^6 \\ = 2.31 \times 10^9 \text{ lb.}$$

### Resolution of Forces for NETS

Using the limiting equilibrium equation:

$$\text{S.F.} = \frac{C_{AA} + C_{BAB} + (N_A - U_A) \tan \phi_A + (N_B - U_B) \tan \phi_B}{S + V_{OC}}$$

and assuming equal cohesion ( $C_A = C_B = C_{AB}$ ) and equal friction angles ( $\phi_A = \phi_B = \phi_{AB}$ ), then

$$\text{S.F.} = \frac{C_{AB}(A_A + A_B) + (N_A - U_A + N_B - U_B) \tan \phi_{AB}}{S + V_{OC}}$$

For a safety factor one, using data for the NETS (all units  $\times 10^9$ ):

$$1 = \frac{C_{AB}(0.00260) + (34.47 - 2.25 + 37.59 - 2.31) \tan \phi_{AB}}{14.86 + 0.48} \\ = C_{AB}(0.000167) + 4.401 \tan \phi_{AB}$$

Solutions to this limiting equilibrium equation are:

<u><math>C_{AB}</math></u>	<u><math>\phi_{AB}</math></u>
0	12.8
250	12.3
400	12.0
500	11.8
1000	10.7
2000	8.6

See Figure 13 for plot of solutions.

## APPENDIX C

### NOTATION

The following symbols are used in this thesis:

- $i$  = angle between minimum and maximum dip
- $n$  = normal force
- $r$  = correlation coefficient
- $s$  = standard deviation
- $u$  = water pressure
- $\bar{x}$  = average
- $C$  = cohesion
- $D$  = dip of tension cables
- $I$  = apparent dip of plane of weakness under slope
- $R_t$  = total force normal to controlling faults mobilized by tension cables
- $S_t$  = force vector from tension cables in opposing slides
- $\sigma_n$  = normal stress
- $\tau$  = shear force (or shear strength)
- $\phi$  = friction angle
- $\phi_A$  = friction angle for plane A
- $\phi_B$  = friction angle for plane B

## REFERENCES

- Abel, J. F., 1971, Uniaxial compressive and tensile strength for typical rocks: unpublished compilation: Dept. of Mining and Geological Engineering, University of Arizona.
- Barron, K., Coates, D. F., and Gyenge, M., 1971, Artificial support of rock slopes: Ontario, Canada, CANMET Report R228, 146 p.
- Barton, M. R., 1974, A review of the shear strength of filled discontinuities in rock: Norwegian Geotechnical Institute, Publication No. 105, 58 p.
- Bateman, A. M., 1935, The copper deposits of Ely, Nevada, in Proceedings, 26th Geological Congress: Washington, D.C., p. 307-321.
- Bauer, H. L., Breitrack, R. A., Cooper, J. L., and Anderson, J. A., 1966, Porphyry copper deposits in the Robinson mining district, Nevada, in Titley, S. R., and Hicks, C. L., eds., Geology of the porphyry copper deposits, southwestern North America: Tucson, University of Arizona Press, p. 232-244.
- Beal, L. H., 1950, Wallrock alteration in the western portion of the Robinson mining district, Kimberly, Nevada: unpublished M.S. thesis, University of California, Berkeley, 92 p.
- Bertacchi, P., and Sampaolo, A., 1974, Some critical considerations on the deformation and failure of rock samples in the laboratory, in Advances in Rock Mechanics, Proceedings, 3rd Congress of the International Society for Rock Mechanics, Denver, Vol. II: Washington, D.C., National Academy of Sciences, p. 21-26.
- Brekke, T. L., and Selmer-Olsen, R., 1965, Stability problems in underground construction caused by montmorillonite-carrying joints and faults: Engineering Geology, v. 1, no. 1, p. 3-19.
- Broadbent, C. D., 1974, Report on sample tests, Job 964-660: unpublished interoffice memorandum between Kennecott Engineering Center and Nevada Mines Division, Ely, Nevada.
- \_\_\_\_\_ 1975, Slope stability recommendations for the Tripp Pit failure zone: unpublished interoffice memorandum between Kennecott Copper Corporation, Nevada Mines Division, and Kennecott Copper Corporation, Metal Mines Division, Engineering Center, Ely, Nevada, 8 p.

- Broadbent, C. D., 1976, Personal communication: Kennecott Copper Metal Mines, Salt Lake City, Utah.
- Call, R. D., 1972, Analysis of geologic structure for open pit slope mine design: unpublished Ph.D. dissertation, University of Arizona.
- Cassun, W. C., 1976, Economic analysis applied to open pit slope design: unpublished M.S. thesis, University of Arizona, 89 p.
- Coates, D. F., 1964, Classification of rocks for rock mechanics: Internat. Jour. Rock Mech. Mining, v. 1, p. 421-429.
- \_\_\_\_\_ McRorie, K. L., and Stubbins, J. B., 1963, Analysis of pit slides in some incompetent rocks: SME Trans., December, p. 94-101.
- Coulson, J. H., 1970, The effects of surface roughness on the shear strength of joints in rock: Missouri River Division, Corps of Engineers, Department of the Army, Technical Report MRD-2-70.
- Crawford, J., 1977, Oral communication: Kennecott Copper Corporation, Nevada Mines Division, Ely, Nevada.
- Deere, D. U., and Miller, R. P., 1966, Engineering classification and index properties for intact rock: Air Force Weapons Laboratory, Kirkland AFB, New Mexico, Technical Report AFWL-TR-65-116.
- Dimock, R. R., 1970, Slope failure—a continuing problem: unpublished paper presented at the Open Pit Slope Stability Seminar Workshop, April 30, 1971, University of Nevada, Reno.
- Fournier, R. O., 1958, Mineralization of the porphyry copper deposit near Ely, Nevada: unpublished Ph.D. dissertation, University of California, Berkeley, 178 p.
- \_\_\_\_\_ 1967a, The porphyry copper deposit exposed in the Liberty open pit mine near Ely, Nevada. Part I. Syngenetic formation: Econ. Geology, v. 62, no. 1, p. 57-81.
- \_\_\_\_\_ 1967b, The porphyry copper deposit exposed in the Liberty open pit mine near Ely, Nevada. Part II. The formation of hydrothermal alteration zones: Econ. Geology, v. 62, no. 2, p. 208-227.
- Goodman, R. E., 1976, Methods in geological engineering in discontinuous rocks: St. Paul, Minnesota, West Publishing Company, 472 p.
- Hamel, J. V., 1972, The slide at Brilliant Cut, in 13th Symposium on rock mechanics: New York, AIME, p. 487-510.

- Hoek, E., and Bray, J. W., 1977, Rock slope engineering, rev. 2nd ed.: London, The Institution of Mining and Metallurgy.
- Horton, R. C., 1960, History of the mineral industry in the White Pine County area, *in* Guidebook to the geology of east-central Nevada: Salt Lake City, Utah, Intermountain Association of Petroleum Geologists, p. 210-219.
- Jaeger, J. C., 1971, Friction of rocks and stability of rock slopes: *Geotechnique*, v. 21, no. 2, p. 97-134.
- \_\_\_\_\_ and Cook, N. G. W., 1969, Fundamentals of rock mechanics: London, Chapman and Hall, Ltd., 585 p.
- James, L. P., 1972, Zoned hydrothermal alteration and ore deposits in sedimentary rocks near mineralized intrusions, Ely area, Nevada: unpublished Ph.D. dissertation, Pennsylvania State University, University Park, PA., 241 p.
- Kim, Y. C., Cassun, W. C., and Hall, T. E., 1977, Slope manual supplement 5-3, Financial computer program: Ontario, Canada, CANMET Report 77-6, 184 p.
- Ko, K. C., 1970, Preliminary investigation on the Tripp Pit slope failure: unpublished interoffice report, Kennecott Copper Corporation, Metal Mining Division, Engineering Department, Job. No. 173, 31 p.
- Kreis, H. G., 1973, Basement porphyritic monzonite and its relationship to ore near Ely, Nevada: unpublished M.S. thesis, University of Arizona, 95 p.
- Krynine, D. P., and Judd, W. R., 1957, Principles of engineering geology and geotechnics: New York, McGraw-Hill Book Company.
- Lambe, T. W., and Whitman, R. V., 1969, Soil mechanics: New York, John Wiley & Sons, Inc.
- Markos, L. J., 1971, Determination of compressive and tensile strength of rock samples, Nevada Mines Division, Kennecott Copper Company, Ely Nevada: Denver, Colorado, Bureau of Mines, Denver Mining Research Center, Report 55-107.
- McDowell, F. W., and Kulp, J. L., 1967, Age of intrusion and ore deposition in the Robinson mining district of Nevada: *Econ. Geology*, v. 62, p. 905-909.
- Merrill, R. H., and Stateham, R. M., 1970, Microseismic investigation of incipient slope movement near the Tripp-Veteran Pit: Denver, U.S. Bureau of Mines, Denver Mining Research Center, Progress Report 55-105.

- Miller, V. J., 1977, Design recommendations for the Tripp slide area: unpublished term project for Advanced Rock Mechanics, Dept. of Mining and Geological Engineering, University of Tucson.
- Nielsen, R. L., 1969, Mineral zoning at Ely, Nevada: Kennecott Exploration Service, Geological Research Division, unpublished report, 42 p.
- Parsons, A. B., 1933, Nevada Consolidated, in The porphyry coppers: New York, AIME, p. 114-133.
- Pennebaker, E. N., 1932, Geology of the Robinson mining district, Nevada: Mining Metall., v. 13, p. 163-168.
- \_\_\_\_\_ 1942, The Robinson mining district, Nevada, in Newhouse, E. H., ed., Ore deposits as related to structural features: Princeton, New Jersey, Princeton University Press, 391 p.
- Piteau, D. R., 1970, Geologic factors significant to the stability of slopes cut in rock, in Planning open pit mines: Johannesburg, South African Institution of Mining and Metallurgy, p. 33-52.
- Pratt, H. R., Black, A. D., and Brace, W. F., 1974, Friction and deformation of jointed quartz diorite, in Advances in Rock Mechanics, Proceedings, 3rd Congress of the International Society for Rock Mechanics, Denver, Vol. IIA: Washington, D.C., National Academy of Sciences, p. 306-310.
- Radosavljevic, Z, Colic, B., and Lokin, P., 1970, Stability of slide slope of the BOR copper mines surface exploitation, in Proceedings, 2nd Congress of the International Institute for Rock Mechanics, Belgrade, Vol. III: Priverdnic Pregled, p. 403-410.
- Ramos, J. M. S., Guimaraes, D. E., and Abrao, A., 1974, Slope stability at CVRD Cane mine, Itabira, Brazil: New York, AIME Preprint 74-F-317.
- Rock Mechanics Laboratory, n.d., unpublished reports: Department of Mines, University of Arizona.
- Sage, R., 1977, Mechanical support, Chapter 6, Pit slop manual: Ontario, CANMET Report 77-3, 111 p.
- Seegmiller, B. L., 1974, How cable bolt stabilization may benefit open pit mining: Mining Eng., v. 26, no. 12, p. 29-34.
- Skempton, A., 1964, Long term stability of clay slopes. Fourth Rankin Lecture: Geotechnique, v. 14, no. 2, p. 75-102.
- Smith, J. G., 1977, Oral communication: Kennecott Copper Corporation, Nevada Mines Division, Ely, Nevada.

- Spencer, A. C., 1917, The geology and ore deposits of Ely, Nevada: U.S. Geol. Survey Prof. Paper 96, 189 p.
- Stagg, K. G., and Zienklewicz, O. C., 1968, Rock mechanics in Engineering practice: New York, John Wiley & Sons.
- Stateham, R. M., and Vanderpool, J. S., 1971, Microseismic and displacement investigation in an unstable slope: U.S. Bureau of Mines Report of Investigation 7470.
- Sultan, H. A., 1977, Oral communication: Dept. of Mining and Geological Engineering, University of Arizona.
- Welsh, J. E., 1965, Stratigraphic control of the structure in the Robinson mining district, White Pine County, Nevada: Ely, Nevada, Kennecott Copper Corporation, Nevada Mines Division, unpublished report, 26 p.
- \_\_\_\_\_ and Breitrack, R. A., 1964, Pennsylvanian Ely Formation, Permian stratigraphy: Ely, Nevada, Kennecott Copper Corporation, Nevada Mines Division, unpublished report, 26 p.
- Westra, G., 1976, The Ruth porphyry copper deposit and its relationship to the Robinson sulfide system near Ely, White Pine County, Nevada: Ely, Nevada, Kennecott Copper Corporation, Kennecott Exploration Inc., unpublished report, 100 p.
- Wilson, W. R., 1976, Unpublished reports: Ely, Nevada, Kennecott Copper Corporation, Nevada Mines Division.
- \_\_\_\_\_ 1977, Oral communication: Ely, Nevada, Kennecott Copper Corporation, Nevada Mines Division.

Spencer, A. C., 1917, The geology and ore deposits of Ely, Nevada. U.S. Geol. Survey Bull. Part 10, 129 p.

Stapp, K. O., and Shanderson, O. C., 1961, Sand sediments in East-Seattle basins, New York. John Wiley & Sons.

Stratton, R. M., and Vanhook, J. L., 1971, Mylonites and dis- placement investigations in an unstable slope: U.S. Bureau of Mines Report of Investigation 7475.

Sullivan, H. A., 1917, Geol. examination Dept. of Mining and Geolog- ical Engineering, University of Arizona.

Wells, J. E., 1961, Stratigraphic control of the structure in the Basin- and mining district, White Pine County, Nevada; Ely, Nevada, Kennecott Copper Corporation, Nevada Mines Division, un- published report, 34 p.

and Botzick, R. A., 1964, Pennsylvania Ely formation, Pa- also geology Ely, Nevada, Kennecott Copper Corporation, Nevada Mines Division, unpublished report, 56 p.

Winters, G., 1972, The bath porphyry copper deposit and its relationship to the Robinson fault system near Ely, White Pine County, Nevada; Ely, Nevada, Kennecott Copper Corporation, Kennecott Corporation Inc., unpublished report, 120 p.

Wilson, W. E., 1974, Unpublished reports; Ely, Nevada, Kennecott Copper Corporation, Nevada Mines Division.

1977, Geol. examination Ely, Nevada, Kennecott Copper Corporation, Nevada Mines Division.



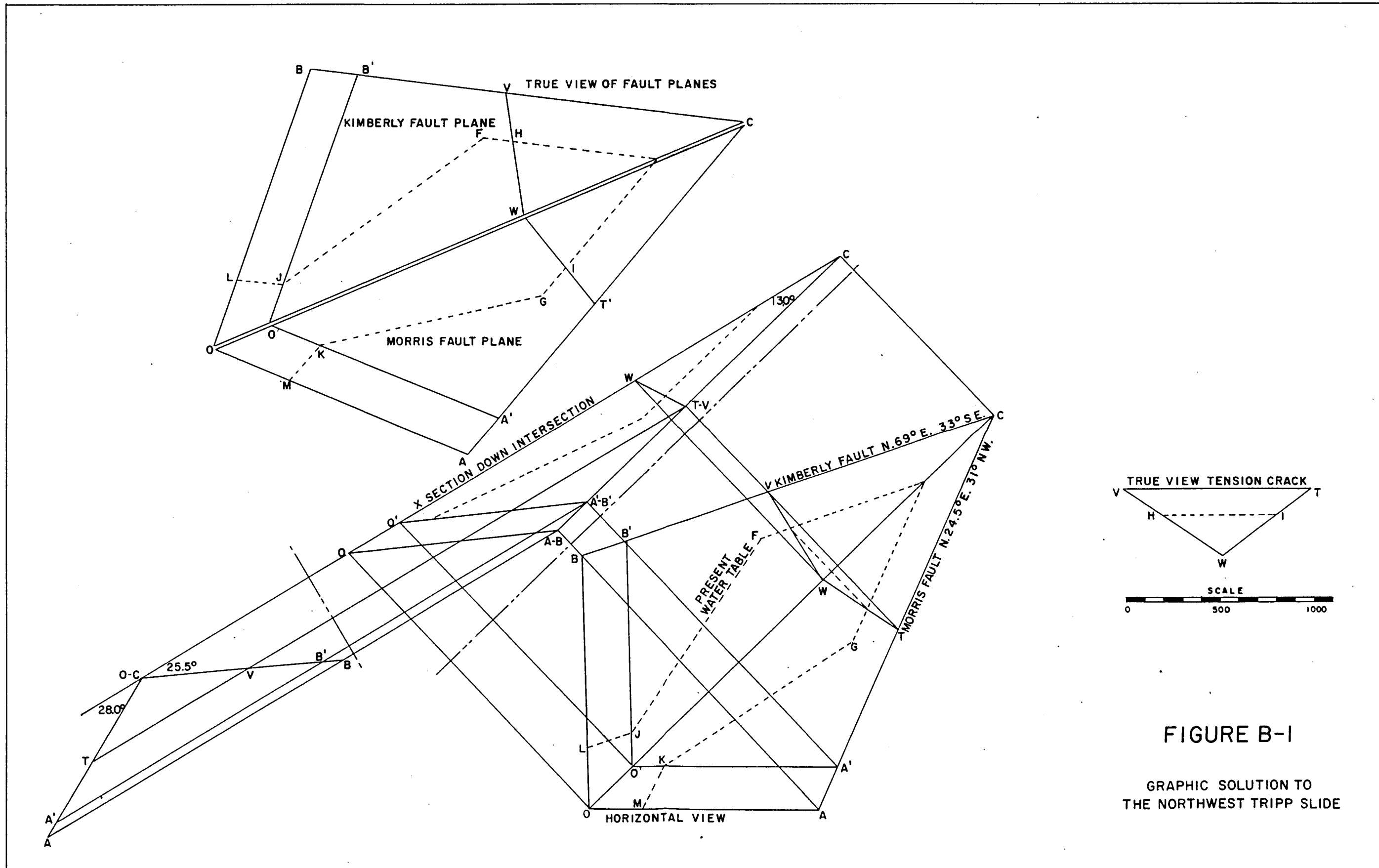


**FIGURE B-1**  
 GRAPHIC SOLUTION TO  
 THE NORTHWEST TRIPP SLIDE

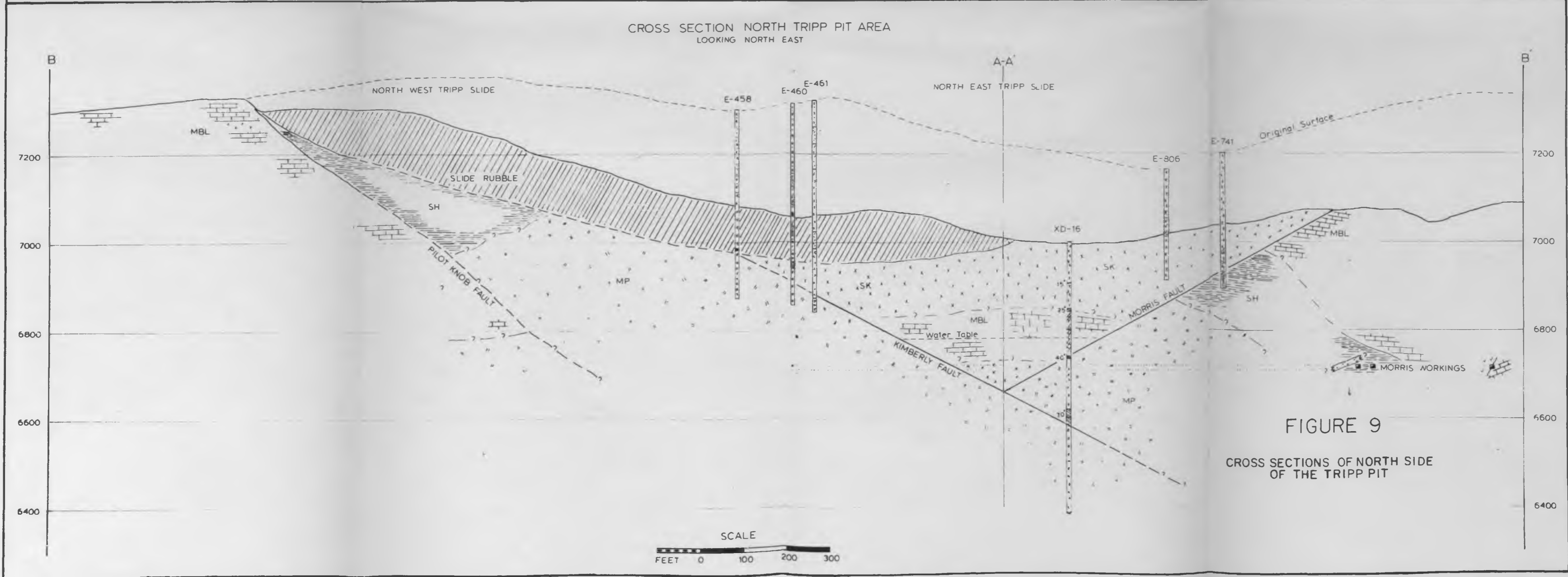
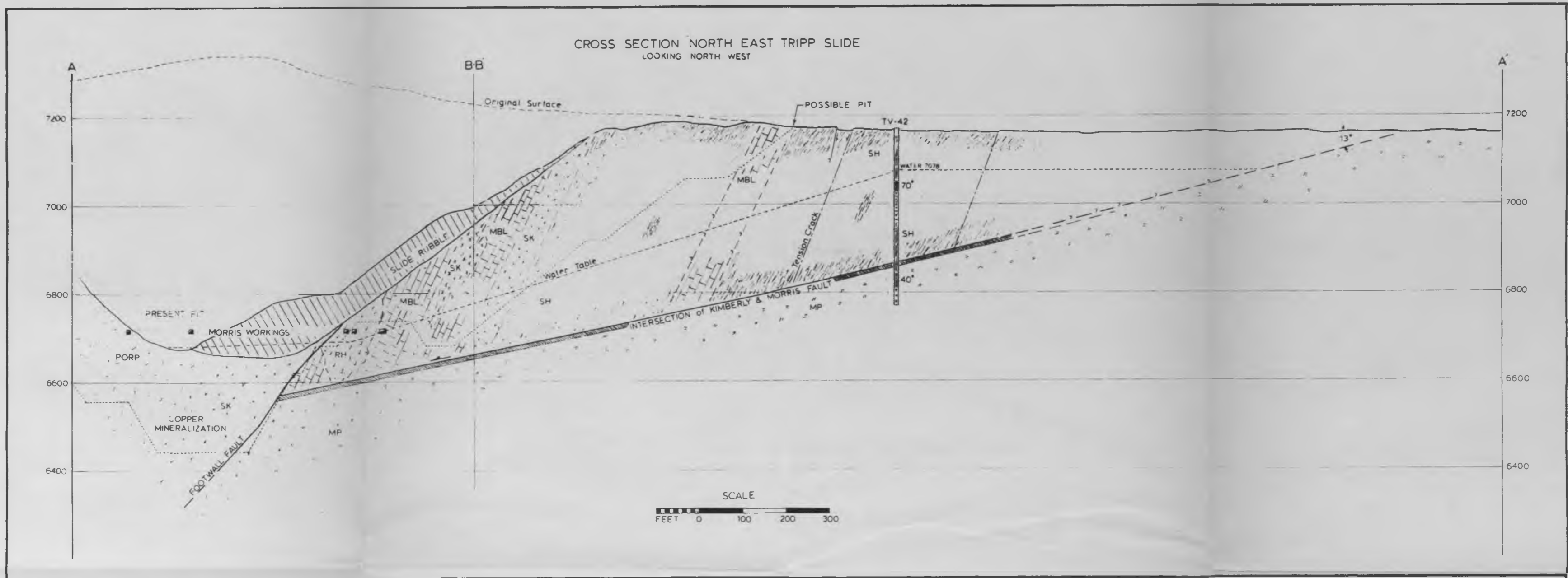
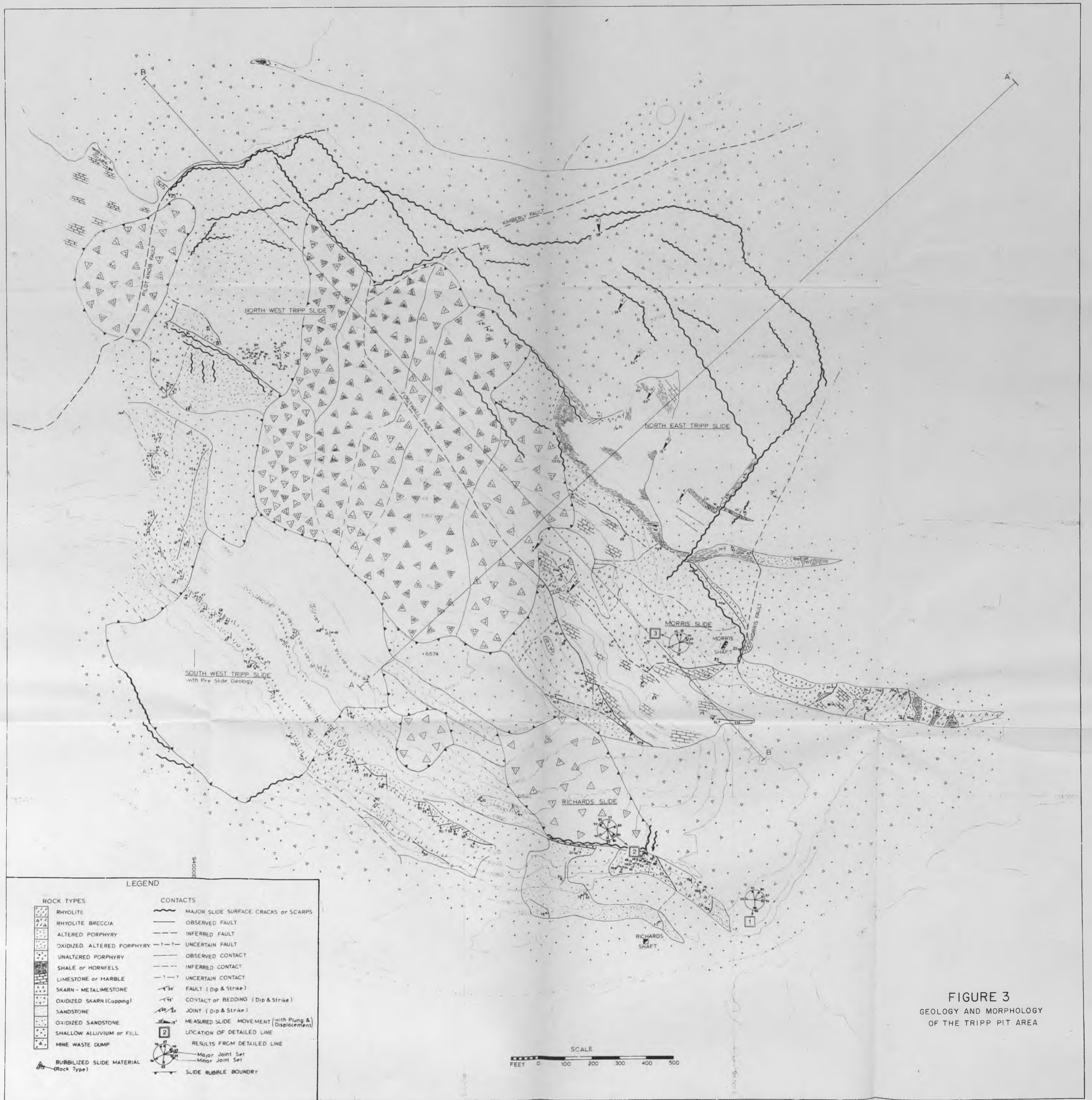


FIGURE 9  
CROSS SECTIONS OF NORTH SIDE  
OF THE TRIPP PIT





FIGURE 8  
TRIPP PIT  
SLIDE MOVEMENT



**FIGURE 3**  
GEOLOGY AND MORPHOLOGY  
OF THE TRIPP PIT AREA

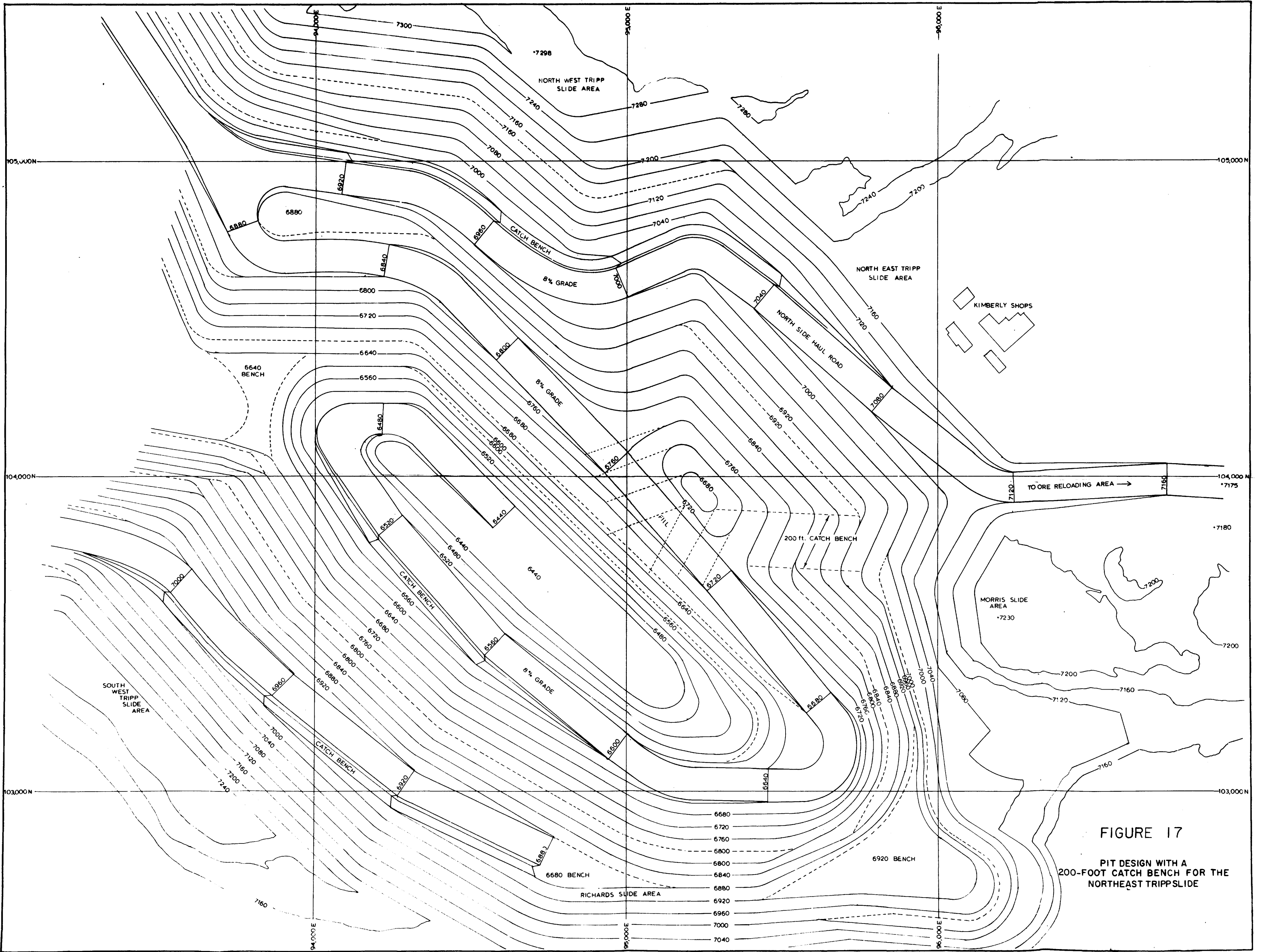


FIGURE 17  
 PIT DESIGN WITH A  
 200-FOOT CATCH BENCH FOR THE  
 NORTHEAST TRIPPSLIDE